Polymer-Nanoparticle Composites: From Orientation Phenomena to Optoelectronic Applications

Dissertation zur Erlangung des Grades „Doktor der Naturwissenschaften“

im Promotionsfach Chemie
am Fachbereich Chemie, Pharmazie und Geowissenschaften
der Johannes Gutenberg-Universität Mainz

Matthias Zorn
geboren in Hachenburg

Mainz, März 2010

Die vorliegende Arbeit wurde unter der Betreuung von [redacted] in der Zeit von April 2007 bis März 2010 am Institut für Organische Chemie der Johannes Gutenberg-Universität Mainz angefertigt

Dekan: [redacted]

1. Berichterstatter: [redacted]

2. Berichterstatter: [redacted]

Tag der mündlichen Prüfung: 19. April 2010

Contents

	Contents	**i**
	Abbreviations	**iii**
	Abstract	**v**
	Zusammenfassung	**vi**
	초록	**viii**
1.	**Introduction**	**1**
1.1.	Nanoparticle-Polymer Hybrid Materials	**1**
1.2.	Nanoparticles	**4**
	1.2.1 Oxidic Semiconductors	**5**
	1.2.2 Quantum Dots	**6**
1.3.	Living Radical Polymerization	**9**
	1.3.1. Nitroxide Mediated Polymerization (NMP)	**10**
	1.3.2. Atom Transfer Radical Polymerization (ATRP)	**11**
	1.3.3. Reversible Addition Fragmentation Transfer Polymerization (RAFT)	**13**
1.4.	Semiconducting Polymers	**14**
1.5.	Self Assembly of Nanoparticles	**17**
	1.5.1 Liquid Crystalline Structures	**17**
1.6.	Optoelectronic Devices Based on Nanoparticles	**20**
	1.6.1. Photovoltaic Devices	**21**
	1.6.2. Light Emitting Devices (LED)	**22**
1.7.	References	**24**
2.	**Scope and Aim of the Work**	**32**

3. Results and Discussion **35**

3.1. Liquid Crystalline Phases of Polymer Functionalized Semiconducting Nanoparticles **36**

3.2. Liquid Crystalline Orientation of Semiconducting Nanorods in a Semiconducting Matrix **61**

3.3. Orientation and Dynamics of ZnO Nanorod Liquid Crystals in Electric Fields **76**

3.4. Light Induced Charging of Polymer Functionalized Nanorods: A "Solar Cell" Concept for a Single Particle **94**

3.5. Quantum Dot-Block Copolymer Hybrids with Improved Properties and Their Application to Quantum Dot Light-Emitting Devices **108**

3.6. Reduced Efficiency Roll-Off in Light-Emitting Diodes Based on Quantum Dot-Conducting Polymer Hybrids **126**

4. Summary **139**

5. Supporting Information

to 3.3 **143**

to 3.4 **144**

to 3.5 **149**

to 3.6 **153**

List of Publications **158**

Acknowledgement **159**

Abbreviations

AC	alternating current
AFM	atomic force microscopy
AIBN	azoisobutyronitril
ATRP	atom transfer radical polymerization
Avg. EQE	average external quantum efficiency
BCP	block copolymer
CAA	cysteamine acrylamide
CdSe	cadmium selenide
CdSe@ZnS	core shell quantum dot (CdSe: core; ZnS: shell)
CdTe	cadmium telluride
$CHCl_3$	chloroform
DA	dopamine acrylamide
DC	direct current
DLS	dynamic light scattering
DMF	dimethylformamid
DS	dielectric spectroscopy
DSC	differential scanning calorimetry
E	energy/electric field strength
EL	electroluminescence
ETL	electron transporting layer
Fc	ferrocene
GPC	gel permeation chromatography
h	Planck´s constant
HDT	hexanedecanthiol
HOMO	highest occupied molecular orbital
HRTEM	high resolution transmission electron microscopy
HTL	hole transporting layer
I-L	current-luminescence
InP	indium phosphide
IR	infrared spectroscopy
ITO	indium tin oxide
I-V	current-voltage
KPFM	Kelvin probe force microscopy
LC	liquid crystal
LED	light emitting diode
LUMO	lowest unoccupied molecular orbital
m	meter
MeOH/MeOD	methanol, deuterated methanol
Mn	number average of the molecular weight
Mw	weight average of the molecular weight
NMR	nuclear magnetic resonance spectroscopy
OA	oleic acid
OLED	organic light emitting diode
P	pressure
PDEGMEMA	poly diethyleneglycolmethylethermethacrylate
PDI	polydispersity index
PEDOT:PSS	poly(3,4-ethylenedioxythiophene) poly(styrenesulfonate)
PEG	polyethyleneglycol
PFPA	pentafluorophenolacrylate

PMMA	polymethylmethacrylate
POM	polarized optical microscopy
PS	polystyrene
PTPA	polytriphenylamine
PV	photovoltaic
QD	quantum dot
Q(D)LED	quantum dot light emitting diode
RAFT	reversible addition fragmentation transfer
R_g	radius of gyration
R_h	hydrodynamic radius
s	interpolymer distance
σ^*	reduced surface coverage
sec	second
SEM	scanning electron microscopy
SnO_2	tin dioxide
Std. σ	standard deviation
τ	relaxation time
T	temperature
t	time
T_c	clearing temperature
TDPA	n-tetradecylphosphonicacid
TEM	transmission electron microscopy
T_g	glass transition temperature
TGA	thermal gravimetric analysis
THF	tetrahydrofuran
TiO_2	titanium dioxide
TOP	trioctylphosphine
TOPO	trioctylphophineoxide
TPA	triphenylamine
TPD	tetraphenylbiphenyldiamin
TPBI	1,3,5-tris-(*N*-phenylbenzimidazol-2-yl)benzene
UV(Vis)	ultraviolet-visible spectroscopy
V	Volt
V(p-p)	voltage (peak to peak)
VFT	Vogel-Fulcher-Taumann
wt%	weight percentage
$Zn(Ac)_2$	zinc diacetate
ZnO	zinc oxide

Abstract

Polymer-nanoparticle hybrids show synergistic effects, demonstrating both, the unique properties of nanosized structures and the good processability and functionalities of polymeric materials. This work shows the synthesis and application of block copolymers containing a soluble, functional block and a short anchor block, which efficiently binds to the surface of nanocrystals.

We functionalized anisotropic, semiconducting nanoparticles, which can be dissolved in organic and polymeric matrices upon modification. The modified nanorods have the ability to form liquid crystalline phases, which behave similar to low molecular liquid crystals with a reversible clearing behaviour. These liquid crystalline phases could also be obtained in hole conducting matrices.

For a macroscopic orientation of the nanorods, electric fields were applied and a switching (in analogy to known liquid crystals) to a homeotropic orientation was observed.

By introduction of dye molecules in the anchor block of a hole conducting block copolymer, all essential components of a solar cell can be combined in a single particle. Light absorption of the dye induces the injection of electrons into the particles, followed by a charging, that was monitored by a special AFM technique.

Light emitting nanocrystals were functionalized analogously with a hole transporting polymer. The stability of the particles could be enhanced by the sterically stabilizing polymer corona and the particles showed improved properties in terms of processing.

We applied these hybrid materials in light emitting devices, which showed better characteristics due to an improved hole injection and well dispersed emitting particles in the active device layer.

The work shows the broad spectrum of properties and applications based on the synergistic effects in hybrid and composite materials.

Zusammenfassung

Hybridmaterialien aus Nanopartikeln und Polymeren vereinigen die einzigartigen Eigenschaften von Nanostrukturen mit Polymereigenschaften, wie guter Löslichkeit und verschiedenen weiteren synthetisch einstellbaren Funktionen.

Das Konzept dieser Arbeit basiert auf der Modifikation von Nanopartikeln mit Blockcopolymeren, die neben einem funktionellen, löslichkeitsvermittelnden Block einen Ankerblock enthalten, der effizient an die Oberfläche anorganischer Materialen anbinden kann.

Anorganiche, anisotrope Nanomaterialien, die mit einem solchen Blockcopolymer sterisch stablisiert wurden, sind löslich in organischen Lösungsmitteln und Polymermatrizen. Auf grund der Anisotropie der Partikel bilden sich flüssigkristalline Phasen aus, die ähnliche Eigenschaften zeigen, wie molekulare Flüssigkristalle. Diese Phasen konnten auch mit halbleitenden Polymeren als Funktionalisierungs- und Matrixpolymer untersucht werden.

In Analogie zu molekularen oder polymeren Flüssigkristallen konnte ein Schalten in elektrischen Feldern beobachtet werden. Die resultierende senkrechte Ausrichtung der Nanostäbe auf der Elektrode ist eine begehrte Morphologie für optoelektronische Anwendungen.

In den Ankerblock eines halbleitenden Blockcopolymers konnten Farbstoffmoleküle eingebracht werden, so dass alle Komponenten einer Solarzelle an einem Partikel vereint werden konnten. Der Farbstoff kann nach der Absortption von Licht Elektronen in den Nanopartikel injizieren, so dass sich dieser auflädt.

Fluoreszierende Nanokristalle (Quantenpunkte) wurden ebenfalls mit einem halbleitenden Polymer modifiziert, wodurch die Stabilität als auch die Verarbeitungsmöglichkeiten des Materials verbessert werden konnten. Diese Hybridmaterialien wurde in Leuchtdioden angewendet, die durch eine verbesserte Injektion positiver Ladungsträger und die gute Dispersion der emittierenden Spezies, optimiert werden konnten.

Diese Arbeit zeigt damit ein breites Spektrum an Eigenschaften und Anwendungen, die auf den synergistischen Effekten der hergestellten und untersuchten Hybrid – und Kompositmaterialien basieren.

초 록

고분자-나노입자 혼성체는, 크기에 따라 다양한 특성을 보이는 나노입자와 우수한 가공성 및 기능성을 지니는 고분자의 특성을 모두 지닐 뿐 아니라, 기존의 물질 및 구조에서 구현할 수 없었던 향상된 특성을 지닌다. 본 연구는, 용해성이 높고 다양한 기능을 지니는 긴 블록과 나노파티클의 표면에 효과적으로 결합할 수 있는 짧은 블록을 갖고 있는 블록 공중합체의 합성하고 그의 광학적 응용에 관한 것이다.

합성된 블록공중합체를 이용하여 비등방성 반도체 나노막대의 표면을 개질함으로써, 나노막대를 유기물 혹은 고분자 매트릭스에 분산하였다. 개질된 나노로드는 저분자 액정 물질과 유사하게 액정상을 형성하며 등방성화 온도 (clearing tempeature) 전후로 가역적인 상변화를 보였다. 두 전극판 사이에 개질된 나노로드를 채우고 전기장을 걸어줌으로써 나노로드의 배열 방향을 변화시킬 수 있었으며, 저분자 액정과 같은 수직 (homeotropic) 배열을 관찰하였다.

정공 전도성 블록 고분자의 앵커 블록에 염료를 결합하여 이를 반도체 나노입자와 결합함으로써 태양광 전지의 필요 요소가 단일 물질에 결합된 혼성체를 제작할 수 있었다. 혼성체에 조사된 빛에 의해 염료에서 여기된 전자가 나노입자에 주입되어 대전 (charging)이 발생되는 것을 새롭게 고안된 원자간력현미경 (AFM) 측정법으로 확인하였다.

발광성 나노입자 또한 정공 전도성 고분자와 화학적으로 결합하여 유-무기 혼성체를 제작하였다. 고분자 사슬 간의 입체 간섭에 의해 나노입자의 입자 안정성이 증가하였으며, 다양한 용액 공정의 가공성 또한 증가하였다.

합성된 유-무기 혼성체를 발광소자의 발광층으로 적용한 결과, 나노입자층 내로의 정공 주입 특성의 향상, 입자층 내의 전자 및 정공 농도 균형의 향성 및 입자층 내의 엑시톤 농도의 감소에 따라, 기존 발광소자보다 향상된 효율 및 안정성을 보였다.

본 연구를 통하여 고분자-나노입자 혼성체의 특성을 폭넓게 이해하고, 그의 다양한 응용 가능성에 대하여 알아볼 수 있었다.

1. Introduction

„There is plenty of room at the bottom“

Richard Feynman already saw fifty years ago the potential hidden in the micro- and nanocosmos. During the last decades nanoscience and nanotechnology became a keyword even in politics and society. Applications based on nanotechnology already found their way into everyday life like polish substances or special paints with lotus effect for self-cleaning surfaces. In particular, development of advanced data storage techniques focuses on miniaturized devices on the nanometer scale.

Combination of polymers and nanoparticles may bring advantages of both of these nanosized components demonstrating synergistic effects. This work focuses on the challenge to combine interesting properties of nanoparticles with those of polymers, to show new combinatorial features of such hybrids and composite materials. We focus on novel self-assembly strategies and polymer nanoparticle hybrids with application in optoelectronic devices.

1.1. Nanoparticle-Polymer Hybrid Materials

Combining two nano sized materials with different properties like nanoparticles and polymers, whose radii are in the nano range, gives rise to materials with unexpected behaviour due to cooperative interactions.[1] These hybrid materials can be combinations of several material classes from the inorganic, organic and biological field. Inorganic - organic hybrids are the most developed. The combination of the high durability and mechanical strength of inorganic structures with the good processing probabilities of organic polymers has already been used for more than 100 years.[2, 3] Filler materials like carbon black or the highly investigated field of clay nanocomposites[4, 5] have already found application in everyday life, like e. g. in tires.[6] But also hybrids from inorganic or organic synthetic structures with biological molecules are interesting materials especially for sensing applications.[7] A classification beyond the components can be made by the kind of interactions between the different materials. Class I

hybrids are connected by weak interactions like van der Waals, hydrogen, weak electrostatic or hydrophobic interactions; class II hybrids exhibit stronger bonding between the single components (like covalent, coordinative or ionic bondings).[8]

Hybrid materials can consist of networks, layered and dispersed systems. Such structures can be synthesized *in situ*. One of the hybrid components can act as a matrix for the synthesized part. Block copolymer with defined microdomains can template e. g. the synthesis of nanoparticles in distinct areas of a film.[9]

The incorporation of nanoparticles is often a challenge due to their immiscibility with a polymeric matrix. Aggregation phenomena are often observed if particles are mixed with polymers depending on the polymer radius of gyration and the nanoparticle size.[10] To achieve well dispersed particles in a polymer matrix, the surface has to be coated with organic ligands of an identical or similar composition like the surrounding polymer.[11] Many particles, like quantum dots but also many other systems, are synthesized with a surfactant to stabilize the particles and make them soluble in organic solvents. The use of polymeric surfactants can introduce different functionalities in addition to solubility, like stimuli responsive,[12] insulating[13] or semiconducting[14] properties. There are two approaches to synthesize polymer-nanoparticle hybrid systems

In the *grafting-from* approach, an initiator or a chain transfer agent (like a halide or a dithioester for (controlled) radical polymerization) can be connected to the particle´s surface. The polymerization is performed in the presence of the functionalized particles to graft polymer brushes directly from the surface.[15] This method produces densely functionalized particles.

In a *grafting-to* approach, the polymer and particles are preformed. This offers a possibility to have well characterized individual components, which can be united under adsorption (sometimes including a ligand exchange) of the anchor group containing polymer on the particle.[16] (see Figure 1)

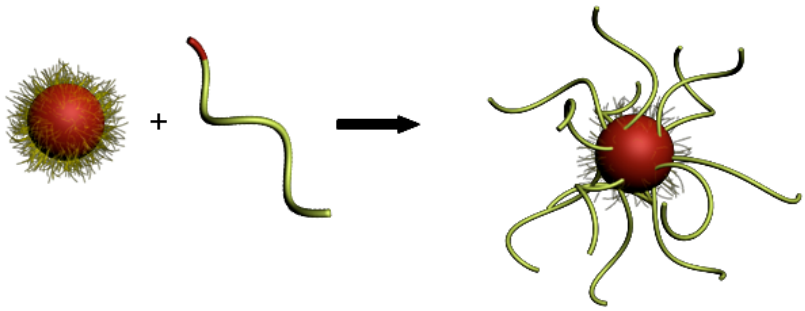

Figure 1.
Polymer modification of a nanoparticle by the *grafting-to* approach (ligand exchange).

Such hybrid systems are soluble in organic solvents suitable for the surrounding polymer corona and polymers of the same chemical composition. Figure 2 shows polymer coated luminescent quantum dots in a polymer matrix. Different morphologies upon polymer modification can be clearly investigated from the nano to micrometer scale. Polymer modified particles are well dispersed in the matrix leading to uniformly luminescent films, while aggregation can be seen in the case of the surfactant (oleic acid) covered particles. In the cross section images 1B/2B segregation and migration of the non-functionalized particles to the interfaces can be investigated, while the particles are uniformly distributed in the film upon polymer modification.

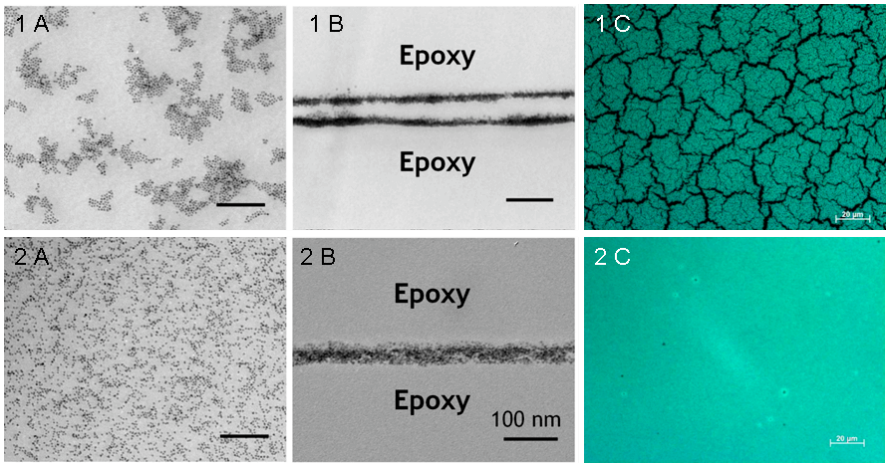

Figure 2
Different morphologies of quantum dots dispersed in polymer matrix 1A: TEM image of aggregated surfactant stabilized QD in a polymer film.1B: Cross section shows segregation of non- functionalized QDs to the interfaces. 1C: Even on a larger scale the segregation can be investigated (fluorescence microscopy image), 2A/2B: polymer modified particles are uniformly distributed in the polymer film, leading to an uniformly luminescent film (2C).

Having a good solubility and good dispersion of nanoparticles in a polymer matrix offers the possibility to self assemble and manipulate the particles in the nanocomposite.[17] Due to the high mobility of functionalized particles it is possible to create e. g. self healing materials.[18]

A very interesting kind of nanocomposite is the combination of semiconductor nanoparticles and semiconducting polymers. By combination of n-type particles and p-type polymers heterojunctions can be formed on a nanoscale. This approach is very promising to improve optoelectronic devices, where a control of the interfaces is essential to efficiently combine or separate charges.[19] Polythiophene and poly(paraphenylenevinylene) based macromolecules were grafted on the surface of cadmium chalkogenide nanocrystals and were applied in solar cells and light emitting devices.[20, 21] Such hybrids show novel photophysics, like strongly changed life time of the excited states and enhanced energy transfer to the luminescent nanocrystal. At the same time the nanocrystals can be well dispersed in a matrix and processability is similar to polymeric materials, which is important for device preparation. In the next chapters, different kind of nanoparticles and polymer, their synthesis and application in devices is discussed.

1.2. Nanoparticles

Nanomaterials are defined as structures with at least one dimension smaller than 100 nm. Properties of nanoparticles are different of those of single atoms or the bulk and show novel electronic, magnetic and optical properties.[22, 23] Due to their small dimensions, their properties cannot be explained with the rules of classical physics but can be described with the help of quantum mechanics. These size related properties lead to novel applications in optoelectronics,[24] data storage systems,[25] biological and medical applications[26] and catalysis[27, 28] In general, the use of nanoscopic materials improves the performance of applications that require a high surface area. Following the preparation of well defined metal clusters with a distinct number of atoms (like the famous Au_{55} by G. Schmid *et al.*),[29]

methods were developed to synthesize large amounts of less well defined nanoscale materials. Beside undefined top down approaches like high energy ball milling,[30] well controllable and adjustable solution and gas phase syntheses were developed to produce nanoparticles with defined morphologies. Many protocols were published on the synthesis of metal[31] semiconductor[32] and metal oxide[33, 34] particles with different size, shape and well-defined morphology.[35-37] Particularly for semiconductor and oxide nanocrystals, various synthetic strategies, for instance, pyrolysis (synthesis in high boiling solvents with organometallic precursors), solvothermal and gas phase techniques as well as nano-templated syntheses have been developed.

Particles with anisotropic shapes (like rods, wires or tubes) offer different properties than spherical nanoparticles, for instance, direction (axis) dependent carrier conductivity or charge polarizability due to their asymmetric wave function distribution along the particle axes, [38] and, in consequence, provide different applications. In particular, the efficiency of photovoltaic devices can be increased by using rod-shaped particles.[39, 40] We will focus on two important groups of nanoparticles that were investigated in this work.

1.2.1 Oxidic Semiconductors

In this thesis different kinds of oxidic semiconductors with an anisotropic shape were functionalized in order to investigate their self-assembly behaviour and liquid crystalline properties in polymer matrices.

TiO_2 is the most prominent oxidic material, used in a variety of applications - from a mass product in chemical industy (used in sunscreen, paint and toothpaste) to technical applications ranging from photovoltaics and photocatalysis to photo-/electrochromics and sensors.[41] It was found that water can be split on a TiO_2 surface under UV irradiation[42] and that TiO_2 can undergo reversible color change in cooperation with other materials for application in photochromic devices.[43] Due to the anisotropic crystal cell of the rutile structure, a rod-like

growing of nanoparticles can be introduced easily for TiO_2 by selecting the right conditions during the growth process.

Since Grätzel introduced the concept of dye sensitized solar cells (DSSC) in the 1990s, TiO_2 is the best investigated material for this kind of photovoltaic device. Therein it acts as an electron conducting material in which electron are injected after light is absorbed by an attached dye (see 1.6.1).

ZnO nanoparticles can also be synthesized in various shapes and structures from wires, rods and spheres[44] to belts and even hierarchical structures.[45] ZnO nanoparticles are also applied in optoelectronic devices and sensing. Recent publications showed that ZnO particles can be used in UV lasing applications.[46]

SnO_2 is the third type of metal oxide investigated in this work. SnO_2 as a semiconducting material is also applied in gas sensing, light and field emission sources. SnO_2 can also be applied as a transparent electrode material. In solar cell application it is a promising material because SnO_2 exhibits very fast electron transportation along with higher recombination dynamics.[47, 48]

1.2.2 Quantum Dots

Nanocrystals of semiconducting materials like CdSe, CdS or InP are the most investigated group of nanosized materials due to their unique optical properties and manifold applications.[49] Due to their small dimensions in the range of the de Broglie wavelength of electrons (referred as quantum confinement effect) they show discrete energy levels (i. e. exitonic states).

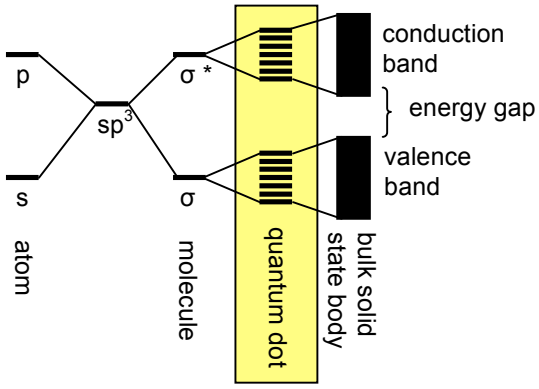

Figure 3.
The electronic energy levels depend on the number of bound atoms. As the number of atoms increases, the discrete energy levels of the atomic orbitals merge into energy bands (in semiconductors). Semiconductor nanocrystals have dimensions in between molecules and bulk material and show discrete energy levels.

Hence, these semiconductor nanocrystals or quantum dots (QD) exhibit properties between those of single atoms and those of the bulk material. The system can be described as an "electron in a box", known from quantum mechanics. Bringing many atoms together causes their orbitals to form molecular orbitals with discrete energy levels. Going to bulk materials, all energy levels are combined in a band, in which the electrons are delocalized and behave like an electron gas.[50] Nanocrystals (in between molecule and bulk) with their small dimensions show discrete energy levels, which give rise to unique electronic and optical properties.[51] By variation of the crystal size, which corresponds to the bandgap of nanomaterials, the emission wavelength can be tuned from UV to the near infrared[52] (see Figure 4). A widening of the band gap is observed with decreasing crystallite size. At the same time the absorption of such nanocrystals is very broad, as they can be excited with any wavelength above the band gap of the semiconductor.

Figure 4.
Emission wavelength of CdSe quantum dots can be tuned over a large spectrum by variation of the particle size.[53]

QD can be synthesized by various combinations of II-VI (group II: Hg, Cd, Zn; group VI: S, Se, Te) and III-V elements (group III: Al, In, Ga; group V: N, P, As). The most famous and intensively investigated systems are cadmium chalcogenide nanocrystals. CdE (E= S, Se, Te) can be prepared in various shapes and narrow size distributions, which allows to adjust their electronic and optical properties.[54]

Optical properties and stability can be adjusted by core-shell heterojunction structures. These core shell structures can be classified as two kinds of quantum dots depending on the energy levels of the shell and the core. In Type I – quantum dots (like CdSe-ZnS), the band edges of the core lie inside the band gap of the outer shell.[55] In Type II – quantum dots (like CdTe-CdSe or CdSe – ZnTe), the valence and conduction band of the shell are higher or lower than the one of the core[56] (see Figure 5)

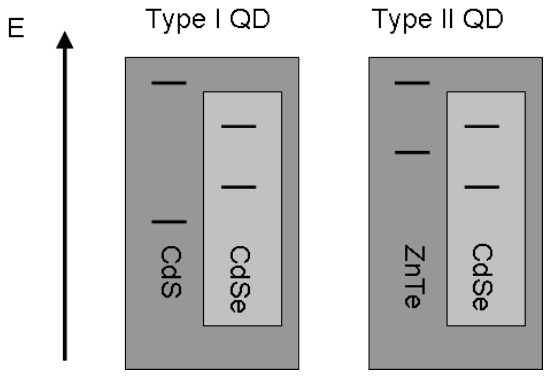

Figure 5.
Energy level positions of Type I and Type II quantum dot. Typical examples for Type I are CdS-CdSe or ZnS-CdSe. A typical Type II quantum dot system is ZnTe-CdSe.

If a Type II QD is excited to generate charge carriers, one of these charge carriers migrates into the core and the other in the shell phase. A recombination of a hole-electron pair at the core –shell interface produces the emission while in Type I –QD recombination is located in the core. A different tuning of the photoluminescence characteristics is possible by choosing appropriate materials. Such core shell QDs can be synthesized in a one-pot synthesis by taking advantage of the different reaction kinetics of the formation of the core and the shell part like done for the particles used in this work.[57]

Due to their unique and superb properties QDs have a huge field of applications, like in dyeing, optoelectronics like solar cells[58] and light emitting devices[59] and for fluorescence imaging of biological samples.[60]

1.3. Living Radical Polymerization

Radical polymerization offers the possibility to synthesize macromolecules from a huge number of vinyl monomers that are initiated with radical starters like peroxides, diazo derivatives, redox systems, organometallics, and photolabile compounds to convert the double bond into a single bond with a radical at the chain end. This radical can add further monomer to build up a polymeric structure. Free-radical polymerization proceeds via a chain mechanism, which basically consists of four different types of reactions involving free radicals: (1) radical generation (initiation), (2) radical addition to a substituted alkene (propagation), (3) atom transfer and atom abstraction reactions (chain transfer and termination by disproportionation), and (4) radical–radical recombination reactions (termination by recombination).[61] (3) and (4) are responsible for a broad molecular weight distribution and it is not possible to reinitiate terminated polymers to create e.g. block copolymers.

To provide end-group control and facilitate the synthesis of block copolymers by sequential monomer addition ionic polymerization techniques were first applied by Swarcz *et al* in the 1950s.[62] Transfer and termination reactions can be prevented and low polydispersities can be reached if the initiator is consumed at early stages of polymerization. However, ionic polymerization techniques can only be utilized for a small number of molecules and have disadvantages due to very sensitive reaction procedures concerning moisture, oxygen or other impurities.

A controlled or living radical polymerization offers the possibility to use all the advantages of radical polymerization together with the benefits of a living polymerization i.e. reaction

control, low polydispersities[63] (PDI < 1.5) and the possibility to synthesize well-defined block and graft copolymers, stars, combs and networks, end-functionalized polymers and many other materials under mild conditions and from a large range of monomers. One of the driving forces for this dramatic increase in interest has been the growing demand for functionalized, well-defined materials as building blocks in nanotechnological applications. Besides the simple experimental procedure a huge variety of monomers are accessible and the choice of solvent is only limited by potential transfer reactions.

The main concept always includes a decrease of the concentration of the reactive species to suppress side and termination reactions. The exchange between the active and dormant species allows slow but simultaneous growth of all chains while keeping the concentration of radicals low enough to minimize termination.

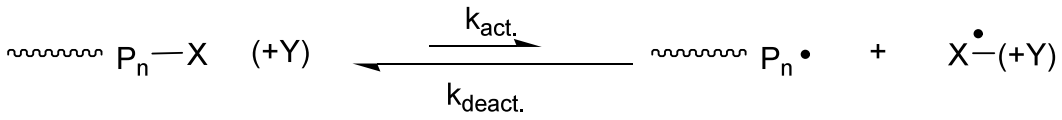

Figure 6.
General scheme for a controlled/living radical polymerization

By addition of a reactant that converts the reactive species into a dormant species the equilibrium is strongly shifted to the side of the dormant species ($k_{deact} >> k_{act}$). At the same time the free radical concentration is dramatically decreased. Mainly three concepts are generally established to decrease the amount of acitive radicals in the reaction mixture.

1.3.1. *Nitroxide Mediated Polymerization (NMP)*

The concentration of the propagating radical can be controlled by addition of a free stable radical (general: stable free radical polymerization SFRP). In most of the cases nitroxides (like 2,2,6,6-tetramethyl-1-piperidynyl-*N*-oxyl (TEMPO) **(3)**) are added as persistent radicals to the polymerization reaction. Coupling of the nitroxide radical with the propagating chain to

form alkoxyamines is sufficiently reversible, termination is reversible, and the active radical concentration can be limited to levels that allow controlled polymerization.

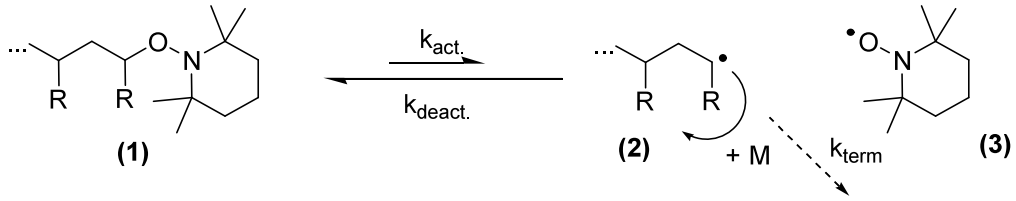

Figure 7.
Schematic mechanism of Nitroxide Mediated Polymerization with TEMPO

The mediating agent/stable radical should not react with itself, nor start new chains or take part in any side reaction. NMP is often performed at high temperatures (< 120 °C) due to thermo cleavable dormant species at the active chain end.[64] The reaction temperature can be lowered by the introduction of bulky substituents that lower the dissociation energy of the dormant species. NMP is an effective method for the polymerization of styrene and its derivatives, while polymerization control for other monomers (like (meth)acrylates) needs the design of special mediating reagents.

Alternatively to adding the stable radical to the monomer-initiator mixture, the dormant species can be formed in advance.[65] This can be an unimer or macroinitiator to prepare block copolymers. This approach offers much better control for the molecular weight and the polymer architecture than the simple addition of the stable radical.[66] Intitiation is started by a thermal dissociation of the dormant species to start the polymer formation.

1.3.2. *Atom Transfer Radical Polymerization (ATRP)*

The Atom Transfer Radical Polymerization (ATRP) originates from the Atom Transfer Radical Addition which is widely used in organic radical synthesis.[67] A transition metal complex is used to convert the growing chain into a dormant species by atom transfer of a halide atom from the metals ligand sphere to the chain, and increase of the oxidation state of the metal center. A transition metal with an expandable coordination sphere that can change

its oxidation number by one is added to the monomer initiator mixture to initiate the cleavage of an alkyl halogen bond (present in the initiator). The formed alkyl radical can start the addition of monomer molecules before the halide atom is retransferred from the metal complex to the propagating chain to form the dormant halide capped species (see Figure 8). Copper was the first metal used for ATRP by Matyjaszewski *et al*. in the 1990s [68, 69] but other transition metals like Mb, Cr, Re, Ru, Fe, Rh, Ni and Pd were also successfully applied to control molecular weight distribution. For every monomer and metal combination the appropriate ligands and initiators have to be found to control the reaction properly.[70] The rate constant for the deactivation step should be several orders of magnitudes higher than the rate constant for activation for the propagating chain. As initiators, whose concentration determines the final molecular weight, halogenated alkanes, benzylic halides, and α-haloesters, -ketones, -nitriles are applied. With different initiator and catalyst systems a large variety of monomers from styrene to (meth)acrylates, (meth)acrylamides and acids can be polymerized by ATRP.

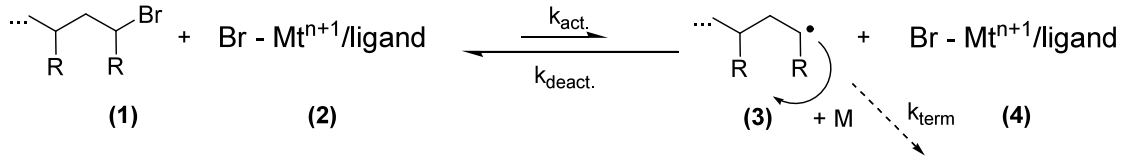

Figure 8.
Schematic mechanism of Atom Transfer Radical Polymerization.

A drawback of ATRP is the presence of the metal complex in the final polymer which obviates the use of the products in medical, biological or electronic application. Furthermore, the complex initiation system is often not compatible with common polymerization media.

1.3.3 Reversible Addition Fragmentation Transfer Polymerization (RAFT)

Another well established way to control radical polymerization is the RAFT process that was first reported by the Australian research groups of Moad, Rizzardo and Thang in the 1990s.[71]

Due to the easy processability, RAFT is arguably the most versatile and convenient controlled radical polymerization technique. In contrast to SFRP/NMP and ATRP there is no inactive dormant species in the RAFT process, but the control originates from a transfer of the propagating radical to another chain.[72] The polymerization has to be initiated like in conventional free radical polymerization (e. g. with AIBN). The proposed mechanism of the RAFT process is shown in Figure 9.[73, 74]

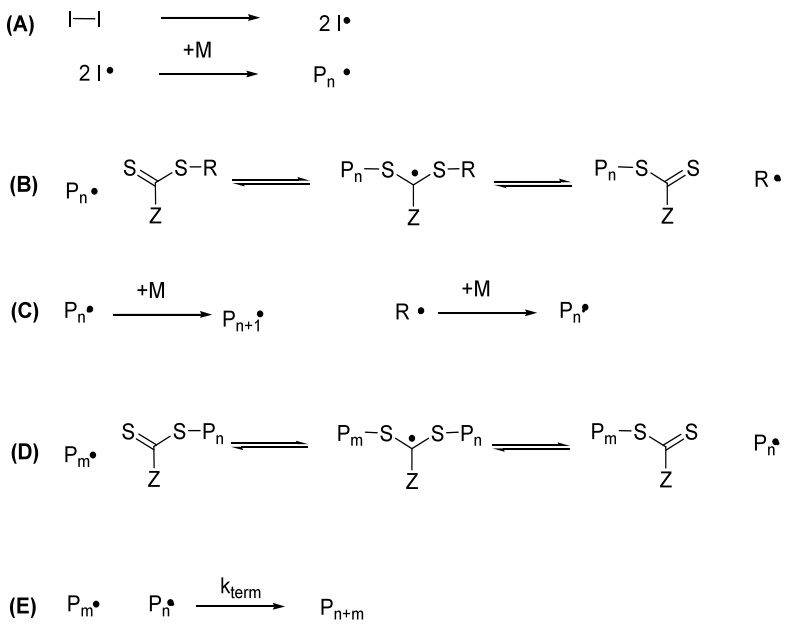

Figure 9.
Mechanism of the RAFT polymerization.[75]

After standard initiation by a radical initiator (A), the propagating chain can attack the RAFT reagent at the reactive C=S double bond (B), followed by fragmentation of the intermediate radical to a RAFT reagent terminated polymer and a new propagating radical, which keeps the polymerization alive. After several monomer additions (C) the growing polymer chain attacks the dithioester terminated inactive polymer chain and transfers the active species to the other chain (D). The rapid equilibrium between the propagating chains and the dormant polymeric

thiocarbonylthio compound offers a narrow molecular weight distribution (PDI < 1.3) due to the equal probability for all chains to grow. If the reaction is stopped most polymer chains carry thiocarbonylthio end groups, which are stable and can be isolated to reinitiate for the formation of block copolymers. Termination (E) is very unlikely due to the fast chain transfer. As chain transfer agents dithioester compounds are the most commonly used species, but a wide range of thiocarbonylthio compounds (like xanthenates,[76] dithiocarbamates,[77] or trithiocarbonates[78]) were successfully applied.[72] By the design of the RAFT reagent various polymer architectures (e. g. star polymers, graft polymers, …) are easily accessible. RAFT polymerization can also be carried out at rather low temperatures[79] (ca. 25°C) and in aqueous solution,[80] offering the possibility to use methods like emulsion or suspension polymerization, which are important industrial polymerization techniques.

1.4. Semiconducting Polymers

Polymers with electronic properties have a lot of applications in several kinds of devices from light emitting devices to organic field effect transistors and organic photovoltaic cells.[81, 82] (Semi-)Conducting polymers combine electric properties of metals and semiconductors with the unique feasibility of a polymeric material, giving rise to future technologies like printable electronics.[83] Hence, a lot of semiconducting polymers were synthesized since Mac Diarmid, Shirakawa and Heeger discovered these materials in the 1970s and were honoured with the Nobel Prize in 2000 for their investigations.[84] In polyacetylene **1** conductivity can be raised by doping to the level of metals. Nevertheless typical polymers are low mobility materials (typically less than $10^{-2} – 10^{-1}$ cm^2 V^{-1} s^{-1}).

Most of these material have a π conjugated backbone or a conducting molecule as a side chain, which makes them capable for transporting charges and interacting with light.

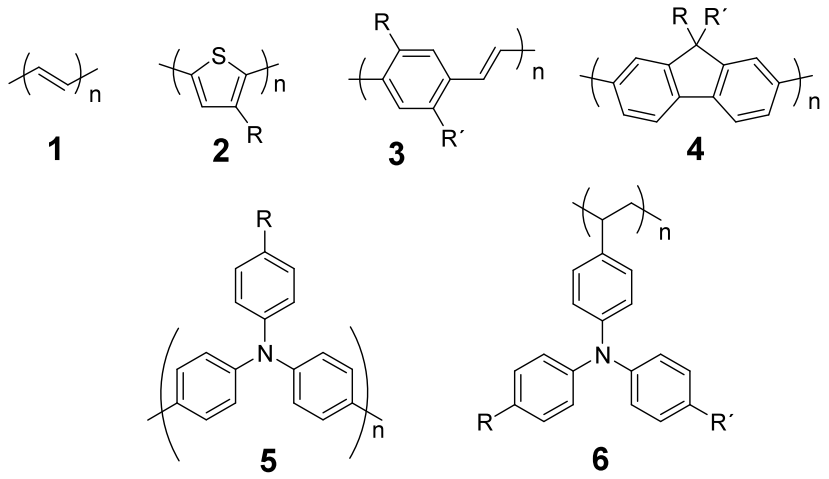

Figure 10.
Semiconducting polymers: 1. polyacetylene, 2. poly(3-alkyl)thiophene, 3. polyphenylenevinylene, 4. polyfluorene, 5. main chain polytriphenylamine, 6. side chain polytriphenylamine.

In the main focus is the application of semiconducting polymers applied in electronic devices.[85] The most prominent examples are alkyl substituted polyl(3-alkyl)thiophenes (**2)** (like poly-3-hexylthiophene; P3HT). P3HT is an interesting material in organic photovoltaics and is already applied in commercialized products.[86]

Polyphenylenevinylene (**3)** (PPV) and polyfluorene (**4)** derivatives[87] became very popular due to their electroluminescent properties and are applied in polymer light emitting diodes,[88] but copolymers of different conjugated monomers (like polyfluorene-*alt*-triphenylamine)[89] have also been shown to be promising materials in terms of stability and charge carrier mobility.

Many of these polymers increase their charge carrier mobility by orders of magnitude in an ordered state (like crystalline or liquid crystalline)[90] while charge carrier mobility drops dramatically in unordered or semi-crystalline samples. P3HT, for example, increases its mobility [91]from 10^{-4} to 0.14 $cm^2\ V^{-1}\ s^{-1}$, depending on the order in the macroscopic sample.

Hence, materials showing mobilities even in an isoptropic, glass-like state are interesting for various applications, although mobility (10^{-6} – 10^{-3} $cm^2\ V^{-1}\ s^{-1}$) does not reach that of crystalline materials.[92] Triphenylamine (TPA) based compounds (**5** or **6**) were already strongly investigated as hole transporting layers in light emitting devices [93, 94] and in a lot of applications taking advantage from the electron-donating molecule (like in copiers, solar

cells[95] and data storage[96]). TPAs can be used as small molecules, or integrated in a polymer backbone (**5)** or side chains (**6**). Dimerized TPA structures (R in **5** is another TPA unit, TPD (tetraphenylbenzylidendiamin) are more stable and show better mobilities. In side chain semiconducting polymer charges are just transported by a hopping mechanism (see Figure 11) from chain to chain.[97, 98] The molecules can be reversibly oxidized (or reduced). In hole conducting polymers single moieties undergo a reversible redox reaction and form radical cations. By this reversible reaction the charges are transported (by charge hopping) from the anode to the cathode.

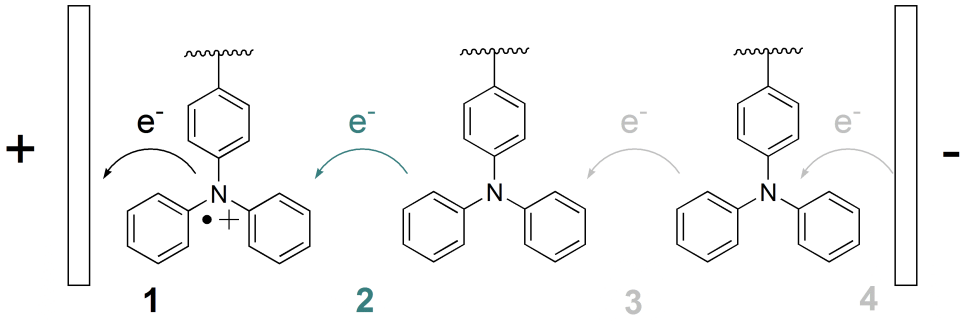

Figure 11.
Hopping mechanism for charge transport in semiconducting polymers (like TPA)

The higher stability of radical carbo cations explains why the majority of semiconducting polymers are p-type materials, while n-type materials need inert conditions for a good performance, due to the high reactivity of radical anions towards oxygen or water.

As electron conducting polymers, perylene and triazine polymers should be mentioned. For application in devices the use of fullerene derivatives (like phenyl-C_{61}-butyric acid methyl ester**,** PCBM) are more common and effective.[99]

1.5. Self Assembly of Nanoparticles

Looking towards application of nanoparticles in different kinds of devices, assembly and arrangement is very important. Self assembly is driven by weak interaction energies between the subunits. The system can lower its free energy by the self assembly process. Well defined nanocrystals with a very low polydispersity form superlattices[100] and organize in colloidal crystals.[101] Even 1D assemblies like chains of nanoparticles based on a templated approach (block copolymer, polyelectrolytes, etc.) were reported in literature.[102, 103]

For anisotropic particles, like nanorods or nanowires, a self assembly into 2D or 3D architectures offers a possibility to take advantage of their collective anisotropic properties like polarized emission[104, 105] or an anisotropic charge transport. This is especially interesting for optoelectronic applications, where the use of rod shaped semiconductors has demostrated to improve the efficiency of photovoltaic devices.[106]

1.5.1 Liquid Crystalline Structures

Liquid crystals (LC), as a kind of self assembled structures, were first found for anisotropic molecules.[107] Starting with investigations of the botanist Friedrich Reinitzer in the 19th century of the strange phase behaviour of cholesteryl benzoate, the concept was generalized; rod shaped, rigid molecules tend to align with their long axis in one direction. This creates a preferred orientation, the director. Alignment of anisotropic stuctures decreases the package volume in the case of a parallel arrangement of the rod-shaped units.[108] In the phase diagram, these mesophases are located between three dimensional ordered crystals and non-ordered, isotropic liquids. With increasing temperature, crystals melt and form a liquid, in which the single molecules (the mesogens) show an orientational order. Due to variations in the direction of the director the liquid appears cloudy. At a distinct temperature, the clearing temperature, the mesogens disorder and form an isotropic, transparent melt. (see Figure 12)

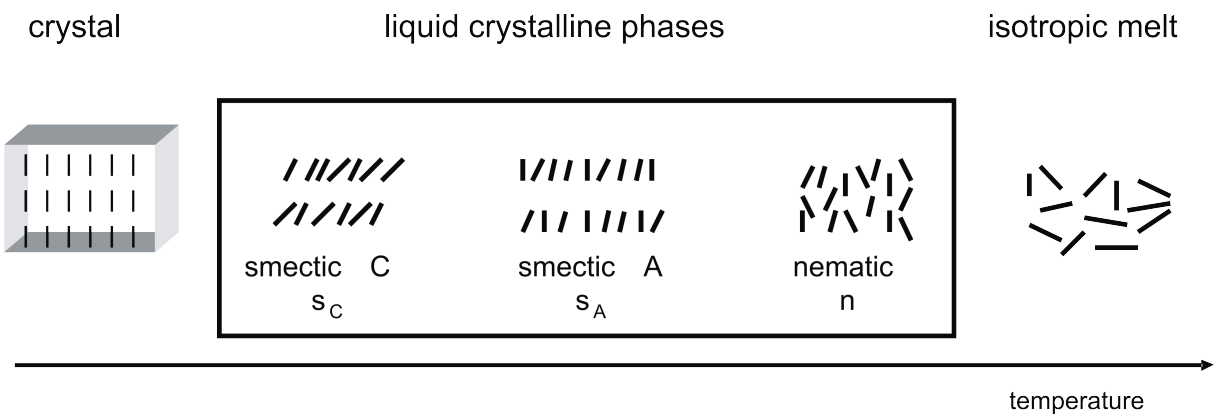

Figure 12
Liquid crystalline phases found for rod-like molecules in an intermediate temperature range between crystalline and isotropic phase.

LCs can be subdivided by different criteria. LCs which form mesophases depending on the the temperature are *thermotropic*. *Lyotropic* LCs, in contrast, exhibit different mesophases as a function of concentration.

Depending on the mesogen shape, three different kinds of phases can be distinguished. Rod-like mesogens give rise to calamitic phases. Depending on the degree of ordering, calamitic phases can be divided into nematic (n) and smectic (s) phases. In the nematic phase the mesogens have no positional order, but a long-range orientational order. Smectic phases, which are found at lower temperatures than nematic phases, exhibit an additional orientational order of the director in a layered structure. A positional order is in one direction. There are many smectic phases which are distinguished by different types and degrees of positional and orientational order. In the smectic C (s_C) phase the mesogens are slightly tilted from the layer normal, while in the smectic A (s_A) phase the mesogen orientation is normal to the layer orientation (see Figure 12).

Besides calamtic mesogens, disc and board-like structures orient in liquid crystalline phases. Liquid crystals formed by disc-like structures are known as discotic phases, board-like mesogens form sanidic phases.

Many of these phases were also observed for nanoparticles with anisotropic shapes. These systems are summarized as mineral liquid crystals.[109, 110] The aspect ratio (length/width) of

rod shaped nanoparticles has to be higher than 3.5 to obtain a stable phase.[111] While birefringence in colloidal dispersion was already observed at the beginning of the 20th century by Zocher,[112] nanoscience explains these phenomena as the self-assembly of nano-sized structures.

Minimization of the systems energy due to the parallel alignment was calculated[113] and experimentally proven. Ionic stabilized oxidic and hydroxidic minerals form birefringent LC phases after sedimentation of rod- and disc-like particles from aqueous solutions.[114-116] For surface functionalized semiconducting nanorods mineral LC phases were observed in organic solvents.[117, 118] These colloidal LC phases are dependent on the volume fraction of the anisotropic material and the temperature.[119] Next to nematic phases higher ordered smectic phases were observed.[120, 121] Smectics, which are expected for samples with a low polydispersity, can also be obtained by demixing of highly polydisperse samples.[122] Spreading nanorods on the water-air interface, followed by compression can produces 2D ordered Langmuir-Blodgett nanorod assemblies,[123] and compression on the interface induced an observable nematic-smectic phase transition,[124] which can be visualized with the analytical tools of nanoscience, like electron microscopy.

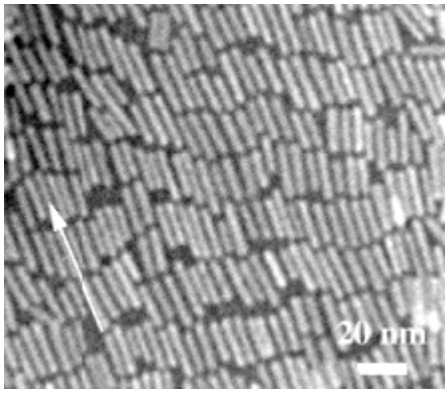

Figure 13.
Smectic arrangement of nanorod mesogens (CdSe) on the water surface on a Langmuir-Blodgett trough.[124]

Meuer et al. applied the concept of mineral LCs to polymer functionalized oxidic semiconductors, which show interesting behaviour and offer new approaches due to the polymeric matrix the mesogens are distributed in.[125]

Analogous orientation methods known for low molecular liquid crystal could be applied to induce a directed self assembly of such liquid crystalline nanoparticle dispersions. Rods can be oriented on patterned substrates, like low molecular LCs on brushed polyimide substrates. If the mesogens are dispersed in a non-volatile medium, like in a polymer-nanoparticle composites, shearing can be applied as an orientation methods.[126] External fields can be applied if the material responds to an external stimulus.

These ordered colloidal materials offer a variety of improvements and applications from oriented particles in solar cell devices to photonic applications. Oriented TiO_2 nanorods, for example, showed anisotropic photocatalytic properties.[127] For semiconducting molecules, it is well known that charge carrier mobility dramatically improves in an ordered phase,[128] a phenomenon that is also expected for oriented nanorod arrays.

1.6. Optoelectronic Devices Based on Nanoparticles

While photovoltaic (PV) devices try to turn light into electricity, light emitting devices use electricity to create light. Both types of devices benefit from the use of nano-sized structures, whether as electron transporting semiconductors with a high surface area to separate charges in dye sensitized PV cells, or as emitting materials in light emitting devices.

1.6.1 Photovoltaic Devices

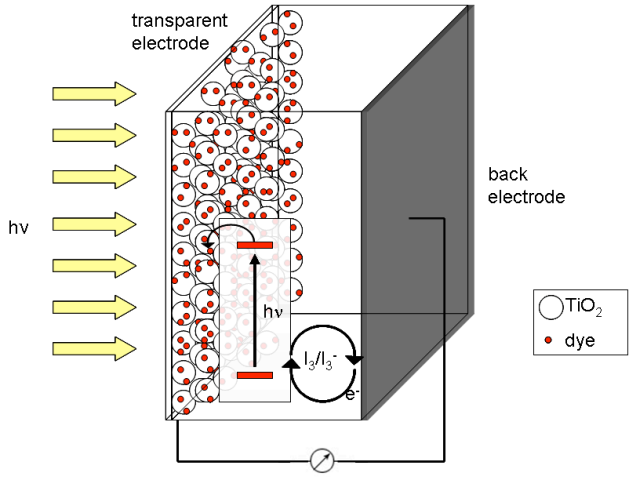

Figure 14.
Scheme of a dye sensitized solar cell (DSSC).

Especially in dye sensitized solar cells (DSSC), semiconductor nanoparticles are the preferred materials to take advantage of the high surface area. The principle of dye sensitized solar cell (DSSC) was introduced for the first time by Michael Grätzel in the early 1990s.[129] DSSCs are generally composed of a colloidal semiconductor (mainly TiO_2), a dye and an electrolyte system (historically an I_3/I_3^- redox system).

The dye absorbs light, generates excitons and injects the promoted electron into the semiconductor conduction band. The redox system reduces the dye and transports the electron to the cathode (see Figure 14).[130] With power conversion efficiencies higher than 11 % and low production costs DSSCs are in competition with silicon based solar cells.

Although the system is already commercialized,[131] many research groups try to improve dye, electrolyte system and morphology of the cells.

To improve the system the liquid electrolyte can be substituted by eutectic salt melt[132] or ionic liquids. Alternatively, hole conducting polymers can be applied as a solid state electrolyte.

Many polymers (like P3HT and PPV derivatives)[133, 134] absorb light. Hence, they work as a hole conductor and sensitizer at the same time.[135]

In case of morphology, anisotropic nanomaterials (like nanorods or –wires) direct the charge along the axis of the structure and simplify charge transport by minimized hopping from particle to particle. Hence, rods oriented or grown perpendicular to a substrate are most promising for application.[136, 137]

1.6.2. Light Emitting Devices (LED)

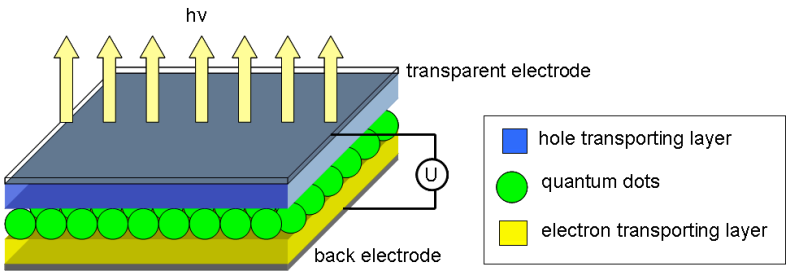

Figure 15.
Scheme of a conventional quantum dot based light emitting diode

In light emitting devices a voltage is applied between two electrodes. On one electrode electrons are injected, while holes are transported from the other electrode. In an emitting layer holes and electrons form excitons and recombine under emission of a photon (electroluminescence). In OLEDs, an organic hole and electron conductor are generally combined in a layered device structure with an emitting material located in the recombination layer. Also, electroluminescent polymers were intensively investigated in terms of good and easy processability.[138] In LEDs of the newest generation, electroluminescent semiconductor nanocrystals are integrated as chromophores. In particular, CdSe based quantum dots (but also non toxic materials like InP) [139] are already used as emitters in this 3rd generation of light emitting devices.[140] The well soluble, surfactant covered nanoparticles exchange organic electroluminescent species as the phosphorus, with a much better stability, high color purity

(full width at half maximum < 35 nm) and easy color tunability by size variation over a wide range in the visible spectrum.

Monolayers of the emitting nanocrystals show the best properties, due to the poor carrier transport property between surfactant carrying QDs.[141] A good energy match between the organic, carrier transport layer and the active QD layer is important to direct exciton recombination in the QDs and avoid a parasitic emission of the organic semiconductors. The combination of QDs with different sizes allows tuning of the emission spectrum[142] and the possibility to create white light emitting diodes.[143] Fabrication with nanocrystal emitters offers the possibility of printable and flexible devices if the particles properties are changed by surface modification.[144] External quantum efficiencies (EQE) of such devices are up to 2.5 %.

1.7 References

[1] P. M. Ajayan, L. S. Schadler, P. V. Braun, *Nanocomposite Science and Technology* , **2003**, Wiley VCH, Weinheim.

[2] L. H. Baekeland, *Sci. Am. 68 (Suppl.)* **1909**, 322.

[3] W. Kulisch in *Functional Properties of Nanostructured Materials*, (Eds: R. Kassing, P. Petkov, W. Kulisch, C. Popov), **2006**, Spinger, Dordrecht, p. 113–124.

[4] A. Okada, A. Usuki, *Materials Science and Engineering: C 3* **1995**, 109, I 15.

[5] K. A. Carrado, *Appl. Clay Sci*. **2000**, 17, 1.

[6] A. Usuki, M. Kojima, A. Okada, Y. Fukushima, O. Kamigaito, *J. Mater. Res.* **1993**, 8, 1179.

[7] H. A. Currie, S. V. Patwardhan, C. C. Perry, P. Roach, N. J. Shirtcliffe in *Hybrid Materials*, (Ed: G. Kickelbick), **2007**, Wiley, Weinheim, p. 255-301.

[8] G. Kickelbick in *Hybrid Materials*, (Ed: G. Kickelbick), **2007**, Wiley, Weinheim, p. 1 – 46.

[9] L. Qi, H. Cölfen, M. Antonietti, *Nano Lett.* **2001**, 1, 61.

[10] M. E. Mackay, A. Tuteja, P. M. Duxbury, C. J. Hawker, B. v. Horn, Z. Guan, G. Chen, R. S. Krishnan, *Science* **2006**, 311, 1740.

[11] A. C. Balazs, T. Emrick, T. P. Russell, *Science* **2006**, 314, 1107.

[12] D. Li, Q. He, Y. Yang, H. Möhwald, J. Li, *Macromolecules* **2008**, 40, 7254.

[13] D. E. Fogg, L. H. Radzilowski, B. O. Dabbousi, R. R. Schrock, E. L. Thomas, M. G. Bawendi, *Macromolecules* **1997**, 30, 8433.

[14] N. I. Hammer, T. Emrick, M. D. Barnes, *Nanoscale Res. Lett*. **2007**, 2, 282.

[15] C. Bartholome, E. Beyou, E. Bourgeat-Lami, P. Chaumont, N. Zydowicz, *Macromolecules* **2003,** 36*,* 7946.

[16] M. K. Corbierre, N. S. Cameron, R. B. Lennox, *Langmuir* **2004,** 20*,* 2867.

[17] S. Meuer, P. Oberle, P. Theato, W. Tremel, R. Zentel, *Adv. Mater.* **2007**, 19, 2073.

[18] S. Gupta, Q. Zhang, T. Emrick, A.C. Balazs, T.P. Russell, *Nat. Mater*. **2006**, 5, 229.

[19] E. Holder, N. Tessler, A. L. Rogach, *J. Mater. Chem*. **2008**, 18, 1064.

[20] J. Liu, T. Tanaka, K. Sivula, A. P. Alivisatos, J. M. J. Frechet, *J. Am. Chem. Soc.* **2004**, 126, 6550.

[21] H. Skaff, K. Sill, T. Emrick, *J. Am. Chem. Soc.* **2004**, 126, 11322.

[22] T. Hyeon, *Chem. Commun*. **2003**, 927.

[23] G. Schmid in *Nanoparticles: From Theory to Application*. (Ed. G. Schmid), **2004** Wiley-VCH, Weinheim, p. 1-3.

[24] J. Boucle, S. Chyla, M. S. P. Shaffer, J. R. Durrant, D. D. C. Bradley, J. Nelson, *Adv. Funct. Mater*. **2008**, 18, 622.

[25] B. D, Terris, T. Thomson, *J. Phys. D: Appl. Phys*. **2005**, 38, R199.

[26] N. L. Rosi, C. A. Mirkin, *Chem. Rev.* **2005**, 105, 1547.

[27] A. T. Bell, *Science* **2003**, 299, 1688.

[28] S. Abbet, U. Heiz in *The Chemistry of Nanomaterials* (Eds.: C. N. R. Rao, A. Müller, A. K. Cheetham) **2004**, Wiley-VCH, Weinheim, p. 551 – 586.

[29] G. Schmid, *Chem. Rev*. **1992**, 92, 1709.

[30] C. C. Koch, Y. S. Cho, *Nanostructured Materials*. **1992**, 1, 3, 207.

[31] Y. Sun, Y. Xia, *Science* **2002**, 298, 2176.

[32] X. Peng, L. Manna, W. Yang, J. Wickham, E. Scher, A. Kadavanich, A. P. Alivisatos, *Nature* **2000**, 404, 59.

[33] Z. R.Tian, J. A.Voigt, J. Liu, B. McKenzie,M. J. McDermott, M. A. Rodriguez, H. Konishi. H. Xu, *Nat. Mater.,* **2003**, 2, 821.

[34] S. O'Brien, L. Brus, C. B. Murray. *J. Am. Chem. Soc.* **2001**, 123, 12085.

[35] C. Burda, X. Chen, R. Narayanan, M. A. El-Sayed, *Chem. Rev*. **2005**, 105, 1025.

[36] Z. R. Dai, Z. W. Pan, Z. L. Wang, *Adv. Funct. Mater*. **2003**, 13, 9.

[37] L. Manna, E. C. Scher, A. P. Alivisatos, *J. Am. Chem. Soc.* **2000**, *122,* 12700.

[38] C. J. Murphy, T. K. Sau, A. M. Gole, C. J. Orendorff, J. Gao, L. Gou, S. E. Hunyadi, T. Li, *J. Phys. Chem. B* **2005**, *109,* 13857.

[39] W. U. Huynh, J. J. Dittmer, A.P. Alivisatos, *Science* **2002**, 295, 2425.

[40] T.-W. Zeng, Y.-Y. Lin, H.-H. Lo, C.- W. Chen, C.-H. Chen, S.-C. Liou,H.-Y. Huang, W. -F. Su, *Nanotechnology* **2006**, 17, 5387.

[41] X. Chen, S. S. Mao, *Chem. Rev.* **2007**, 107, 2891.

[42] A. Fujishima; T. N. Rao, D. A. Tryk,. *J. Photochem. Photobiol. C* **2000**, 1, 1.

[43] A. Hagfeldt,.N. Vlachopoulos, M. Grätzel,. *J. Electrochem. Soc.* **1994**, *141*, L82.

[44] Z. L. Wang, *Materials Today*, **2004**, 26.

[45] J. Y. Lao, J. G. Wen, Z. F. Ren, *Nano Lett*. **2002**, 2, 1287.

[46] M. H. Huang, S. Mao, H. Feick, H. Yan, Y. Wu, H. Kind, E. Weber, R. Russo, P. Yang, *Science* **2001**, 292, 1897.

[47] J. M. Kroon, N. J. Bakker, H. J. P. Smit, P. Liska, K. R. Thampi, P. Wang, S. M. Zakeeruddin, M. Grätzel, A. Hinsch, S. Hore, U. Würfel, R. Sastrawan, J. R. Durrant, E. Palomares, H. Pettersson, T. Gruszecki, J. Walter, K. Skupien, G. E. Tulloch, *Prog. Photovoltaics* **2007**, 15, 1.

[48] N.-G. Park, M. G. Kang, K.S. Ryu, K. M. Kim, S. H. Chang, *J. Photochem. Photobiol. A.* **2004**, 161, 105.

[49] T. Trindade, P. O'Brien, N. L. Pickett, *Chem. Mater.* **2001**, 13, 3843.

[50] W. J. Parak, L. Manna, F.C. Simmel, D.Gerion, P. Alivisatos in *Nanoparticles: From Theory to Application.* (Ed.: G. Schmid), **2004,** Wiley-VCH, Weinheim, p. 4 – 49.

[51] A. P. Alivisatos, *Science* **1996**, 271, 933.

[52] E. H Sargent, *Adv. Mater.* **2005**, 17, 515.

[53] A. L. Rogach, D. V. Talapin, H. Weller in *Colloids and Colloid Assemblies* (Ed.: F. Caruso) **2004**,Wiley-VCH, Weinheim, pp.52–95

[54] C. B. Murray, D. J. Noms, and M. G. Bawendi, *J. Am. Chem. Soc.* **1993**, 115*,* 8706.

[55] B. O. Dabbousi, J. Rodriguez-Viejo, F. V. Mikulec, J. R. Heine, H. Mattoussi, R. Ober, K. F. Jensen, M. G. Bawendi, *J. Phys. Chem. B* **1997**, 101*,* 9463.

[56] S. Kim, B. Fisher, H.-J. Eisler, M. Bawendi, *J. Am. Chem. Soc.* **2003**, 125, 11466.

[57] W. K. Bae, K. Char, H. Hur, S. Lee, *Chem. Mater.* **2008**, *20,* 531.

[58] K. W. Johnston, A. G. Pattantyus-Abraham, J. P. Clifford, S. H. Myrskog,D. D. MacNeil, L. Levina, E. H. Sargent, *Appl. Phys. Lett*. **2008**, 92, 151115

[59] A. J. Shields, *Nat. Photonics* **2007**, 1, 215.

[60] M. Bruchez Jr., M. Moronne, P. Gin, S. Weiss, A. P. Alivisatos, *Science* **1998**, 281, 2013.

[61] B. Yamada, P. B. Zetterlundin *Handbook of Radical Polymerization*, (Eds.: K. Matyjaszewsky, T. P. Davis) **2002**, Wiley and Sons, Inc., Hoboken, p. 117-187.

[62] M. Szwarc, *J. Polym. Sci.Part A: Polym. Chem*.**1998**, 36, ix – xv.

[63] D. Columbani, *Prog. Polym. Sci*. **1997**, 22, 1649.

[64] W.A. Braunecker, K. Matyjaszewski, *Prog. Polym. Sci*. **2007**, 32, 93.

[65] E. E. Malmström, C. J. Hawker, *Macromol. Chem. Phys*. **1998**, 199, 923.

[66] D.H. Solomon. *J. Polym. Sci. Part A: Polym Chem,* **2005**, 43, 5748.

[67] D. P. Curran, *Synthesis* **1988**, 489.

[68] J.-S. Wang, K. Matyjaszewski, *Macromolecules* **1995**, 28, 7901.

[69] J.-S. Wang, K. Matyjaszewski, *J. Am. Chem. Soc.* **1995**,117, 5614.

[70] K. Matyjaszewski, J. Xia, *Chem. Rev*. **2001**, 101, 2921.

[71] J. Chiefari, Y. K. Chong, F. Ercole, J. Krstina, J. Jeffery, T. P. T. Le, R. T. A. Mayadunne, G. F. Meijs,C. L. Moad, G. Moad, E. Rizzardo, S H. Thang, *Macromolecules* **1998**, *31,* 5559.

[72] G. Moad, E. Rizzardo, S H. Thang, *Aust. J. Chem*. **2005**, 58, 379.

[73] Y. K. Chong, T. P. T. Le, G. Moad, E. Rizzardo, S. H. Thang, *Macromolecules* **1999**, 32, 2071.

[74] C. Barner – Kowollik, T. P. Davis, J. P. A. Heuts, M. H. Stenzel, P.Vana, M. Whittaker, *J. Polym. Sci. Part A: Polym. Chem*. **2003**, 41, 365.

[75] G. Moad, E. Rizzardo, S. H. Thang, *Polymer* **2008**, 49, 1079.

[76] S. Perrier, P. Takolpuckdee, *J. Polym. Sci. Part A: Polym.Chem,* **2005**, 43, 5347.

[77] R. T. A. Mayadunne, E. Rizzardo, J. Chiefari, Y. K. Chong, G. Moad, S. H. Thang, *Macromolecules* **1999**, 32*,* 6977.

[78] R. T. A. Mayadunne, E. Rizzardo, J. Chiefari, J. Krstina, G. Moad, A. Postma, S. H. Thang, *Macromolecules* **2000**, 33, 243.

[79] J. F. Quinn, E. Rizzardo, T. P. Davis, *Chem. Commun.*, **2001**, 1044.

[80] M. Mertoglu, S. Garnier, A. Laschewsky, K. Skrabania, J. Storsberg, *Polymer* **2005**, 46, 7726.

[81] C. J. Brabec, N. S. Sariciftci, J. C. Hummelen, *Adv. Funct. Mater.* **2001**, 11, 15.

[82] Y.- J. Cheng, S.- H. Yang, C.- S. Hsu, *Chem. Rev*. **2009**, 109, 5868.

[83] G. B. Blanchet, Y.-L. Loo, J. A. Rogers, F. Gao, C. R. Fincher, *Appl. Phys. Lett*. **2003**, 82, 463.

[84] A. J. Heeger, *Angew. Chem. Int. Ed*. **2001**, 40, 2591.

[85] B. de Boer, A. Facchetti, *Polym. Rev.* **2008**, 48, 423.

[86] http://www.konarka.com/ (14. January.2010).

[87] U. Scherf. E. J. W List, *Adv. Mater*. **2002**, 14, 477.

[88] J. H. Burroughes, D. D. C. Bradley, A. R. Brown, R. N. Marks, K. Mackay, R. H. Friend, P. L. Burn, A. B. Holmes, *Nature* **1990**, 347, 539.

[89] L.- L Chua, P. K. H. Ho, H. Sirringhaus, R. H. Friend, *Adv. Mater*. **2004**, 16, 1609.

[90] W. Pisula, M. Zorn, J. Y. Chang, K. Müllen, R. Zentel, *Macromol. Rapid Commun*. **2009**, 30, 1179.

[91] B. S. Ong, Y. Wu, P. Liu, S Gardner, *J. Am. Chem. Soc*. **2004**, 126, 3378.

[92] J. Pacansky, R. J. Waltman, H. Seki, *Bull. Chem. Soc. Jpn*. **1997**, 70, 55.

[93] X.-C. Li, Y. Liu, M. S. Liu, A. K.-Y. Jen, *Chem. Mater*. **1999**, 11, 1568.

[94] E. Bellmann, S. E. Shaheen, S. Thayumanavan, S. Barlow, R. H. Grubbs, S. R. Marder, B. Kippelen, N. Peyghambarian, *Chem. Mater*. **1998,** 10*,* 1668.

[95] M. Sommer, S. M. Lindner, M. Thelakkat, *Adv. Funct. Mater*. **2007**, 17, 1493.

[96] Y. Shang, Y. Wen,, S. Li, S. Du, Xi. He, L Cai, Y.Li, L. Yang, H. Gao, Y. Song, *J. Am. Chem. Soc*. **2007**, 29, 11674.

[97] J.-L. Bredas, D. Beljonne, V. Coropceanu, J. Cornil, *Chem. Rev*. **2004**, 104, 4971.

[98] V. I. Arkhipova, P. Heremans, E. V. Emelianova, G. J. Adriaenssens, H. Bässler, *Appl. Phys. Lett*. **2003**, 82, 3245.

[99] M. Reyes-Reyes, K. Kim, D. L. Carroll, *Appl. Phys. Lett*. **2005**, 87, 083506.

[100] C. B. Murray and C. R. Kagan, M Bawendi, *Annu. Rev. Mater. Sci.* **2000**. 30, 545.

[101] D. V. Talapin, E.V. Shevchenko, A. Kornowski, N. Gaponik, M. Haase, A. L. Rogach, H. Weller, *Adv. Mater.* **2001**, 13, 1868.

[102] Z. Tang, N. A. Kotov, *Adv. Mater.* **2005**, 17, 951.

[103] S. Srivastava, N. A. Kotov, *Soft Matt*. **2009**, 5, 1146.

[104] A. Rizzo, C. Nobile, M. Mazzeo, M. De Giorgi, A. Fiore, L. Carbone, R. Cingolani, L. Manna, G- Gigli, *ACS Nano* **2009**, 3, 1506.

[105] R.A.M. Hikmet, P. T. K. Chin, D. V. Talapin, H. Weller, *Adv. Mater* **2005**, 17, 1436.

[106] K. Yu, J. Chen, *Nanoscale Res. Lett*. **2009**, 4, 1.

[107] *Handbook of Liquid Crystals* (Eds.: D. Demus, J. Goodby, G.W. Gray, H.-W. Spiess, V. Vill) **1998**,Wiley-VCH, Weinheim.

[108] P. J. Flory, G. Ronka, *Mol. Cryst. Liq. Cryst.* **1979**, 54, 289.

[109] J. C. P. Gabriel, P. Davidson, *Adv. Mater*. **2000,** 12, 9.

[110] P. Davidson, J. C. P. Gabriel, *Curr. Opin. Colloid Interface Sci.* **2005**, 9, 377.

[111] P. Bolhuis, D. Frenkel, *J. Chem. Phys*. **1997**, 106, 8.

[112] H. Zocher, *Z. Anorg. Allg. Chem.* **1925**, 147, 91

[113] A. T. Titov, P. Kral, *Nano Lett.* **2008**, 8, 3605.

[114] J.-C. P. Gabriel, P. Davidson, *Top. Curr. Chem.* **2003**, 226, 119.

[115] M. P. B. van Bruggen, F. M. van der Kooij, H. N. W. Lekkerkerker, *J. Phys.: Condens. Matter* **1996**, 8, 9451.

[116] M.C. D. Mourad, E. J. Devid, M. M. van Schooneveld, C. Vonk, H. N. W. Lekkerkerker, *J. Phys. Chem. B* **2008**, 112, 10142.

[117] L. Li, J. Walda, L. Manna, A. P. Alivisatos, *Nano Lett*. **2002**, 2, 557.

[118] L.-S. Li, A.P. Alivisatos, *Adv. Mater*. **2003**, 15, 408.

[119] L.-S. Li, M. Marjanska, G. H. J. Park, A. Pines, A. P. Alivisatos, *J. Chem. Phys.* **2004**, 120, 1149.

[120] D. Frenkel, H. N. W, Lekkerkerker, A. Sroobants, *Nature* **1988**, 332, 822.

[121] C. Querner, M. D. Fischbein, P. A. Heiney, M. Drndic, *Adv. Mater.* **2008**, 20, 2308.

[122] G. J.Vroege, D. M. E. Thies-Weesie, A. V. Pethukhov, B. J. Lemaire, P. Davidson, *Adv. Mater.* **2006**, 18, 2565.

[123] L. Mai, Y. Gu, C. Han, B. Hu, W. Chen, Z. Liu, W. Guo, Y. Dai, *Nano Lett*. **2009**, 9, 826.

[124] F. Kim, S. Kwan, J. Akana, P. Yang, *J. Am. Chem. Soc.* **2001,** *123,* 4360.

[125] S. Meuer, P. Oberle, P. Theato, W. Tremel, R. Zentel. *Adv. Mater*. **2007,** 19, 2073.

[126] G. Schmidt, M. M. Malwitz, *Curr. Opin. Colloid Interface Sci.***2003,** 8, 103.

[127] A. Dessombz, D. Chiche, P. Davidson, P. Panine, C. Chaneac, J.-P. Jolivet, *J. Am. Chem. Soc.* **2007**, 129, 5904.

[128] W. Pisula, M. Zorn, J. Y. Chang, K. Müllen, R. Zentel, *Macromol. Rapid Commun*., **2009**, 30, 1179.

[129] B. O´Regan, M. Grätzel, *Nature* **1991**, 353, 737.

[130] M Grätzel, *J. Photochem. Photobiol. C* **2003**, 4, 145.

[131] http://www.g24i.com (29. January 2010).

[132] Y. Bai, Y. Cao, J. Zhang, M. Wang, R. Li, P. Wang, S. M. Zakeeriddin, M. Grätzel, *Nat. Mater.* **2008**, 7, 626.

[133] C. Y. Kwong, W. C. H. Choy, A. B. Djurisic, P. C. Chui, K. W. Cheng, W. K. Chan, *Nanotechnology* **2004**, 15, 1156.

[134] T.-W. Zeng, Y.-Y. Lin, H.-H. Lo, C.-W. Chen, C.-H. Chen, S.-C. Liou, H.-Y. Huang, W.-F. Su, *Nanotechnology* **2006**, 17, 5387.

[135] Y.-G. Kim, J. Walker, L. A. Samuelson, J. Kumar, *Nano Lett.* **2003**, 3 523.

[136] C. Y. Kuo, W. C. Tang, C. Gau, T. F. Guo, D. Z. Jeng, *Appl. Phys. Lett.* **2008**, 93, 033307.

[137] A. I. Hochbaum, P. Yang, *Chem. Rev.* **2010,** 110*,* 527.

[138] J. H. Burroughes, D. D. C. Bradley, A. R. Brown, R. N. Marks, K. Mackay, R. H. Friend, P. L. Burns, A. B. Holmes, *Nature* **1990**, 347, 539.

[139] R. Xie, D. Battaglia, X. Peng, *J. Am. Chem. Soc.* **2007**, 129, 15432.

[140] V.L. Colvin, M. C. Schlamp, A. P. Alivisatos, *Nature* **1994**, 370, 354.

[141] S. Coe, W.-K. Woo, M. Bawendi, V. Bulovic, *Nature* **2002**, 420, 800.

[142] P. O. Anikeeva, J. E. Halpert, M. G. Bawendi, V. Bulovic, *Nano Lett*. **2007**, 7, 2196.

[143] M. Goo, B. Richter, S. Kirstein, *Adv. Mater*, **1997**, 9, 802.

[144] V. Wood, M. J. Panzer, J. Chen, M. S. Bradley, J. E. Halpert, M. G. Bawendi, V. Bulovic, *Adv. Mater*. **2009**, 21, 2151.

2. Scope and Aim of the Work

As shown in the introduction, nanoscience and nanotechnology offer solutions to create more efficient optoelectronic devices, in the case of solar cells as well as light emitting devices. To create such highly efficient materials there are many factors that have to be controlled in which solubility and suppression of agglomeration of the nanoparticles is one of the main issues.

The aim of this project is to create functional block copolymers by living radical polymerization that anchor to the particle surface, containing a functional, solubility mediating block and an anchor block. Due to the universality of controlled radical polymerization various combinations of monomers can be polymerized to create tailored macromolecules for modification. Standard polymers like polystyrene or polymethyl methacrylate shall be used to solubilize the inorganic particles in organic media, but also functional polymers showing semiconducting or a stimuli responsive behaviour can be applied for surface modification. In contrast to dispersion of charged particles in an aqueous solution, the organically modified particles offer the possibility to apply particle dispersions from organic solvents. This prevents the inserting of ions into the system, which might interfere in subsequent applications.

Hence, modification with non polar polymers based on styrene was one goal. The universality of the concept was another point to be addressed. In particular, the modification of the most frequently used oxidic semi conductors that can be functionalized by dopamine anchor moieties followed by the modification of various inorganic materials by changing the anchor units was an aim of the project. The multidentate anchor block binds very efficiently to the particle surface and is able to replace surfactant molecules (also due to entropic considerations).

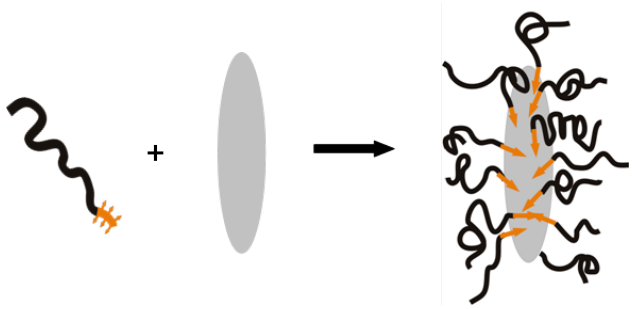

Scheme of the polymer functionalization of nanoparticles.

The soluble polymer coated structures should be well dispersable in matrices of the same chemical composition. With increased solubility and mobility, the coated particles should show self assembly phenomena if anisotropic particles were used. An orientation of nanoobjects makes all properties of anisotropic particles available on a macroscopic scale, comparable to liquid crystalline structures.

To use these advantages in optoelectronic applications, polystyrene as an isolating matrix should be changed to a hole conducting matrix to create a p-n junction in the system. Such a matrix can transport (or inject) positive charges into the covered particle. The possibility to align semi conducting nanorods in this functional matrix would be desirable.

Behaving like liquid crystalline phases, similar orientation principles known for low molecular - or polymeric liquid crystals can be applied. By orientation in an electric field a perpendicular arrangement of the mesogens (in this case the polymer modified nanorods) to an electrode can be induced. This morphology is promising to increase the performance of nanorod based solar cells, because the charge carriers can be directed to the electrode on a direct way, with reduction in hopping processes from particle to particle. This concept shall be proven in the work by applying an electric field and investigate the behaviour of the liquid crystalline structure.

Further on, the flexibility of the post polymerization approach shall be used to integrate different functionalities into the anchor block. It also offers a localization of

functional molecules at the interface between the particle and the polymer corona. For example, dyes can be fixed at the donor-acceptor interface to optimize charge separation in dye induced charge transfer applications, like dye sensitized solar cells. The dye can absorb light and inject the electron into the particle while the positive charge carrier can be transported by the polymeric hole conducting shell. Hence, such dye functionalized particles should be charged upon illumination, analogous to a dye solar cell concept.

As a second kind of nanoparticles with application in optoelectronics, highly luminescent quantum dots shall be stabilized by a polymer shell. The processing of the covered QD should behave in parts like a polymer. The use of functional polymers, like hole transporting polymers, can combine the functionalities of different layers in a device in one hybrid structure. In the case of optoelectronic application these hole conducting polymers can transport charge carriers sufficiently to the particle core, where the excitons can recombine. These materials shall be applied in light emitting devices based on QD emitting layers. Synthesis of chemically and electrically stable polymers for surface modification may even improve the devices in terms of stability at high current densities.

3. Results and Discussion

3.1.

Liquid Crystalline Phases of Polymer Functionalized Semiconducting Nanoparticles

Matthias Zorn, Stefan Meuer, Muhammad Nawaz Tahir, Yuriy Khalavka, Carsten Sönnichsen, Wolfgang Tremel, Rudolf Zentel

J. Mater. Chem., **2008**, 18, 3050 – 3058.

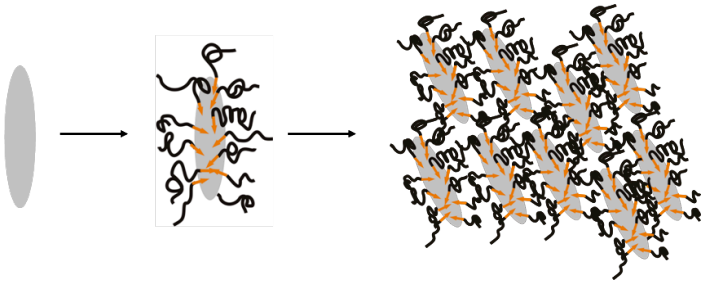

Polymer modification is a good method to solubilise nanoparticles and make them mobile in organic solvents and polymer matrices. We synthesized acrylate (Stefan Meuer) and styrene based polymers (Matthias Zorn) for this purpose. The polymers were synthesized by RAFT polymerization. As a second block we used pentafluorophenylacrylate, which can be converted by primary amines into anchor groups for different materials.

The block copolymers were synthesized with low polydispersities (< 1.2) and could be functionalized with dopamine and cysteamine to bind efficiently to oxidic or chalcogenidic semiconductors.

Next to the already published work about polymer functionalization of TiO_2 with PMMA and PDEGMEMA by Stefan Meuer the concept was extended to polystyrene, which has advantages looking towards orientation methods based on applied electric fields. The non-polar styrene polymers contain much less ionic pollution than PMMA or PDEGMEMA polymers. Sonication of the polymer with different nanoparticles allows the surface modification. Most prominent oxidic semi conductors like TiO_2, SnO_2, ZnO and CdTe (provided by Muhammad Nawaz Tahir and Yuriy Khalavka) were modified with polystyrene

(by Matthias Zorn). For CdTe it was necessary to introduce a thiol containing anchor group. We used cysteamine for this purpose. The polymer content was characterized by thermo gravimetry for all semiconductor polymer conjugates and surface modification was evaluated quantitatively. An ideal ratio between soluble and anchor block was found by systematic investigation of different block copolymers (by Stefan Meuer) and this ideal ratio (100 units soluble block and 10 units of the anchoring moiety) was taken as a standard for the styrene block copolymer synthesis.

The styrene functionalized nanoparticles are well dispersible in styrene oligomers. Due to solubility and mobility of the systems in an oligostyrene matrix, the system self assembled in liquid crystalline structures. These mineral liquid crystals show a reversible clearing at characteristic temperatures for the different modified materials.

Introduction

The use of nano-objects in the real macroscopic world requires – besides their preparation – also their macroscopic organization and orientation. The organization of nanometre sized objects can be realised in colloidal crystals[1] and lyotropic liquid crystals (LC)[2]. Generally the formation of lyotropic liquid crystals[3-5] from rigid-rod objects as result of form-anisotropy is well understood[6,7] and such phases offer the potential to orient anisotropic nanoparticles. In this respect the orientation of functional semiconducting nanoparticles is interesting for materials science and especially for photovoltaics.[8-11] E.g. oriented semiconducting materials might improve the device performance in solar cells by alignment of electron-carrying nano-rods perpendicular to the electrode.[12] Following this concept it was shown by Alivisatos and co-workers that the efficiency of nanoparticle solar cells could be enhanced, if rod-shaped particles are chosen.[13] Research in this direction is, so far, limited by the solubility of functional nano-particles, which is needed to obtain the LC-phase at high concentration.

Historically lyotropic LC-phases in water have been observed for various rigid-rod objects like V_2O_5 ribbons,[14,15] tabacco mosaic viruses[16] and TiO_2 nanorods[17]. Aqueous solutions offer the opportunity to stabilize nano-objects electrostatically by surface charges. But as a major drawback, the charges used to stabilize the system disable any electronic use. Therefore ion free mineral liquid crystals from uncharged anisotropic nanoparticles in organic solvents are needed.

This requires the "solubilisation" of the nano-objects in organic solvents. For this purpose the particles have to be surface functionalised with a soluble corona to overcome the strong adhesion forces among them.[18, 19] The concept of "hairy rods", which was originally developed for stiff main chain liquid crystalline polymers, is very promising for such inorganic nano-objects too.[3] In that concept, a stiff insoluble core is solubilized by linking long chains (the hairs) on its surface. Alkyl chains are often used[20, 21] to stabilize nanoparticles of sphere- or rod-like shape and they are also used for delaminated clay fragments.[22] In some

cases they allow the preparation of highly concentrated solutions, which give rise to a liquid crystalline ordering, if anisotropic nanoparticles are used.

Polymeric surfactants[19, 22, 23] offer here advantages for the solubilization of inorganic nano-objects: polymers themselves are objects of nanometre dimensions. Therefore polymer coated surface are stabilized sterically up to distance of nanometres and not just for angstroms as with alkyl chains. Then polymer chains have a lot of free volume inside, which can be filled by solvent. This large interaction volume between solvent and functionalized surface leads to good solubility in solvents for the polymer. In addition, new polymers designed for surface functionalization have multiple anchor units for surface attachment. Hence, adsorption-desorption equilibria reactions are avoided, and a robust fixation of the multi-dentate polymer ligand to the surface can be achieved. Using this concept we could recently observe smectic and nematic phases in highly concentrated solutions of TiO_2 nanorods,[19] which were coated with block copolymers. This concept could also be applied successfully to carbon nanotubes.[24] In addition we were able to solubilize TiO_2 nano-rods in a functional organic matrix and thus to orient semiconducting inorganic nano-rods in an organic hole conducting matrix by self-assembly.[25]

In order to see, if the concept to (i) solubilize anisotropic inorganic nano-particles with block copolymers and (ii) to observe LC-phases in highly concentrated solutions can be generalized, we extended our work to various semiconducting nano-particles, which require different anchor blocks and thus more polymer synthesis (see Figure 1). Concerning the inorganic part we concentrated on nanorods from semiconductors like TiO_2, ZnO, SnO_2 and CdTe, which are discussed mostly for optoelectronic applications. Concerning the block copolymer synthesis we used RAFT polymerization and a reactive ester intermediate.[26] We focus here mostly on the surface functionalization with newly synthesized block copolymers and describe first results concerning the observation of LC-phases in various solvents

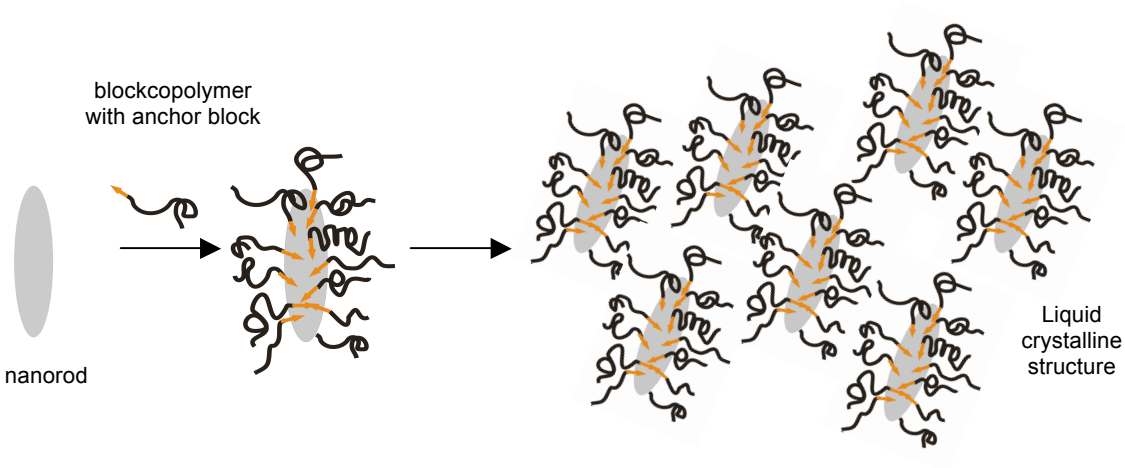

Figure 1.
Scheme for functionalization and liquid crystalline ordering.

Results and Discussion

Semiconducting nanorods:

The oxidic semiconducting nanorods were all prepared by hydrothermal methods.[27, 28, 29] This synthetic route can produce the particles in a high quantity and without stabilizing surfactants on the nanorod surface. The products of these syntheses are of moderate polydispersity for TiO_2 and SnO_2. The size distribution of ZnO nanorods is broader. CdTe was synthesized with TOPO as stabilizing ligand. Table 1 presents the physical date like average size in length and width as well as their surface which is the background for the calculations of surface coverages, which is described later in this work. Size distributions can be found in figure 2. In all cases the preparation methods allow to synthesize rods with high aspect ratios (length/width), that posses the potential to act as mesogens, if a good mobility and solubility can be achieved by a polymeric corona as a shell around the particle (see Figure 2 and Table1).

Table 1.
Physical properties of nanorods used in this study.

material	density [g/cm^3]	l [nm]	d [nm]	l/d	surface [nm^2]	nanorods / mg	surface/ [nm^2/mg]
TiO_2	4.26	30	6	5.2	600	$3.03\text{x}10^{14}$	$1.82\text{x}10^{17}$
ZnO	5.61	120	19	6.4	7800	$5.20\text{x}10^{12}$	$4.05\text{x}10^{16}$
SnO_2	6.95	20	4	5.0	280	$5.72\text{x}10^{14}$	$1.58\text{x}10^{17}$
CdTe	6.20	23	4	5.8	310	$5.58\text{x}10^{14}$	$1.75\text{x}10^{17}$

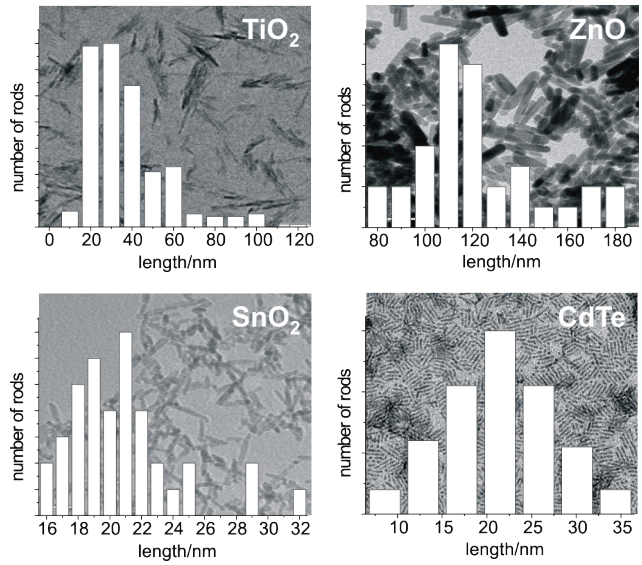

Figure 2.
Electron microscopy images of nanorods used in this study. The width of the images is 370 nm for TiO_2, 200 nm for SnO_2, 450 nm for ZnO and 870 nm for CdTe. The length distributions of the nanorods are inlayed.

Functional block copolymers.

To synthesize the polymers which are needed to solubilise the inorganic particles in organic solvents reversible addition fragmentation transfer (RAFT) polymerization was chosen.[30] The block copolymers for the surface modification of the inorganic nanorods presented above were synthesized according to the scheme presented in Figure 3. In the first step of the synthesis the block that acts as solubilizer is polymerized. It is made of methyl methacrylate, (diethylene glycol monomethyl ether) methacrylate or styrene. After purification of the first block it can be used as a macroinitiator leading to a diblock copolymer. As a second block, we chose a reactive ester monomer (pentafluorophenylacrylate), which allows varying the anchor group by a simple polymer analogous reaction with any primary amine that can be used as an anchor group for the nanorod material.[26]

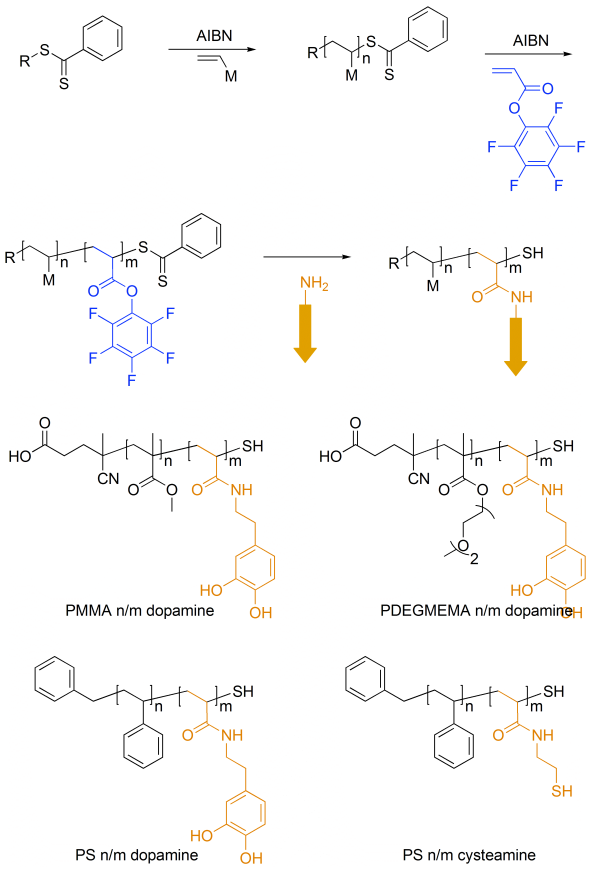

Figure 3.
Synthesis of reactive block copolymers and polymer analogous reaction to anchor unit functionalized polymers.

The block lengths of the soluble block were determined by GPC (determined by light scattering with known dn/dc ratios) and are therefore well accessible. The polydispersity index (PDI) of almost all polymers made is between 1.14 and 1.21. These are very good values for diblock copolymers after a polymer-analogous reaction. The polymers made from (diethylene glycol momomethyl ether) methacrylate have larger PDIs. This phenomenon might be due to diethylene glycol dimethacrylate (acts as a cross linker) impurities from the monomer synthesis.

As an anchor group to functionalize the oxidic nanorods dopamine was chosen, which is known to bind preferentially to the reactive edges of the oxidic nanocrystal.[31] The conversion of the reactive block can be monitored by ^{19}F-NMR, IR and UV spectroscopy. The polymers

can be dissolved in THF which is a solvent for both blocks. The synthesized block copolymers are collected in Table 2.

Table 2.
Block lengths, molecular weights and polydispersities of anchor unit functionalised diblock copolymers used in this study.

polymer m/n anchor	soluble units	anchor units	M_n [g/mol]	M_w [g/mol]	PDI
PMMA 100/20 dopamine	100	20	14,700	17,600	1.20
PMMA 100/40 dopamine	100	40	18,900	22,900	1.21
PMMA 100/60 dopamine	100	60	23,000	27,400	1.19
PMMA 110/20 dopamine	110	20	15,200	17,800	1.17
PMMA 110/40 dopamine	110	40	19,400	23,300	1.20
PMMA 110/60 dopamine	110	60	23,500	28,000	1.19
PMMA 140/20 dopamine	140	20	17,800	20,300	1.14
PMMA 140/40 dopamine	140	40	22,000	25,500	1.16
PMMA 140/60 dopamine	140	60	26,100	30,300	1.16
PMMA 70/30 dopamine	70	30	12,800	15,000	1.17
PDEGMEMA 40/30 dopamine	40	30	14,500	17,500	1.21
PDEGMEMA 190/30 dopamine	190	60	47,400	72,500	1.53
PS 90/10 dopamine	90	10	11,600	13,300	1.15
PS 90/10 cysteamine	90	10	11,100	13,000	1.17

For functionalization of CdTe thiol groups were introduced by polymer analogous reaction of the reactive block copolymer with cysteamine. The reaction with cysteamine results in a total conversion as examined also by IR spectroscopy and shown in ^{19}F-NMR spectra (disappearance of the three signals of the pentafluorophenylacrylate).

Functionalized nanorods / Hybrid systems:

Combining the semiconducting nanorods with anchor functionalized polymers leads to interesting inorganic organic hybrid systems (see Figure 1). In general, the functionalization process is done in dilute solution (both polymer and nanorods) to prevent interparticle cross linking. Bidentate ligands containing enediol moeity such as dopamine serves as robust anchor group to many metal oxides.[32] It has been proved spectroscopically by Rajh et al. and

his study suggested that such ligands convert the under-coordinated surface sites back to a bulk-like lattice structure which results in a really robust binding.[33] The binding of dopamine anchor units on TiO_2 nanorods is optically traceable. The functionalization kinetics can be monitored by UV-Vis spectroscopy as dopamine has a strong absorption band around 285 nm. We investigated the decrease of the polymer concentration in solution in presence of excess nanorods. Figure 4A shows the absorption spectra of a dopamine functionalized polymer in a quartz cuvette with TiO_2 nanorods lying at the bottom. UV-Vis spectra were taken and show a weakening of the absorption band over time. This is due to adsorption of the polymer on the TiO_2 nanorods at the bottom of the cell. After two days, the spectrum was run again and the signal of the dopamine units were found again in comparable strength to the beginning of the experiment but blue shifted to 269 nm. This effect can be explained by solubilised TiO_2 nanorods that started to diffuse freely in the cuvette. The dopamine units bind to the nanorod surface and form a charge transfer complex with unsaturated surface titanium ions. The electron density of dopamine is reduced in this complex (the HOMO is lowered), which corresponds to a blue shift in its absorption spectra (the HOMO – LUMO distance increased). The effect was observed without the use of ultrasound or stirring of the sample, which proves the high mobility of these hairy rods.

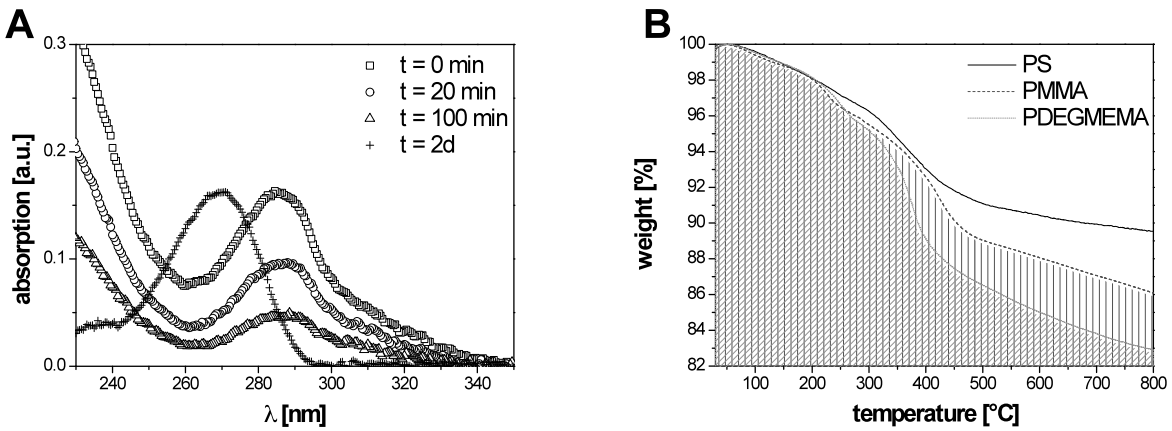

Figure 4.
A: Adsorption kinetic of PMMA 70/30 dopamine on TiO_2 nanorods monitored by UV-Vis spectroscopy; B: TGA analysis of PS, PMMA and PDEGMEMA coated TiO_2 nanorods.

To investigate the functionalization process in detail, various diblock copolymers with PMMA, PS and poly(diethyleneglycolmonomethylether)methylmethacrylate as soluble block and dopamine functionalised reactive ester blocks as anchor blocks were used. The block length of both blocks was varied (see Table 2). The functionalization was carried out in THF solutions with a weight ratio of TiO_2 nanorods to polymers of 2 : 1. The solutions were stirred over night and cleaned from unbound polymer by repeated centrifugation of the functionalized nanorods and removal of the supernatant solution.

The amount of bound polymer was measured using thermo gravimetry (see Figure 5B). The samples were heated up to 800 °C under a nitrogen atmosphere and the weight loss was measured as a function of temperature. As TiO_2 withstands these temperatures, the weight loss is only due to the decomposition of the polymer (usually by depolymerization). With known molecular weight (Table 2) and nanorod surface (Table 1) it is possible to calculate roughly the number of polymer chains per nanorod.

The TiO_2 nanorods used were in average 30 nm long and 6 nm wide, so that the nanorods have a surface of about 600 nm^2 and a volume of 800 nm^3 in average. Taking the density of crystalline rutile into account, $3x10^{14}$ nanorods are present per milligram powder (see Table 1). Thus the calculated surface of the nanorods is 1.8 x 10^{17} nm^2/mg or 1800 m^2/g. Tables 3 and 4 summarize the calculated amounts of chains per nanorod for each block copolymer. A plot of repeat units of the soluble block and anchor block vs. adsorbed chains per nanorod is shown in Figure 5. The number of adsorbed chains per nanorod increases as the number of repeat units in the soluble block as well as in the anchor block decreases. Thus a maximum of adsorbed chains is found for block copolymers with about 10 to 30 repeat units in the anchor and 40 to 100 in the soluble block (see xz and yz trajectories in Figure 5). As expected the number of adsorbed chains increases as the anchor block gets shorter. There should be – of course – a minimum length that is needed for a stable connection. But this length is shorter than the shortest anchor blocks examined. On the other side, the length of the soluble block is

also limiting the grafting density. When the coil diameter of the soluble block is larger than the area accessible to the anchor block, the coils will hinder each other. Thus the grafting density gets down, when the soluble block is too large.

Table 3.
Adsorption characteristics of diblock copolymers PS, PMMA and PDEGMEMA X/Y dopamine on TiO_2 nanorods.

soluble units **X**	anchor units **Y**	chains / nanorod	nm^2 / chain	s [nm]	R_g [nm]	σ*
70[a]	30	25	24.3	4.9	3.6	1.7
100[a]	20	21	28.6	5.3	3.8	1.6
	40	16	38.0	6.2	4.3	1.6
	60	9	65.8	8.1	4.8	1.1
110[a]	20	14	42.7	6.5	3.9	1.1
	40	17	35.3	5.9	4.4	1.7
	60	13	48.0	6.9	4.9	1.5
140[a]	20	15	40.2	6.3	4.2	1.4
	40	13	44.6	6.7	4.7	1.5
	60	10	58.4	7.6	5.1	1.4
40[b]	30	22	27.0	5.2	2.9	1.0
190[b]	60	3	254.4	15.9	5.9	0.4
90[c]	10	28	21.4	4.6	3.4	1.7

a: methyl methacrylate, b: diethylene glycol monomethyl ether) methacrylate, c: styrene

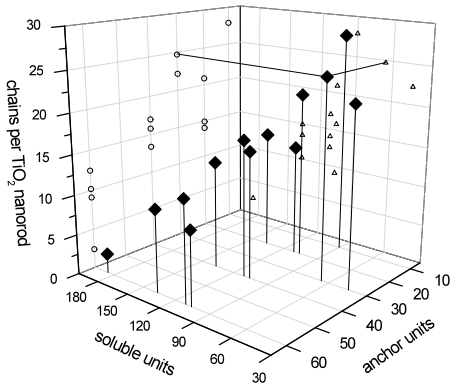

Figure 5.
Adsorbed chains per TiO_2 nanorod of PS, PMMA and PDEGMEMA X/Y dopamine diblock copolymers.

Table 4.
Adsorption characteristics of diblock copolymers PS 90/10 dopamine/cysteamine on various nanorods.

nanorod	chains / nanorod	nm^2 / chain	s [nm]	R_g [nm]	σ*
TiO_2[a]	30	21	4.6	3.4	1.7
ZnO[a]	1800	4	2.0	3.4	9.1
SnO_2[a]	20	14	3.8	3.4	2.5
CdTe[b]	200	15	3.9	3.4	2.4

a: functionalized by **PS 90/10 dopamine**, b: functionalized by **PS 90/10 cysteamine**

Formula 1:

$$A_{chain} = A_{nanorod} / N_{adsorbed\ chains}$$

Formula 2:

$$s = \sqrt{A_{chain}}$$

Formula 3:

$$\sigma^* = \pi R_g^2 / s^2 = \pi R_g^2 / A_{chain}$$

Related to these number is the area that is covered per polymer chain and the inter polymer distance.[34] The area that is covered per polymer chain is calculated by dividing the nanorod surface by the number of chains per nanorods (see Formula 1). The interpolymer distance s is defined as the square root of this area (see Formula 2). Another useful ratio is known as reduced coverage σ* and is calculated by Formula 3 (R_g values were calculated from known R_g to M_w relations of PMMA and PS; the values for Poly(diethylene glycol monomethyl ether) methacrylate were estimated from polyhexyl methacrylate).[35] This value resembles the degree of coverage: A value of two marks the onset of large steric interactions, which lead to deformed polymer coils on the surface (brush regime).[36] Values smaller than one correspond to distances between two polymers on the surface that are larger than the cross section of that coil in solution. This regime of σ* values < 1 is also called mushroom regime (all calculated values can be found in Table 3). Almost all σ* values are between 1 and 2. Thus the polymer functionalized surface consists of close packed polymer mushrooms that fill the surface completely. In one case, a σ* value of 0.4 was found. In this case the surface morphology should consist of isolated mushrooms. The soluble block of that polymer had 190 and the anchor block 60 repeat units. Both values are not optimal when compared to the trends from the other diblock copolymers, so that such a low coverage is not astonishing. Considering these calculations one should consider that there might be various sources of errors, e.g. from

asymmetry in polydispersity and therefore the absolute values might not be correct. However comparison with literature data presented below gives comparable values. In addition, all compared systems were treated identically. So the trends in these values are correct.

The interpolymer distances vary from 5 to 8 nm for the polymers from Table 3. Literature known interpolymer distances from 3 to 25 nm with σ* values from 2.6 to 10.3 can be found in different systems, where – as in our case – diblock copolymers with short anchor blocks were used.[34, 37] These literature values were measured on a planar and chemically homogeneous surface like silicon or aluminium oxide while our experiments were carried out on nanorod surfaces.

The same block copolymer can behave differently on various nanoparticles. A block copolymer of styrene with dopamine anchor units was used to functionalize TiO_2, ZnO and SnO_2 nanorods (see Table 4). The reduced coverages σ* from functionalized TiO_2 and SnO_2 are similar with a slight increase from TiO_2 (σ* = 1.7, s = 4.6 nm) to SnO_2 (σ* = 2.5, s = 3.8 nm). However the reduced coverage for ZnO particles is significantly larger (σ* = 9.1, s = 2.0 nm). This effect might be due to different crystal structure. TiO_2 and SnO_2 crystallise in a rutile structure whereas ZnO crystallized as wurtzite. All cations form stable octahedral complexes, but in the case of zinc also tetrahedral complexes are possible. Thus, dopamine might bind more efficient to the zinc atoms, which are more flexible with regard to coordination geometry. Another reason might be different degrees of physiosorption of the soluble block.

To investigate the functionalization of non-oxidic compounds, we investigated the functionalization of thiol functionalized polystyrene on CdTe nanorods. The reduced coverage observed was 2.4 and the interchain distance 3.9 nm, which is quite similar to the values for SnO_2 (Table 4). As the precursor diblock copolymer was the same for both cases the same number of reactive ester moieties was available for the reaction with the anchor units. Thus both diblock copolymers (carrying thiol anchor units for CdTe and dopamine anchor units for

the oxidic nanorods) are identically in block lengths of soluble and anchor block. The fact that a similar surface coverage is found indicates that both anchor units are interacting similar with the surfaces.

The solubility of functionalized nanorods was investigated using various experiments. Starting from the optical properties, functionalized particles dispersed in suitable solvents for the diblock copolymers form stable, non-sedimenting dispersions upon ultrasonification. In comparison with the TiO_2 nanorods, dispersions of ZnO ($\rho = 5.6$ g/cm^3) and SnO_2 ($\rho = 7.0$ g/cm^3) tend to sediment faster due to the higher densities. As the pristine nanorod powders can – however – not be broken up completely, highly opaque dispersion are obtained, where the strong scattering comes solely from undispersed material. This can be shown by polarized microscopy and scanning electron microscope images (see Figure 6). The pristine material consists of larger aggregates that can be seen in the microscope as scattering particles of around 5 µm (see Figure 6A and C). Upon polymer functionalization the aggregates are broken up and dispersed particles together with larger aggregates are found. After filtration (0.2 µm PTFE syringe filter) the larger aggregates are removed and solely dispersed particles are remaining (see Figure 6B). These dispersions are now clear and oriented domains can be found after evaporation of the solvent (see Figure 6D). These dispersions have been investigated by dynamic and static light scattering[19, 41] in various solvents and in all cases single nanorods are found. The similarity of the results obtained with different block copolymers, different anchor groups and different inorganic nanorods demonstrates that our concept for surface functionalization of nano-objects is generally applicable.

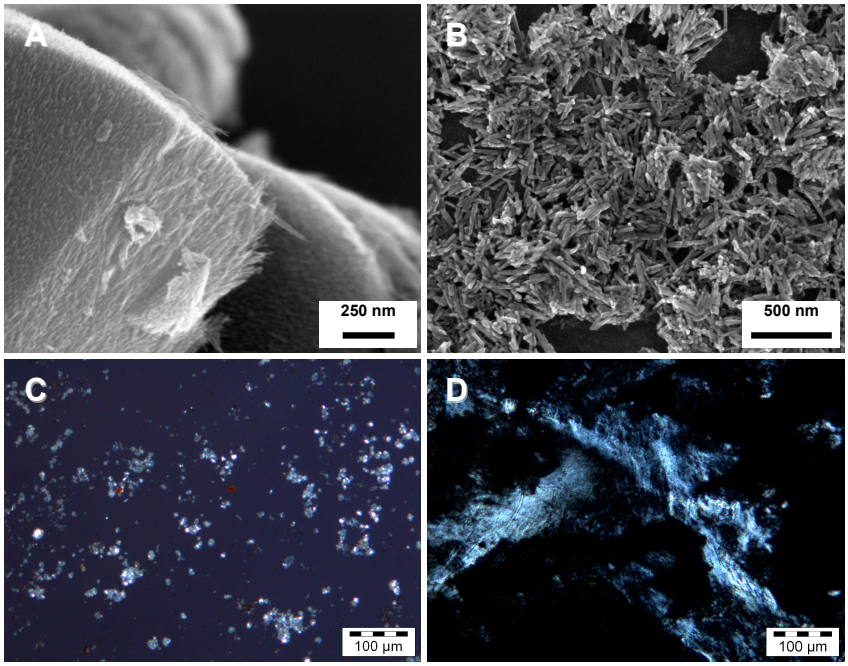

Figure 6.
ZnO nanorods: A: SEM image of pristine nanorods; B: SEM image of PS 90/10 dopamine functionalised nanorods; C: polarized microscopy image of pristine nanorods; D: polarized microscopy image of PS 90/10 dopamine functionalised nanorods (evaporated from 20 µl solution of 1.7 mg functionalized nanorods in 1 mL THF sheared between glass slides).

Liquid crystalline phases.

As described before, polymer functionalization and solubilisation of semiconducting nanorods was successful. When the concentration of these hairy-rods is increased (by evaporation of the solvent), birefringent domains are formed as presented in ref. 19 for functionalized TiO_2 nanorods and in Figure 6 for ZnO.

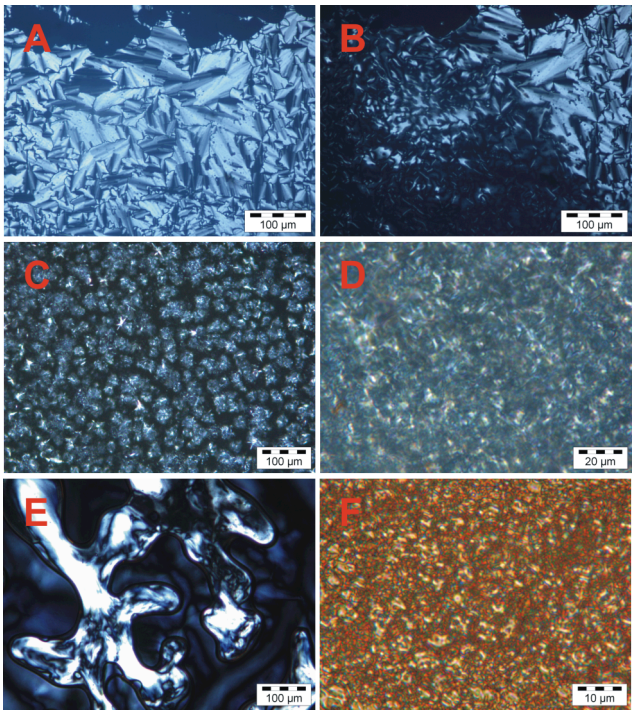

Figure 7.
Polarized microscopy images of A, B: PMMA 70/30 dopamine functionalized TiO_2 nanorods (50 wt%). Smectic-nematic phase transition around 55 °C (A: 45 °C, B: 55°C); C: PDEGMEMA 40/30 dopamine functionalized TiO_2 nanorods (50 wt%) in excess PDEGMEMA 40/30 dopamine matrix at room temperature. T_c ~90 °C; D: PS 90/10 dopamine functionalized SnO_2 nanorods (70 wt %) in oligo-PS matrix at room temperature, T_c ~ 60 and 68 °C; E: PS 90/10 dopamine functionalized ZnO nanorods (70 wt%) in oligo-PS matrix at room temperature. T_c ~ 200 and 230 °C, F: PS 90/10 cysteamine functionalized CdTe nanorods (70 wt%) in oligo-PS matrix at room temperature. T_c ~ 60 and 69 °C.

Generally this behaviour is observed for all nanorods in common solvents like THF, $CHCl_3$, dichlorobenzene and DMF when a glass slide is drop coated with filtered solution. Above certain concentrations of the particles in a solvent appropriate for PMMA, poly(diethylene glycol monomethyl ether) methacrylate and polystyrene birefringent domains can be observed. The exact volume fractions could not be determined because of the volatility of the solvents and the small amounts of particles and solvent needed on a glass slide to observe LC-phases. The textures that can be observed after evaporation of the solvent (THF) are similar. Compared with TiO_2 the birefringent domains are smaller in the case of SnO_2, whereas the domains are slightly bigger in the case of ZnO nanorods. After evaporation of the solvent the birefringent domains cannot be sheared and a clearing temperature cannot be determined due to a lack of mobility of the functionalized rods without a liquid matrix.

In order to investigate the temperature dependence of the LC behaviour for these different polymer functionalised nanorods an appropriate high boiling solvent has to be found. Oligomeric PEG (M_n = 400 g/mol) is a suitable solvent for PMMA, as both can be mixed in any composition[38] and does not evaporate even at elevated temperatures. Upon mixing PMMA functionalised TiO_2 nanorods with PEG 400, liquid crystalline phases are found in a volume fraction regime between 0.2 and 0.7 (for the hairy-rods). A typical texture can be found in figure 8A and 8B. They show textures common for a smectic (below 55 °C) and a nematic (between 55 and 65 °C) phase. Another way to reduce the volume fraction of the TiO_2 nanorods is to use more functionalization polymer than needed to form a polymer matrix around the hairy-rods. This was done with the low T_g polymer (diethylene glycol monomethyl ether) methacrylate (glass transition temperature below 0 °C) which shows a waxy, honey like consistency at room temperature and is therefore mobile enough. Liquid crystalline phases are found in these mixtures (see Figure 7C) with a pure polymeric matrix. The clearing temperature is around 90 °C and the system "freezes" around the T_g of the polymer matrix. This principle should also be useful for other polymer matrices, as heating above the T_g should allow the self organization of embedded nanorods by a liquid crystalline phase.

In the case of the polystyrene functionalized particles it was possible to disperse them in low molecular weight polystyrene (M_n = 580 g/mol). We prepared mixtures of about 70 wt% functionalized particles and 30 wt% of the polystyrene oligomers. Although the viscosity of the mixtures was too high at room temperature, a fluent system could be found when heating to about 35 °C. With this oligomeric solvent clearing temperatures of the liquid crystalline phases can be found. For TiO_2 the clearing of the solution could be observed between 86 and 92°C and for SnO_2 birefringence disappeared between 60 and 68°C (see Figure 7D). For ZnO a different texture was found: if a little pressure is put on the sample between two glass slides large and bright birefringent areas are observable (see Figure 7E and 7F). The clearing point of this phase, which is between 200 and 230 °C, is much higher than for the other phases.

This may be due to the much larger dimensions of the ZnO rods, which results in less mobility. For CdTe also liquid crystalline textures could be found in polarisation microscopy (see Figure 7E). In comparison with the structures of the oxidic nanorods the textures showed a red birefringence, due to the absorbance of CdTe nanorods. They showed a similar texture to those of the styrene modified SnO_2 nanorods, which also have a comparable size. The clearing temperature was found between 60 and 69°C in polarised optical microscopy.

Conclusion

In this work, we focussed on the polymer functionalization of semi conducting nanorods in order to orient them. The chosen inorganic materials TiO_2, SnO_2, ZnO and CdTe were functionalised with PMMA, PDEGMEMA and PS block copolymers synthesized by RAFT polymerization. The synthesis of the polymers was carried out using a macroinitiator approach followed by the polymerization of a reactive ester monomer. Polymer analogous reaction with an anchor unit gave anchor group functionalized diblock copolymers of low polydispersity. The functionalized inorganic nanorods were soluble in organic solvents and formed stable dispersions. Their degree of surface coverage was investigated by TGA measurements and shows a clear dependency of the polymer architecture. A maximal coverage was found for short anchor blocks (around 20 repeat units) and soluble blocks of 40 to 100 repeat units. As expected the number of adsorbed chains decreases as the anchor block gets longer. On the other side, the length of the soluble block is also limiting the grafting as the coils hinder each other. It was possible to cover oxidic as well as chalcogenic inorganic materials sufficiently with a polymer corona by using appropriate anchor units in the diblock copolymers showing the generality of this functionalization concept.

Liquid crystalline phases of functionalized nanorods were found and investigated in organic media. In organic solvents, liquid crystals were found in concentrated solutions and showed clear lyotropic behaviour. After evaporation of the solvents, the oriented particles are

immobilised. To avoid such problems, high boiling solvents as oligomeric PEG or PS were used as organic matrix. They allow it to investigate temperature dependant phase transitions. In all cases we found liquid crystalline textures and clearing temperatures in a broad range between 60 and 230 °C. The clearing temperature depends on the particle size as well as the used matrix. The LC phases could only be found above the glass transition temperatures of the matrix as the system is otherwise frozen in a glassy state. We also investigated polymeric matrices with low glass transition temperatures and found the same behaviour as for oligomeric matrices.

We were able to demonstrate the generality of the functionalization principle by grafting different oxidic and chalcogenic nanorods with different types of polymers. Afterwards, various organic matrices were used to form liquid crystalline composites. We were able to self organize the nanorods as liquid crystals by their property to behave as mesogenes which is due to their anisotropy. Future work will be done to investigate the orientation of semi conducting materials in order to improve optoelectronic device efficiencies.

Experimental

Methyl methacrylate and styrene (from Acros) and (diethylene glycol monomethyl ether) methacrylate ((2-methoxy-ethoxy)-ethylmethacrylate from Aldrich) were distilled before usage, benzyl dithiobenzoate (RAFT reagent),[39] pentafluorophenoleacrylate[26] were synthesized as described in literature. αα'-azoisobutyronitrile (AIBN from Fluka) was recrystallized from diethyl ether, dopamine hydrochloride (3-hydroxy tyramine hydrochloride, from Acros) was used as purchased, dioxane and tetrahydrofurane (THF) were dried and distilled before usage, all other solvents were also distilled before use.

Gel permeation chromatography (GPC) was carried out in THF as solvent and the detector system contained refractive index (Jasco), UV-VIS (Jasco) and light scattering (Wyatt) detectors.

Thermo gravimetry was carried out in a Perkin Elmer Pyris 6 TGA under nitrogen atmosphere. NMR spectra were obtained in a Bruker AC 300. Infrared spectroscopy was done in a Bruker Vector 22, UV-Vis spectroscopy was measured in a Shimadzu UV 2102 PC UV-Vis Scanning Spectrophotometer.

The syntheses of **PMMA 70/30 dopamine** and **PDEGMEMA 40/30 dopamine** are already described in literature and all other variations of the block length were synthesized accordingly.[19]

Synthesis of TiO_2 nanorods: The synthesis of TiO_2 nanorods was carried out using the method reported in ref. 19.

Synthesis of SnO_2 nanorods: SnO_2 nanorods were synthesized by the modified method as reported by Cheng et al.[28] In a typical procedure, $SnCl_4$ x 5 H_2O (0.001 moL) was dissolved in methanol (10 ml). To this 20 ml of tetramethyl ammonium hydroxide (25% w/w in methanol) were added. The solution with dissolved precursor was transferred to a Teflon-lined stainless steel autoclave and heated at 150 °C for 24 h. A white-gray precipitate was collected, purified, and dried in air at ambient temperature.

Synthesis of ZnO nanorods:[29] For the synthesis of ZnO nanorods, $Zn(Ac)_2$ x $2H_2O$ (1.09 g) was dissolved in 10 mL of methanol. 20 mL of the tetra methyl ammonium hydroxide (25% w/w in methanol) was added with stirring at room temperature. The solution was transferred to a Teflon-lined stainless steel autoclave and heated at 50 °C for 24 h followed by a period at elevated temperature 150 °C for another 24 h. The white precipitate was collected and purified by washing with water and dried in air at room temperature.

Synthesis of CdTe nanorods: The CdTe nanocrystals are synthesized in a coordinating solvent by sequential chalcogenide precursor injection similar to the procedure reported by Shien et al.[40] The cadmium precursor is prepared by degassing a mixture of 0.114 g CdO (0.89 mmol), 0.43 g n-tetradecylphosphonic acid (TDPA) (0.155 mmol) and 7 g of trioctylphosphine oxide (TOPO) at 65 °C for three hours. The mixture is heated slowly to

320 °C under argon and then cooled to the 300 °C. Tellurium precursor is prepared by dissolving 0.2 g of Te powder in 4 mL of trioctylphosphine (TOP) and stirring for 72 hours at room temperature. Rods are synthesized by injecting the Te precursor in 0.25 mL volumes four times, every 2 minutes, into the hot reaction mixture. To remove the reaction mixture, the nanords are precipitated with isopropanol, washed by centrifugation and resuspension in toluene (twice). Finally, the particles were dissolved in 20 mL of chloroform.

Polystyrene-b-dopaminacrylamide (**PS 90/10 dopamine**): To synthesize the macroinitiator 6.4 mL (56 mmol, 140 eq.) styrene, 97 mg (0.4 mmol, 1 eq) of the chaintransfer agent benzyl dithiobenzoate and 6.5 mg (0.04 mmol, 0.1 eq) AIBN (azoisobutyronitrile) were added all together with 3 mL tetrahydrofuran in a Schlenk tube. Oxygen was exchanged by nitrogen in three freeze-pump-thaw cycles and polymerization was carried out at 65 °C for 12h. The macroinitiator was purified by precipitation in methanol for three times to give 3.8 g (67 %) of the desired polymer. To synthesize the reactive block copolymer, 2 g (0.16 mmol, 1 eq) of the macroinitiator was dissolved with AIBN (2.6 mg, 0.016 mmol, 0.1 eq), pentafluorophenylacrylate (760 mg, 3.2 mmol, 20 eq) and THF in a Schlenck tube and oxygen was exchanged by nitrogen in three freeze-pump-thaw cycles. The mixture was polymerised for 48 h at 65 °C and the polymer was purified by precipitating in methanol for three times to yield 1.74 g (63 %) of the reactive block copolymer. For the polymer analogous reaction 700 mg (0.06 mmol, 1 eq.) reactive diblock copolymer, dopamine hydrochloride (171 mg, 0.9 mmol, 15 eq) and triethylamine (90 mg, 0.9 mmol, 15 eq) were dissolved in 2 mL THF and stirred under nitrogen at room temperature for 5 h. Afterwards the solution was filtered and precipitated in methanol for three times to yield 520 mg (74 %) of the desired product **PS 90/10 dopamine**. M_n (GPC) = 11590 g/mol, PDI (GPC) = 1.15. ^{1}H-NMR (300MHz, $CDCl_3$/MeOD 4:1): δ[ppm]: 7.06 (m, 3H, Ph-H), 6.57 (m, 2H, Ph-H), 6.14 (m, 3H, $ArH_{dopamine}$), 3.52 (m, 2H, CONH-C*H*$_2$-CH_2-Ph), 3.39 (m, 2H, CONH-C*H*$_2$-CH_2-Ph), 2.97 (m, 1H, CH_2-C*H*-), 2.38 (m, 1H, CH-C*H*$_2$), 1.87 (m, 1H, CH-C*H*$_2$), 1.84 (m, 1H), 1.39

(m, 2H). ^{19}F-NMR (400 MHz, $CDCl_3$): no signals found. IR: ν_{max}/cm^{-1}: 3374 ($OH_{dopamine}$), 3027 (CH), 2923 (CH), 1650 (CONH).

Poly(styrene-b-cysteamidacrylate) (**PS 90/10 cysteamine**): To synthesize the blockcopolymer with thiol anchorgroups the reactive diblockcopolymer (700 mg, 0.06 mol, 1 eq.) and cysteamin (69.4 mg, 0.9 mmol, 15 eq.) were dissolved in 2 mL THF and stirred under nitrogen at room temperature for 5 h. Afterwards the solution was precipitated in methanol for three times to yield of the desired product **PS 90/10 cysteamine** (580 mg, 81 %). M_n (GPC) = 10570 g/mol, PDI (GPC) = 1.19. ^{1}H-NMR (300MHz, $CDCl_3$/MeOD 4:1): δ[ppm]: 6.88 (m, 3H, Ph-H), 6.43 (m, 2H, Ph-H), 3.58 (m, 2H, NH-C*H*$_2$-CH$_2$-SH), 3.08 (m, 2H, NH-C*H*$_2$-CH$_2$-SH), 3.02 (m, 1H, CH$_2$-C*H*-), 2.44 (m, 1H, CH-C*H*$_2$), 1.91 (m, 1H, CH-C*H*$_2$), 1.67 (m, 1H, CH-C*H*$_2$), 1.27 (m, 1H, CH-C*H*$_2$). ^{19}F-NMR (400 MHz, $CDCl_3$): no signals found. IR: ν_{max}/cm^{-1}: 2561 (SH), 1667 (CONH), 697 (CS).

Preparation of polymer/nanorods hybrids: (for TiO_2, SnO_2 and ZnO) 10 mg of nanorod powder were dispersed in THF by sonifiaction. After 10 min 5 mg of the functionalization polymer was added and the mixture was sonificated for further 20 min, and stirred over night under N_2 atmosphere. To get rid of the excess of functionalization polymer the solution was centrifuged (4000 rpm) and the supernatant solution was exchanged against distilled THF for three times.

CdTe nanorods were functionalized by dissolving 2 mg of PS 90/10 dopamine in 1 mL solution of CdTe in chloroform (2 mg/ml). The reaction mixture was stirred for 1 d at 40 °C. The functionalized rods were purified by centrifugation (4700 rpm / 4°C) and exchanging the supernatant solution by distilled THF for three times.

Before investigations of the liquid crystalline behaviour the solution were freshly filtered (0.45 μm PTFE syringe filter).

Acknowledgement

We would like to thank the "Fonds der chemischen Industrie" for having founded parts of this work (stipend for S. Meuer) as well as the "International Research Training Group: Self organized Materials for Optoelectronic Applications" (stipend for M. Zorn). SEM pictures were kindly taken by S. Weber (Max Planck Institute for Polymer Research, Mainz).

References

1 P. G. Bolhuis, D. A. Kofke, *Phys. Rev. E*, 1996, **54**, 634.

P. Bartlett, P. B. Warren, *Phys. Rev. Lett.*, 1999, **82**, 1979.

2 M. Stegemeyer, Guest Ed. in *Liquid crystals*, Steinkopf, Darmstadt/Germany/Springer, New York/USA, 1994; D. Demus, J. Goodby, G. W. Gray, H.-W. Spiess, V. Vill in *Handbook of Liquid Crystals*, Wiley-VCH, Weinheim, Germany, 1998.

3 M. Ballauff, *Angew. Chem*., 1989, **101**, 261.

4 C. Noël, P. Navard, *Progr. Polym. Sci.*, 1991, **16**, 55.

5 P. Davidson, J. C. P. Gabriel, *Curr. Opin. Colloid Interface Sci.*, 2005, **9**, 377.

6 P. J. Flory, *Proc. R. Soc. London Ser. A*, 1956, **254**, 73; P. J. Flory, G. Ronca, *Mol. Cryst. Liq. Cryst.*, 1979, **54**, 289.

7 G. Petekidis, D. Vlassopoulos, G. Fytas, N. Kountourakis, *Macromolecules*, 1997, **30**, 919.

8 M. Grätzel, *Inorg. Chem*., 2005, **44**, 6841.

9 P. Suri, R. M. Mehra, *Sol. Energy Mater. Sol. Cells,* 2007, **91**, 518.

10 W. J. E. Beek, M. M. Wienk, R. A: J. Janssen, *Adv. Mater*., 2004, **16**, 1009.

11 J. Sites, J. Pan, *Thin Solid Films*, 2007, **515**, 6099.

12 P. K. Sudeep, T. Emrick, *Polym. Rev.*, 2007, **47**, 155.

13 W. U. Huynh, J. J. Dittmer, A. P. Alivisatos, *Science*, 2002, **295**, 2425.

14 H. Zocher, *Z. Anorg. Allg. Chem.*, 1925, **147**, 91.

[15] C. A. Brunello, C. F. O. Graeff, *J. Non-Cryst. Solids,* 2002, **304**, 265.

[16] F. C. Bawden, N. W. Pirie, J. D: Bernal, I. Fanhucken, *Nature*, 1936, **138**, 1051.

[17] A. Dessombz, D. Chiche, P. Davidson, P. Panine, C. Chanéac, J.- P. Jolivet, *J. Am. Chem. Soc*. 2007, **129**, 5904; L. J. Michot, I. Bihannic, S. Maddi, C. Baravian, P. Levitz, P. Davidson, *Langmuir*, 2008, **24**, 3127.

[18] M. N. Tahir, N. Zink, M. Eberhardt, H. A. Therese, U. Kolb, P. Theato, W. Tremel, *Angew. Chem.*, 2005, **45**, 4809; M. N. Tahir, M. Eberhardt, P. Theato, S. Faiß, A. Janshoff, T. Gorelik, U. Kolb, W. Tremel, *Angew. Chem. Int. Ed.*, 2006, **45**, 908.

[19] S. Meuer, P. Oberle, P. Theato, W. Tremel, R. Zentel, *Adv. Mater.*, 2007, **19**, 2073.

[20] L. Li, J. Walda, L. Manna, A. P. Alivisatos, *Nano Lett.*, 2002, **2**, 557; B. J. Lemaire, P. Davidson, J. Ferre, J. Jamet, D. Petermann, P. Panine, I. Dozov, D. Stoenescu, J. Jolivet, *Faraday Discuss.*, 2005, **128**, 271

[21] N. R Jana, *Chem. Comm*., 2003, **15**, 1950.

[22] Z. X. Zhang, J. S. van Duijneveldt, *J. Chem. Phys.*, 2006, **124**, 154910; E. S. H. Leach, A. Hopkinson, K. Franklin, J. S. van Duijneveldt, *Langmuir*, 2005, **21**, 3821.

[23] D. van der Beek, H. Reich, P. van der Schoot, M. Dijkstra, T. Schilling, R. Vink, M. Schmidt, R. van Roij, H. N. W. Lekkerkerker, *Phys. Rev. Lett.*, 2006, **97**, 087801; M. P. B. van Bruggen, F. M. van der Kooij, H. N. W. Lekkerkerker, *J. Phys.: Condens. Matter*, 1996, **8**, 9451.

[24] a) S. Meuer, L. Braun, R. Zentel, *Chem. Comm.*, 2008, in press; b) R. Daussin, S. Cuenot, A.-S. Duwez, C. Pagnoulle, C. Detrembleur, C. Bailly, R. Jérôme, *Chem. Mater*., 2004, **16**, 4005; c) G. J. Bahun, C. Wang, A. Adronov, *J. Polym. Sci., Part A: Polym. Chem.*, 2006, **44**, 1941.

[25] M. Zorn, R. Zentel, *Macromol. Rapid Comm.*, 2008, **29**, 922.

[26] a) M. Eberhardt, P. Theato, *Macromol. Rapid Commun.,*. 2005, **26**, 1488; b) M. Eberhardt, R. Mruk, R. Zentel, P. Theato, *Eur. Polym. J.*, 2005, **41**, 1569.

[27] X.-L. Li, Q. Peng, J.-X. Yi, X. Wang, Y. Li, *Chem. Eur. J.*, 2006, **12**, 2383.

[28] B. Cheng, J. M. Russell, W, Shi, L. Zhang, E. T. Samulski, *J. Am. Chem. Soc.*, 2004, **126**, 5972.

[29] B. Cheng, W. Shi, J.M. Russell-Tanner, L. Zhang, E. T. Samulski*, Inorg. Chem*., 2006, **45**, 1208.

[30] C. Barner-Kowollik, T. P. Davis, J. P. A. Heuts, M. H. Stenzel, P. Vana, M. Whittaker, *J. Polym. Sci. Part A: Polym. Chem.*, 2003, **41**, 365.

[31] P. Z Araujo, P. J. Morando, M. A. Blesa, *Langmuir*, 2005, **21**, 3470.

[32] C. Xu, K. Xu, H. Gu, R.heng, H. Liu, X. Zhang, Z. Guo, B. Xu, *J. Am. Chem. Soc.*, 2004, **126**, 9938.

[33] T. Rajh, L. X. Chen, K. Lukas, T. Liu, M. C. Thurnauer, D. M. Tiede, *J. Phys. Chem. B*, 2002, **106**, 10543; L. de la Garza, Z. V. Saponjic, N. M. Dimitrijevic, M. C. Thurnauer, T. Rajh, *J. Phys. Chem. B*, 2006, **110**, 680.

[34] A. G. Koutsioubas, N. Spiliopoulos, D. Anastassopoulos, A. A. Vradis, G. D. Priftis, *J. Polym. Sci., Part B: Polym. Phys.*, 2007, **45**, 2060.

[35] *Polymer Handbook*, ed. J. Brandrup, E. H. Immergut, E. A. Grulke, A. Abe, D. R. Bloch, 4th edn., 2005, ch. VII / E, pp. 232ff.

[36] R. Baranowski, M. P. Whitmore, *J. Chem. Phys.*, 1995, **103**, 2343.

[37] A. C. Costa, M. Geoghegan, P. Vlček, R. J. Composto, *Macromolecules*, 2003, **36**, 9897.

[38] H. Ito, T. P. Russell, G. D. Wignall, *Macromolecules*, 1987, **20**, 2213.

[39] Y. K. Chong, J. Krstina, T. P. T. Le, G. Moad, A. Postma, E. Rizzardo, S. H. Thang, *Marcomolecules*, 2003, **36**, 2256.

[40] F. Shien, A. E. Saunders, B.A.Korgel, *J. Phys. Chem. B*, 2005, **109**, 8538.

[41] S. Meuer, Ph.D. Thesis University of Mainz, 2008.

3.2.

Liquid Crystalline Orientation of Semiconducting Nanorods in a Semiconducting Matrix

Matthias Zorn, Rudolf Zentel

Macromol. Rapid Commun., **2008**, 29, 922 - 927.

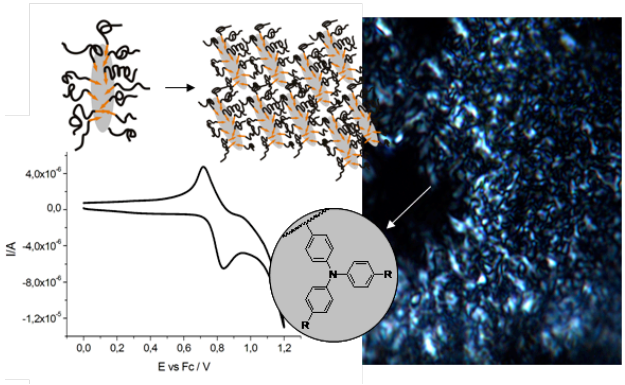

The concept of nanorods oriented by their self assembly behaviour is a highly interesting topic concerning the improvement of solar cells based on nanorod semiconductors. The transport of electrons is faster, if the electrons can travel along the long nanorod axis. For this application it is important to orient the electron conducting nanorods in a hole conducting matrix to form a p-n junction.

Hence, a hole conducting triphenylamine monomer was controlled polymerized by RAFT polymerization. The hole conducting block was characterized by cyclovoltammetry to show the transport properties of the material by reversible redox cycles. As a second block we used pentafluorophenylacrylate, offering the possibility to flexibly integrate anchoring moieties. Block copolymers containing triphenylamine (with and without methyl groups at the phenyl rings) and the reactive ester were converted with dopamine to anchor them to the different semiconducting materials (TiO_2, SnO_2, ZnO).

The surface coverage was analyzed quantitatively by thermo gravimetry experiments.

The TPA functionalized particles were well dispersable in a TPA monomer and oligomer matrix. Glass temperature of these oligomers is between 15 and 30 °C (DSC) and they show a low viscosity at temperature higher than 40°C. Hence, the particles can be oriented analogous to the PS particles in the semi conducting matrix. They show similar liquid crystalline behaviour like in a PS matrix, and clear above a certain temperature, which offers an interesting concept for the orientation of semiconducting particles in a semiconducting matrix.

Introduction

Polymer nanoparticle composite materials are very attractive in order to combine the unique properties of inorganic nanomaterials with the benefits of the easy processing and tailored features of polymeric materials.[1] The inorganic nanoparticle materials, that can be embedded, may contribute their conductive, semiconductive, magnetic or mechanical properties to yield new properties of the hybrid material.[2] Especially in the field of optoelectronic applications many researchers are focussed on nanoscale inorganic semiconductors to improve device characteristics and enhance e.g. the efficiency of photovoltatics[3, 4] It was also shown that the use of rod-like structures is improving the device characteristic of solar cells.[5] On the polymer-side semiconducting and stimuli-responsive properties can be integrated into the composite material. As semiconducting polymers beside poly thiophenes and poly (*para*-phenylene vinylenes) the group of polytriphenylamines is promising for the use in solar cell applications.[6] Hydrid solar cell concepts often combine nanocrystalline TiO_2, which acts as an electron conductor, and polymeric hole conductors, which offer a lot of advantages compared to liquid electrolytes, that were reported first by Grätzel et al. in the 1990´s.[7]

Beside the preparation of polymer-nanoparticle hybrids the orientation of nanoparticles by self-assembly is a hot topic in the field of nanotechnology. It can be achieved by forming liquid crystalline phases using the anisotropy of nanoobjects themselves. For this purpose it is necessary to combine their anisotropy with solubility and mobility in a solvent. The phenomenon that anisotropic mineral particles tend to form liquid crystalline structures was first reported in 1925 by Zocher, who found that anisotropic V_2O_5 particles show a parallel ordering of the colloids during sedimentation.[8] Binding organic molecules to the nanorod surface enhances the solubility in organic media.[9] Following this concept we could recently show that also diblock copolymers containing a soluble block and an anchor block are good surfactants to produce stable nanoparticle dispersions in various solvents and oligomers.[10] Thus anisotropic inorganic nanorods, like TiO_2, SnO_2, ZnO and CdTe can be used as

mesogens to obtain liquid crystalline ordering.[11] As soluble polymers –so far- classical polymers like PMMA or PS have been used.

As a new concept we present now the self-assembly of functional inorganic nano-objects within a functional organic matrix; i.e the self-organization of semiconducting inorganic nanorods within an organic semiconducting matrix composed of oligo-triphenylamines. Such a parallel alignment of inorganic electron conducting semiconductors might improve charge transport due to a better percolation and increase thus the transport of electrons to the electrode.[1] In addition the formation of a self-assembled nanostructure within a hole conducting organic matrix might facilitate charge separation and be therefore useful for photovoltaics. Here we present: (1) the preparation of block copolymers by RAFT polymerization of triphenylamine monomers and a reactive ester monomer and the subsequent incorporation of the anchor block, (2) the functionalization of the inorganic nanorods and (3) their self-organization into liquid crystalline phases

Results and Discussion

As a semiconducting polymer we chose poly (triphenylamines); as monomers vinyltriphenylamine (TPA) and the *para* methylated vinyltriphenylamine (TPA-Me) were used. The methylation of the *para*-position avoids dimerization of the triphenylamines due to electrochemical oxidation.[12] The monomers were synthesized according to literature in a copper catalyzed Ullmann coupling of the accordant diphenylamine and bromobenzene followed by a Vilsmeyer reaction and a Wittig reaction to produce a polymerizable vinyl group.[13]

The polymer for nanorod functionalization was polymerized by RAFT polymerization, which offers the opportunity to synthesize block copolymers with a low polydispersity index by a living radical mechanism (see Figure 1). We choose the RAFT macroinitiator approach by first polymerizing the hole conducting monomer, because the method allows it to synthesize

blockcopolymers with an reactive ester as a second block.[14] For this purpose we used a chain transfer agent, which is known to polymerize styrene analogous monomers efficiently.[15] Thus the semiconducting block (macroinitiator) could be obtained (Figure 1a) in yields between 55 and 69 % (Table 1). Due to the incomplete conversion it was, however, not possible to determine the molecular weight by the initiator to monomer ratio. After purification of the macroinitiator pentafluorophenylacrylate (PFPA) was used as monomer for the second block (Figure 1b, Table 1). The reactive ester groups of this monomer are known to react with any primary amine.[16] At least the polymer to functionalize the nanoparticles is obtained by reaction of the reactive blockcopolymer with dopamine as an anchor group (Figure 1c) for the oxidic semiconducting nanomaterials.

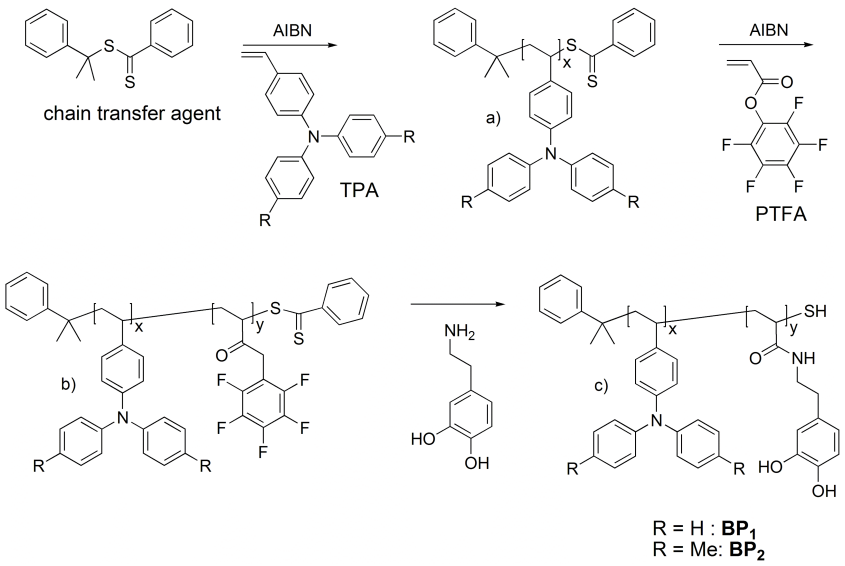

Figure 1.
Reaction scheme for diblock copolymer synthesis and polymeranalogous reaction; a) macroinitiator (also used as oligo 1 and 2); b) reactive blockcopolymer, c)block copolymer containing dopamine anchor groups for particle functionalization (BP1 and BP2).

The conversion of the reactive block was investigated by IR spectroscopy. The absorption of the ester bond (1786 cm^{-1}) belonging to the pentaflourophenolacrylate disappears after stirring the dissolved polymer with an excess of the amine containing anchor group. After conversion

absorption at 1647 cm^{-1} can be detected showing the formation of an amide bond. Polymers prepared according to this scheme are collected in Table 1.

Table 1.
Triphenylamine polymers and blockcopolymers synthesized according to figure 1(BP1: R = H, BP2: R = Me)

	x TPA	M_n/ g mol^{-1} a)	PDI a)	yield /% a)	y PFPA	$M_{n/}$ g mol^{-1} b)	PDI b)	yield/ % b)	M_n/ g mol^{-1} c)	T_g/°C
BP1	87	2.36×10^4	1.09	55	13	2.70×10^4	1.19	66	2.65×10^4	156[c]
BP2	102	3.05×10^4	1.12	69	9	3.26×10^4	1.22	58	3.26×10^4	143[c]
Oligo 1	41	1.23×10^4	1.14	67	-	-	-	-	-	15[a]
Oligo 2	34	9.31×10^3	1.30	61	-	-	-	-	-	27[a]

a) macroinitiator from triphenylamine; b) block copolymer with reactive ester block; c) block copolymer after introduction of the anchor groups

Starting from low polydispersities (around 1.1), the polydispersity increases slightly after adding the reactive ester block, which is also typical for the method. Nevertheless the polydispersity of the block copolymers was around 1.2 which is a good value for living radical polymerization. The molecular masses of the block copolymers synthesized for nanoparticle functionalization are around 30,000 g/mol. After the polymer analogous reaction with dopamine the GPC traces show some aggregate formation due to the hydrophilicity of the anchor group.

The polymers for the surface functionalization **BP 1** and **BP 2** contain approximately 100 triphenylamine units and 10 units of the dopamine anchor group. This composition was chosen, because prior experiments with copolymers from PMMA or PS and an anchor block had shown that copolymers of this composition bind especially well onto the nanorods.[11] As a matrix oligomeric triphenylamines (**oligo 1** and **2**) were synthesized as described for the macroinitiator, but with a higher ratio of the chain transfer agent in relation to the monomer. Thus a rather low molecular weight could be obtained (Table 1). The redox properties of the

triphenylamine polymers were investigated by cyclovoltammetry, which shows their hole conducting properties. The redox potential of oligomers and functional polymers (0.65 and 0.71 for methylated and unmethylated monomer) was identical and in agreement with literature data.[17, 18] Thus the dopamine anchor does not influence the hole conducting properties of the triphenylamine unit.

The inorganic nanorods used for this study (Table 2) consisted of TiO_2, SnO_2 and ZnO, materials which are widely used in optoelectronics. Their full characterization is presented in ref. 11. For particle functionalization the nanorods are treated with ultrasound in THF, which is a good solvent for the triphenylamine block copolymers. After ten minutes of sonication the polymer is added in a mass ratio of one wt-% blockcopolymer to two wt-% of the inorganic nanomaterial to the yet rarely dispersed nanorods and the mixture is again treated with ultrasound for ten minutes. To improve the degree of functionalization further the nanorod polymer mixture is stirred for 12 h. Afterwards the excess of polymer is removed by repeated centrifugation of the functionalized nanorods and exchange of the supernatant solution of tetrahydrofuran for four times. The degree of surface coverage (= amount of adsorbed polymer) is determined by thermogravimetry and collected in Table 2. Surface coverage is found to be comparable to that of polystyrene coated particles reported recently.[11] For TiO_2 and SnO_2 about the same values are found, while the coverage of ZnO nanoparticles is higher. This may result from the fact that ZnO can coordinate both in an octahedral and a tetrahedral way. The values of the reduced surface coverage σ^*, which is bigger than 1 for all samples, indicates a high grafting density. Values < 1 would indicate a low grafting density ("mushroom regimes") on the particle surface.

Table 2.
Characteristics of inorganic nanorods and polymer surface coverage data.

	average length (TEM)/nm	aspect ratio	chains per nanorod	s / nm	σ*
TiO_2	30	5.5	20	6	3.2
SnO_2	20	4.9	10	6	3.5
ZnO	120	6.3	1000	3	14.6

s: interpolymer distance; σ*: reduced surface coverage

After polymer functionalization the nanoparticles form stable dispersions in an appropriate solvent for the polymer corona. Tetrahydrofuran and dioxane but also higher boiling solvents like toluene and xylene can be used to generate stable dispersions. In comparison with TiO_2, SnO_2 and ZnO dispersions tend to sediment faster due to the higher density of these materials. Closer inspection of these materials shows that they still contain larger aggregates. These aggregates can be removed by filtration (0.45 μm PTFE syringe filter). Light scattering proves that the filtered dispersions consist of individual nanorods.

With increasing nanoparticle concentration (evaporation of solvent) birefringent areas can be observed in polarized optical microscopy (POM). The nanoparticle solutions show typical liquid crystalline behavior, because the anisotropic nanorods are acting as mesogenes and orient parallel to each other. This behavior is analogues to that of PMMA functionalized TiO_2 nanorods investigated previously.[10] After evaporation of the solvent oriented domains are formed that can no longer be sheared, due to lack of mobility.

To investigate thermotropic liquid crystalline properties of these anisotropic nanomaterials the monomers TPA (T_m = 91.8°C) and TPA-Me (T_m = 52.3°C) can be used as a non-volatile matrix. 70 wt% solutions of the functionalized nanorods in these monomers (30 wt %) form LC-phases with clearing temperatures above or around (in the case of TPA) the melting temperatures of the monomer.

Another interesting matrix is the triphenylamine oligomer **oligo 2**. It offers the potential to self-organize the inorganic electron conducting nanoparticles inside a glassy hole conducting polymer. 70 wt% mixtures of the functionalized nanorods in 30 wt% **oligo 2** soften above 65 °C. At higher temperatures these mixtures can be sheared easily and clearing points can be detected, which are around 70°C both for TiO_2 and SnO_2 and at around 200 °C for ZnO nanorods. The high value for ZnO nanorods is most probably a consequence of the large length of these rods (Table 2). This result is quite similar to those reported for polystyrene coated nanorods in an oligostyrene matrix.[11] The textures that can be observed for the LC phases of the functionalized nanorods in **oligo 2** are presented in Figure 2. While TiO_2 nanorods show a Schlieren texture typical for a nematic phase, the SnO_2 nanorods often show birefringent *bâtonnet* structures. Dispersed ZnO nanorods show the –by far- largest domains with uniform birefringence due to parallel alignment of the rods (see Figure 2).

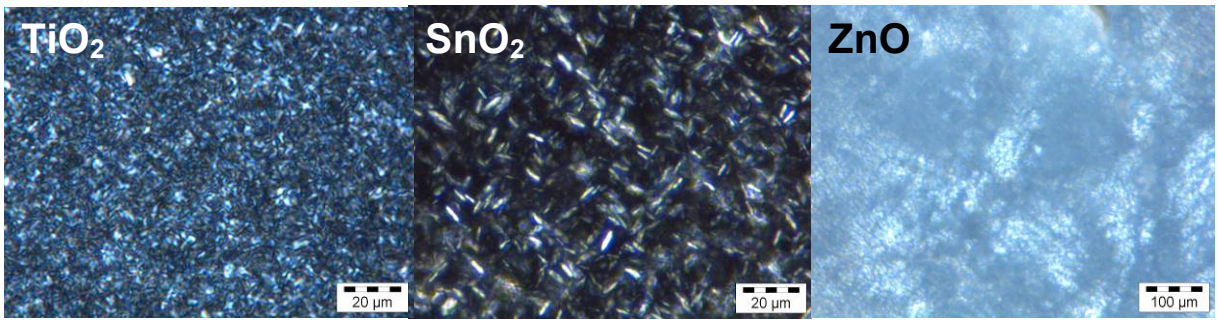

Figure 2: LC textures of polytriphenlyamine coated particles (BP2) in oligo 2

Conclusion

We were able to synthesize block copolymers consisting of a hole-conducting block and an anchor block prepared via a reactive ester approach. Block copolymers with dopamine anchor groups bind to oxidic semiconductors like TiO_2, SnO_2 and ZnO. Thus it becomes possible to combine inorganic electron conducting (acceptor) materials with a corona of an organic hole conducting (donor) polymer like polytriphenylamine, giving interesting hybrid materials. The

polytriphenylamine grafted to the inorganic nanorod leads also to stable nanorod dispersions in appropriate solvents. At higher concentration the nanorods form liquid crystalline phases in various solvents and in a low T_g oligotriphenylamine matrix. This offers the potential to orientate semiconducting inorganic nanorods in a hole conducting polymer matrix by self-assembly.

Experimentals

All raw materials were purchased by Aldrich. α,α'-azoisobutyronitrile (AIBN, from Fluka) was recrystallized from diethyl ether, dopamine hydrochloride and cysteamine (3-hydroxy tyramine hydrochloride, from Acros) were used as purchased. Solvents used to prepare nanoparticle dispersions all were distilled before usage. Tetrahydrofuran and dioxane used for polymerization was dried over Na/K and distilled. Triphenylamine monomers and the chain transfer agent were synthesized according to literature.[13, 15] Nanoparticle synthesis is described in literature.[11, 19 - 22]

Gel permeation chromatography (GPC) was carried out in THF as solvent and the detector system contained refractive index (Jasco), UV-VIS (Jasco) and light scattering (Wyatt) detectors.

Thermo gravimetry was carried out in a Perkin Elmer Pyris 6 TGA under nitrogen atmosphere. NMR spectra were obtained in a Bruker AC 300. Infrared spectroscopy was done in a Bruker Vector 22, UV-Vis spectroscopy was measured in a Shimadzu UV 2102 PC UV-Vis Scanning Spectrophotometer. Differential Scanning Calorimetry (DSC) was measured on a Perkin Elmer DSC 7 with 10 K min^{-1} scanning rate. Cyclovoltamograms were obtained with an Autolab P30 potentiostat. We used an undivided cell and three electrode configurations with a platinum mesh as counter electrode. As reference electrode an Ag/AgCl (LiOH/EtOH) electrode was chosen. We used acetonitrile as a solvent containing 0.1 M tetrabutylammonium tetrafluoroborate (Aldrich) as a conducting salt. The samples were drop

coated on a gold coated silicon wafer, which was used as working electrode. The system was calibrated against a ferrocene standard, which enables determine the oxidation potential.

Poly (triphenylamine-b-dopamineacrylamide) **BP 1**: 2.5 g vinyltriphenylamine (9.2 mmol, 150 eq), 15.1 mg 2-phenylpropan-2-ylbenzodithioate/chain transfer agent (0.06 mmol, 1eq) and 0.9 mg AIBN (0.006 mmol, 0.1 eq) were dissolved in 4 mL dioxane in a Schlenck tube. Oxygen was exchanged by nitrogen in three freeze-pump-thaw cycles and polymerization was carried out at 90 °C for 24 h. The polymer was purified by precipitation in methanol to yield in 1.45 g (55%) of a yellow-orange polymer.

To synthesize the reactive blockcopolymer 1 g (0.004 mmol, 1eq) of the macroinitiator and 300 mg pentafluorophenylacrylate (0.12 mmol, 30 eq) were dissolved in 3 mL of dioxane and oxygen was exchanged by nitrogen in three freeze-pump-thaw cycles. Polymerization was carried out at 90°C for 3 d. The polymer was purified by precipitation in methanol to yield in 0.88 g (66%) of the reactive blockcopolymer.

To synthesize the anchor block containing polymer 0.88 mg of the reactive blockcopolymer (0.003 mmol, 1eq) was dissolved in tetrahydrofuran and dopamine hydrochloride (0.034 mmol, 13 eq) and triethylamine (0.034 mmol, 13 eq) was added to the mixture. The solution was stirred over night and the polymer solution was filtered and precipitated in methanol for three times to yield in 0.64 mg (72%) of the desired polymer.

^{1}H-NMR (300MHz, d_8-THF/MeOD 4:1): δ[ppm]: 7.09 – 6.48 (m, 14xH, Ph-H), 3.75 (m, 2yH, CONH-C*H*$_2$-CH$_2$-Ph), 3.38 (m, 2yH, CONH-C*H*$_2$-CH$_2$-Ph), 2.78 (m, 1yH, C*H*$_2$-CH), 2.55 (m, 1xH, CH$_2$-C*H*), 2.47 (m, 1yH, C*H*$_2$-CH), 2.10 (m, 1H, CH$_2$-C*H*), 1.75 (m, 2xH, C*H*$_2$-CH). ^{19}F-NMR (400 MHz, d_8-THF/CD$_4$OD 4:1): no signals found. IR: ν_{max}/cm^{-1}: 3374 (OH$_{dopamine}$), 3027 (CH), 1653 (CONH).

Poly(para-methyl triphenylamine-b-dopamineacrylamide) **BP 2**: 2.5 g *para* methyl – vinyl triphenylamine (8.3 mmol, 150 eq), 13.6 mg 2-phenylpropan-2-ylbenzodithioate (0.05 mmol, 1eq) and 0.8 mg AIBN (0.005 mmol, 0.1 eq) were dissolved in 4 mL dioxane in a Schlenck tube. Oxygen was exchanged by nitrogen in three freeze-pump-thaw cycles and polymerization was carried out at 90 °C for 3 d. The polymer was purified by precipitation in methanol to yield 1.72 g (69 %) of a yellow-orange polymer.

To synthesize the reactive blockcopolymer 1 g (0,004 mmol, 1eq) of the macroinitiator and 300 mg pentafluorophenylacrylate (0.12 mmol, 30 eq) were dissolved in 3 mL of dioxane and oxygen was exchanged by nitrogen in three freeze-pump-thaw cycles. Polymerization was carried out at 90°C for 3 d. The polymer was purified by precipitation in methanol to yield in 0.76 g (58 %) of the reactive block copolymer.

To synthesize the anchor block containing polymer 0.76 mg of the reactive blockcopolymer (0.002 mmol, 1eq) was dissolved in tetrahydrofuran and dopamine hydrochloride (0.023 mmol, 14 eq) and triethylamine (0.023 mmol, 14 eq) was added to the mixture. The solution was stirred over night and the polymer solution was filtered and precipitated in methanol for three times to yield in 0.67 mg (89 %) of the desired polymer

^{1}H-NMR (300MHz, d_8-THF/CD_4OD 4:1): δ[ppm]: 7.09 – 6.46 (m, 12xH, Ph-H), 3.73 (m, 2yH, CONH-CH_2-CH_2-Ph), 3.37 (m, 2yH, CONH-CH_2-CH_2-Ph), 2.77 (m, 1yH, CH_2-CH), 2.56 (m, 1xH, CH_2-C*H*), 2.46 (m, 1yH, CH_2-CH), 2.14 (m, 6xH, Ph-Me), 2.10 (m, 1H, CH_2-C*H*), 1.75 (m, 2xH, CH_2-CH). ^{19}F-NMR (400 MHz, d_8-THF/CD_4OD 4:1): no signals found. IR(KBr) ν_{max}/cm^{-1}: 3374 ($OH_{dopamine}$), 1654 (CONH).

Oligo-triphenylamine (**oligo 1**): 1 g vinyltriphenylamine (3.6 mmol, 60 eq), 15.1 mg 2-phenylpropan-2-ylbenzodithioate/chain transfer agent (0.06 mmol, 1eq) and 0.9 mg AIBN (0.006 mmol, 0.1 eq) were dissolved in 3 mL dioxane in a Schlenck tube. Oxygen was exchanged by nitrogen in three freeze-pump-thaw cycles and polymerization was carried out

at 90 °C for 24 h. The polymer was purified by precipitation in methanol to yield in 0.67 g (67 %) of a yellow-orange polymer.

^{1}H-NMR (300MHz, $CDCl_3$): δ[ppm]: 7.09 – 6.48 (m, 14H, Ph-H), 2.55 (m, 1H, CH_2-C*H*), 2.30 (m, 1H, CH_2-C*H*), 1.75 (m, 2H, CH_2-CH).

Oligotriphenylamin (**oligo 2**): 0.8 g *para* methyl –vinyl triphenylamine (2.6 mmol, 60 eq), 12.7 mg 2-phenylpropan-2-ylbenzodithioate (0.04 mmol, 1eq) and 0.7 mg AIBN (0.004 mmol, 0.1 eq) were dissolved in 3 mL dioxane in a Schlenck tube. Oxygen was exchanged by nitrogen in three freeze-pump-thaw cycles and polymerization was carried out at 90 °C for 24 h. The polymer was purified by precipitation in methanol to yield in 0.48 g (61 %) of a yellow-orange polymer.

^{1}H-NMR (300MHz,$CDCl_3$): δ[ppm]: 7.08 – 6.49 (m, 12H, Ph-H), 2.56 (m, 1H, CH_2-C*H*), 2.14 (m, 6H, Ph-Me), 1.75 (m, 2H, CH_2-CH).

Acknowledgement

We would like to thank the “International Research Training Group: Self Organized Materials for Optoelectronic Applications” (DFG) for financial support (stipend for Matthias Zorn). Thanks to Dr. Mohammad Nawaz Tahir (AK Tremel) for kindly providing nanorod materials. Thanks to Karl Fischer and Coworkers (AK Schmidt) for doing Light Scattering Experiments.

References

[1] P.K. Sudeep, T. Emrick, *Polym. Rev.* **2007**, 47, 155.

[2] G. Schmidt, M.M. Malwitz, *Curr. Opin. Colloid Interface Sci*. **2003**, 8, 103.

[3] J. M. Kroon, N. J. Bakker, H .J .P. Smit, P. Liska, K. R. Thampi, P. Wang, S. M., Zakeruddin, M. Grätzel, A. Hinsch, S. Hore, U. Würfel, R. Sastrawan, J. R. Durrant, E. Palomares, H. Pettersson, T. Gruszecki, J. Walter, K. Skupien, G. E.Tulloch, *Prog. Photovol.: Res. Appl*, **2007**, 15,1.

[4] S.-S. Kim, J. Jo, C. Chun, J.C.Hong, D.-Y- Kim, *J. Photochem. Photobiol. A* **2007**, 188, 364.

[5] W. U. Huynh, J. J. Dittmer, A. P. Alivisatos, *Science* **2002**, 295, 2425.

[6] J. Hagen, W. Schaffrath, P. Otschik, R. Fink, A. Bacher, H.-W. Schmidt, D. Haarer, *Synth. Met.* **1997**, 89, 215.

[7] M. Grätzel, *Nature* **2001**, 414, 338.

[8] H. Zocher, *Z.Anorg. Allg. Chem*. **1925**, 147, 91.

[9] L. S. Li, J. Walda, L. Manna, A. P. Alivisatos, *Nano Lett*. **2002**, 2, 557.

[10] S. Meuer, P. Oberle, P.Theato, W. Tremel, R. Zentel, *Adv. Mater*. **2007**, 19, 2073.

[11] M. Zorn, S. Meuer, Y. Khalavka, M. N.Tahir, W. Tremel, R. Zentel. *J. Mater. Chem*. **2008**,18, 3050.

[12] L. Hagopin, G. Köhler, R. I. Walter, *J. Phys. Chem.* **1967**, 71, 2290.

[13] M. Behl, E. Hattemer, M. Brehmer, R. Zentel, *Macromol. Chem. Phys*. **2002**, 203, 50

[14] M. Eberhardt, P. Theato, *Macromol. Rapid Commum.* **2005**, 26, 1488.

[15] Y. K. Chong, J. Krstina, T. P. T. Le, G. Moad, A. Postma, E. Rizzardo, S. H. Thang, *Marcomolecules* **2003**, 36, 2256.

[16] M. N. Tahir, M. Eberhardt, P. Theato, S. Faiß, A. Janshoff, T. Gorelik, U. Kolb, W. Tremel, *Angew. Chem. Int. Ed*. **2006**, 45, 908.

[17] K. Choi, R. Zentel, *Macromol. Chem. Phys*. **2006**, 207, 1870;

K. Choi, S.J. Yoo, Y.-E. Sung, R. Zentel, Chem. Mater. **2006**, 18, 5823 .

[18] M. Sommer, S.M. Lindner, M. Thelakkat, *Adv. Funct. Mater*. **2007**, 17, 1493.

[19] X.- L. Li, Q. Peng, J.- X. Yi, X. Wang, Y. Li, *Chem. Eur. J.* **2006**, 12, 2383.

[20] B. Cheng, J.M. Russell, W, Shi, L. Zhang, E.T. Samulski, *J. Am. Chem. Soc.* **2004**, 126, 5972.

[21] B. Cheng, W. Shi, J.M. Russell-Tanner, L. Zhang, E.T. Samulski*, Inorg. Chem*. **2006**, 45, 1208.

[22] F. Shien, A.E. Saunders, B.A.Korgel, *J. Phys. Chem. B* **2005**, 109, 8538.

3.3.

Orientation and Dynamics of ZnO Nanorod Liquid Crystals in Electric Fields

Matthias Zorn, Muhammad Nawaz Tahir, Björn Bergmann, Wolfgang Tremel, Chris Grigoriadis, George Floudas, Rudolf Zentel

Macrmol. Rapid Commun. **2010**, DOI: marc.201000049

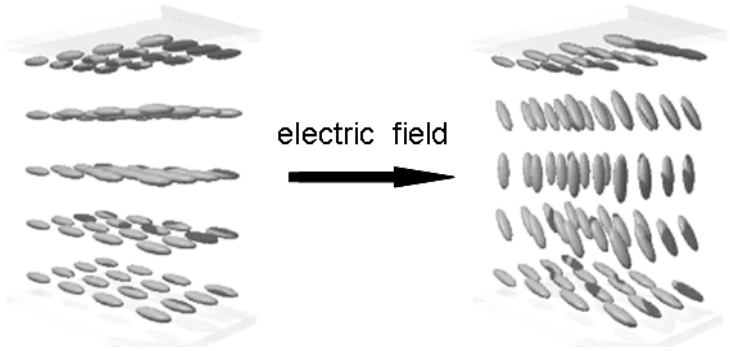

Nanorods standing perpendicular on an electrode are the desired morphology for a dye sensitized solar cell composed of anisotropic particles. In this setup, electrons can travel the longest distances in a single nanorod, with a minimization of the charge hopping from particle to particle. As shown in the previous chapters, polymer functionalized, anisotropic nanoparticles show liquid crystalline behaviour. As known from low molecular and polymeric liquid crystals, electric fields can induce a homeotropic alignment. We tested the influence of an electric field on a liquid crystalline phase composed of polystyrene functionalized ZnO nanorods in an oligostyrene matrix. The nanorods were synthesized by Muhammad Nawaz Tahir (AK Tremel). As shown by dielectric spectroscopy data (Chris Grigoriadis, George Floudas), the effective dipole moment of the nanorods in the oligomer matrix is too low for an orientation. Nevertheless, the cooperative effect of the liquid crystalline phase enables the system to react on the applied electric fields. The reaction can be monitored by the vanishing

birefringence under crossed polarizers. The switching velocity shows the expected dependence of the field strength.

By changing the polymer matrix to a higher molecular weight, it was possible to visualize the oriented mesogens with electron microscopy. Due to the large mesogens a typical Fredericks transition known from low molecular liquid crystals in displays, could be visualized for the first time.

Introduction

The use of nanoscale inorganic particles is a research field of high interest with applications in optoelectronic devices.[1] Organized patterns arising from the self-assembly of nanostructures may enhance the efficiency of optoelectronic devices. Furthermore they allow fundamental studies of charge transport through nanoparticle assemblies.[2] Especially the perpendicular orientation of anisotropic nanoparticles on an electrode is a promising new approach towards improved photovoltaics.[3] Such ordered structures can be achieved by growing techniques from a substrate.[4] On the other hand, a wet chemical synthesis of nanoparticles is straightforward and enables chemists to easily synthesize large amounts of particles with different shapes, aspect ratios, crystallinities and surface modifications.[5] In addition, patterned substrates can be used to direct the self-assembly of nanorods in a vertical orientation.[6]

Nanorods possessing strong dipole moments can be aligned in external electric fields. For CdSe and CdS nanorods (dipole moments as large as 1450 D) Russell et al. and Alivisatos et al. showed superlattices and self-corralling perpendicular to the electrodes for particle suspensions dried under an DC electric field.[7] The alignment is a result of the dipole in the distorted non-centrosymmetric crystallographic lattice of the nanoparticle. However, not all nanocrystals possess such a large dipole moment. For ZnO in particular, distortions of the ideal wurtzite lattice (the basis for the dipole moment) strongly depend on the aspect ratio and growth conditions of the nanoparticles.[8, 9] Thus the preparation of nanoparticles with a given anisotropy and high dipole moment is non-trivial and only very few publications deal with the effect of electric fields on anisotropic oxidic nanostructures.[10, 11]

There is, however, an alternative way to orient anisotropic objects, which uses their cooperativity in liquid crystalline (LC) phases. In this case not the individual object, but the LC-domain interacts with the electric field.[12, 13] That is why the combination of inorganic nanoobjects and LC-materials is fascinating.[14] In a more general way such cooperative liquid crystalline (LC) behavior can be observed for structures with high aspect ratios (> 3.5)

independent of their chemistry. LC phases can also be observed from rod- or disc-like inorganic particles, if they are well dispersible in an external medium.[15-19] To increase solubility and prevent agglomeration a modification of the particle surface is essential. Besides standard surfactants that are often introduced during the particle synthesis, a post-modification with polymers is an interesting approach. In this way, besides solubility other functionalities, like semi conducting properties or stimuli responsive features can be added to inorganic nanoparticles.[19- 21] Especially the use of block copolymers with a short anchor block that attaches to the inorganic particle (multi dentate binding) and a longer soluble or even functional block, that sterically stabilizes the colloids in an organic medium, is an interesting new approach. In a previous work we have shown that these polymer-coated nanorods form LC phases.[21]

Mineral liquid crystals embedded in polymer matrices can be oriented using the same methodology employed for low molar mass liquid crystals like shearing, convective or flow forces[22] and other external fields. The orientation in electric fields (switching, in particular), is a well-known method to orient low molecular mass or polymeric liquid crystals used in display applications. The method requires only a slight anisotropy in the dielectric polarizability although a large dielectric anisotropy facilitates an easier orientation.[7] This is especially useful in oxidic semiconductors like ZnO, a potential material for hybrid photovoltaic devices, which often possesses only a low dipole moment.

In this study we report the influence of electric field on liquid crystalline phases of polystyrene (PS) functionalized ZnO nanorods. We employ dynamic probes in order to understand the mobility and dipole moment of the rods in detail, while the switching of the rods can be investigated in a simple setup by following the change in birefringence. We further study the impact of AC electric fields and show images of LC phases composed from inorganic nanorods that are embedded in a higher molecular weight PS and effectively oriented under an applied DC field.

Experimental Part

All chemicals were purchased by Sigma-Aldrich, Fisher Scientific, Merck and Fluka. THF was distilled over sodium before used. The liquid crystal test cells were purchased by E.H.C Co., Ltd., Tokyo, Japan (KSRO-10/A311N1NSS, Y type cell, 4x4 mm, ITO electrode, SiO and polyimide coated, parallel rubbed). SEM images were taken on a Field Emission Scanning Microscope (FE-SEM, LEO, 1550-VP) operated at 5 kV. TEM was measured on a Hitachi 7600 with an operating voltage at 90 kV. Film thicknesses of the electric set up were determined with a calliper.

Nanoparticle and Polymer Synthesis

Polystyrene-bl-dopamineacrylamide (PS_{90}-*bl*-DA_{10}): Styrene was polymerized with benzyl dithiobenzoate as chain transfer agent in tetrahydrofuran in a nitrogen atmosphere at 65 °C for 12h. The macroinitiator was purified by precipitation in methanol (yield: 67 %), M_n (GPC): 9360 g/mol (PDI (GPC) = 1.12.

The reactive block copolymer PS-*bl*-PFPA was synthesized by adding pentafluorophenylacrylate to the macroinitiator with AIBN in THF under a nitrogen atmosphere. The mixture was polymerized for 48 h at 65 °C and the polymer was purified by precititation in methanol (yield: 63 %) M_n (GPC) = 11590 g/mol, PDI (GPC) = 1.15.

For the polymer analogous reaction the reactive block copolymer was stirred with dopamine hydrochloride and triethylamine in THF under nitrogen at room temperature for 5 h. Afterwards the solution was filtered and precipitated in methanol to yield the desired product PS_{90}-*bl*-DA_{10}.

^{1}H-NMR (300MHz, $CDCl_3$/MeOD 4:1): δ[ppm]: 7.06 (m, 3H, Ph-H), 6.57 (m, 2H, Ph-H), 6.14 (m, 3H, $ArH_{dopamine}$), 3.52 (m, 2H, CONH-C*H*$_2$-CH_2-Ph), 3.39 (m, 2H, CONH-C*H*$_2$-CH_2-Ph), 2.97 (m, 1H, CH_2-C*H*-), 2.38 (m, 1H, CH-C*H*$_2$), 1.87 (m, 1H, CH-C*H*$_2$), 1.84

(m, 1H), 1.39 (m, 2H). ^{19}F-NMR (400 MHz, $CDCl_3$): no signals found. IR: ν_{max}/cm^{-1}: 3374 ($OH_{dopamine}$), 3027 (CH), 2923 (CH), 1650 (CONH).

ZnO nanorods were prepared as reported in previous work.[8] Functionalization was done by sonication of the ZnO nanorods and the polymer in THF. The solution was centrifuged, the solvent was exchanged and the particles redispersed for three times to get the pure hybrid. Thermal gravimetry measurements show a dense surface coverage with the polymer (around 35 wt% organic content). Calculated to the particle surface the data show that the particles are stabilized by a brush-like polymer corona (4 nm^2 per polymer chain). This shows that the particles are well functionalized and sterically stabilized. TEM images show clearly the polymer corona around the particles (see Figure 1 (inlet))

The particles were dried in vacuum, weighed and redispersed in an organic polymer solution to get the investigated solutions.

Dielectric spectroscopy (DS)

The dielectric measurements were performed at different temperatures in the range 143–403 K, at atmospheric pressure, and for frequencies in the range from 10^{-2} to 10^6 Hz using a Novocontrol BDS system composed of a frequency response analyzer (Solartron Schlumberger FRA 1260) and a broadband dielectric converter. The sample cell consisted of two electrodes 20 mm in diameter and the sample with a thickness of about 50 μm maintained by Teflon spacers. The complex dielectric permittivity $\varepsilon^*=\varepsilon'-i\varepsilon''$, where ε' is the real and ε'' is the imaginary part, is generally a function of frequency ω, temperature T, and pressure P, although here only the frequency and temperature dependencies have been investigated.[23] There are two principal mechanisms that contribute to ε^* in our case: orientation polarization of permanent dipoles (ε^*_{dip}) and conductivity contribution (ε^*_{cond}) as:

$$\varepsilon^*(\omega,T,P) = \varepsilon^*_{dip}(\omega,T,P) - i\frac{\sigma(T,P)}{\varepsilon_f \omega} \qquad (1)$$

where σ is the dc conductivity and ε_f the permittivity of free space (=8.854 pF/m). The orientational contribution was fitted using the empirical equation of Havriliak and Negami.[24]

$$\varepsilon^*_{dip}(\omega,T,P) = \varepsilon_\infty(T,P) + \sum_{k=1}^{2} \frac{\Delta\varepsilon_k(T,P)}{\left[1+(i\omega\tau_{HN}(T,P))^{m_k}\right]^{n_k}} \qquad (2)$$

where $\Delta\varepsilon_k(T,P)$ is the relaxation strength of the process under investigation, τ_{HN} is the relaxation time of the equation and m, n ($0<m$, $mn\leq 1$) describe the symmetrical and asymmetrical broadening of the distribution of relaxation times and $\varepsilon_\infty(T,P)$ is the dielectric permittivity at the limit of high frequencies. The relaxation times at maximum loss (τ_{max}) are presented herein and have been analytically obtained by the Havriliak-Negami equation as follows:

$$\left[\sin\left(\frac{\pi m}{2+2n}\right)\right]^{1/m} \tau_{max} = \tau_{HN}\left[\sin\left(\frac{\pi mn}{2+2n}\right)\right]^{1/m} \qquad (3)$$

At lower frequencies, ε'' rises due to the conductivity ($\varepsilon''=\sigma/(\omega\varepsilon_f)$,).

Orientation in AC field

The nanorod polymer solution (60% ZnO-PS hybrid: 40% PS 980) was deposited on the electrode area of a liquid crystal test cell at 80°C. After removal of the solvent the top electrode was placed on the composite and a LC phase was formed by shearing the suspension between the electrodes. The solution was observed with a microscope with crossed polarisers. An AC field with 100 Hz, 50-400 V(p-p) was applied. Film thicknesses were determined between 20 and 30 µm. For the kinetics a video was made and the brightness of the images was quantified with Image J - software in dependence of time. The beginning velocity was determined depending on the field strength.

Orientation in DC field

The polymer coated particles were dispersed in a solution of PS (90% ZnO-PS hybrid: 10% PS 25k) in toluene (10 mg/ 0.1 mL) and dropped through a syringe filter (200 nm pore size) on a silicon wafer (polished, n-doped with phosphorus, resistance 1-10 Ω, thickness 500-550 μm). Kapton was used as a spacer. As top electrode a Kapton foil with aluminium layer (Sheldahl, Northfield, Minnesota) was used with Kapton directly contacted to the polymer particle solution to prevent short circuit. The solvent was slowly evaporated in a saturated toluene atmosphere. After 3 h the field was turned off and the sample was broken for SEM imaging.

Results and Discussion

For the investigation of switching processes in mineral liquid crystals we employ ZnO nanorods with a length of 150 nm and a width of 20 nm (both 30% coefficient of variation). The rods were synthesized in a sol-gel process and can be produced in large quantities.[8] For surface functionalization, block copolymers were synthesized by RAFT polymerisation.[21] Benzyl benzodithioate was used as a chain transfer reagent to produce polystyrene with a low molecular size distribution (PDI ~ 1.1). From this macroinitiator, pentafluorophenylacrylate (PFPA) was polymerized as a short block to prepare PS-*bl*-PFPA (ratio ~ 90:10), that can be transferred quantitatively to an anchor block for nanoparticles and surfaces with primary amine carrying functional groups like dopamine (catechol)[21] (see Figure 1). For this work PS-*bl*-DA was used dopamine, which binds well to oxidic nanorods. This is done by sonicating the inorganic material and the block copolymer (PS_{90}-*bl*-DA_{10}). The hybrid material is purified by centrifugation and exchange of the solvent for several times. The nanorod/polymer hybrid can be well dispersed in any solvent suitable for the polymer corona as well as in polymer matrices of the same chemical composition like the polymer brushes bound to the particle surface. The changed solubility behavior and dispersibility in a polymer matrix is

evidence for the modified surface. As already reported, light scattering of these structures shows that the rods are individually dispersed.[19] Calculations based on TGA analysis show a brush like surface coverage.[21] Figure 1 shows a TEM image of a film of PS functionalized ZnO particles embedded in a PS (25k) matrix. The rods are individually dispersed in the film, but already have the tendency to orient parallel to each other like in a liquid crystalline phase, as a result of the high form anisotropy. The polymer bound to the surface can be clearly visualized, if the PS corona is stained with RuO_4 to enhance the contrast.

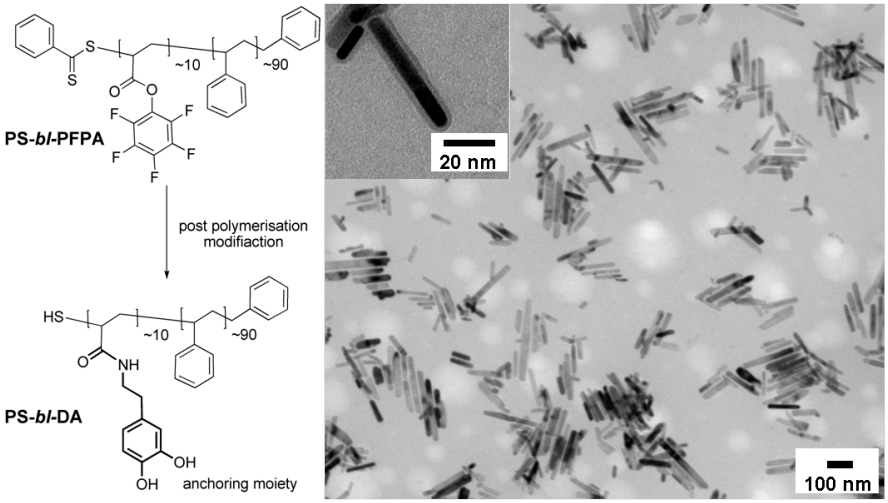

Figure 1.
(Left): Synthesis of PS-*bl*-DA from PS-*bl*-PFPA (M_n (GPC) = 11590 g/mol, PDI (GPC) = 1.15) by post polymerization modification. (Right): TEM image of PS functionalized ZnO nanorods in a polystyrene (25k) film. The inlet in the TEM image shows a single nanorod coated with polymer (stained with RuO_4).The rods show the tendency to align parallel like in LC structures.

These brushed nanorods have as molecular analogs the hairy-rod structures known from liquid crystalline polymers.[25] Due to the form anisotropy and functionalization, the ZnO nanorods are well-soluble even at high inorganic weight fraction; they are mobile in low viscous matrices and can form large uniformly birefringent liquid crystalline phases after shearing in a polymer matrix.[21] Due to the large length of the nanorods (150 nm) the clearing temperature of the LC-phase is very high (around 250 °C). Since the polymer nanoparticle mixture decomposes at these high temperatures, it cannot be determined accurately. (This is different from the much shorter modified TiO_2 or SnO_2 nanorods,[21] which show reversible

clearing below 100 °C.) Birefringent textures are observable from 20 to 90 wt% of the nanorod/polymer hybrid in the PS matrix. In the case of ZnO the LC phases are mobile at temperatures above the glass temperature (T_g) of the polymer matrix (in the case of a PS oligomer with M_n=980 g/mol, T_g is at 14°C (DSC)).

Application of an electric field on this system induces a rotational force on the director (a phenomenon known as Fredericks transition)[26] and the energy of the system is minimized by the alignment of the rods parallel to the electric field. This transition requires sufficient local mobility as well as shape anisotropy and a dipole moment. For this purpose we employ dielectric spectroscopy (DS) to study the mobility of the ZnO nanorods in an oligostyrene matrix as well as their dipole moment.

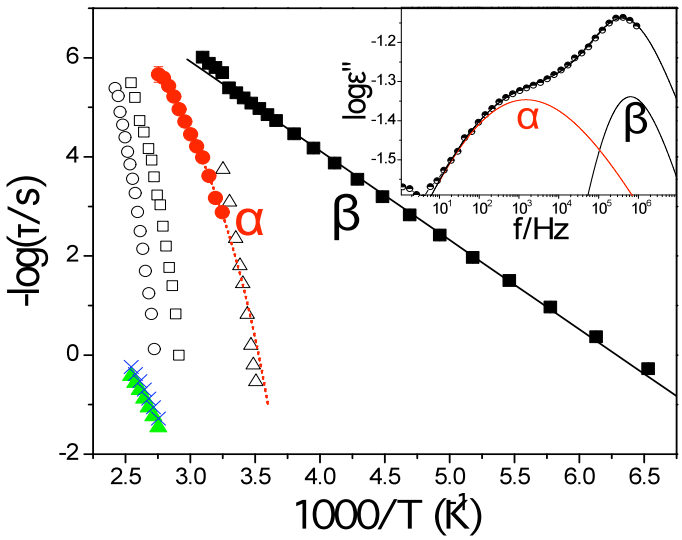

Figure 2.
Arrhenius representation of the dielectrically active relaxation times in polystyrene-*b*-dopamine acrylamide (PS_{90}-*b*-DA_{10}) functionalized ZnO particles embedded in a polystyrene matrix with M_n=980 g/mol) (the composition is 30/70); (filled squares): β-process, (filled circles): α-process, (filled up triangles): slow process and (X) ion-mobility process. The open symbols correspond to the homopolymer PS segmental relaxations; (open triangles) PS with M_n=760 g/mol), (open squares): PS with M_n=2940 g/mol and (open circles): PS with M_n=5030 g/mol).[28] The line is a fit of the β-process relaxation times to an Arrhenius temperature dependence whereas the dashed line is the result of the fit of the α-relaxation times to the VFT equation (see text). The inset gives a representative fit of the dielectric loss to a summation of two Havriliak-Negami functions at *T*=313 K.

The results of the dynamic investigation for the polystyrene-*b*-dopamine acrylamide (PS_{90}-*b*-DA_{10}) functionalized ZnO particles embedded in a polystyrene matrix with M_n=980 g/mol) with a 30/70 composition are shown in Figure 2. Two relaxation processes are observed and a

representative fit to the dielectric loss data at 313 K is also shown in the inset to Figure 2. The fast process (β-process) has an Arrhenius temperature dependence according to: $\tau=\tau_0\exp(E/RT)$, where τ_0 (=5x10^{-12} s) is the characteristic time in the limit of very high temperatures, and E is the apparent activation energy (=35 kJ/mol). The weak $\tau(T)$ dependence identifies the interfacial DA block (most probably the amide bond) as responsible for the β-process. The α-process, on the other hand, with the steeper T-dependence conforms to the Vogel-Fulcher-Tammann (VFT) equation as: $\tau=\tau_0\exp(B/T-T_0)$, where B (=1490 K) is the activation parameter and T_0 (=220±26 K) is the "ideal" glass temperature located below the calorimetric glass temperature. In Figure 2, literature values of PS segmental relaxation times are included for different molecular weights.[27] The α-process in the composite has the same $\tau(T)$ dependence as the local segmental process in a homo polystyrene of ~760 g/mol, that is close to the molecular weight of the PS matrix. However, despite the similarity in local friction, the dielectric strength of the α-process in the hybrid system is 10 times higher ($T\Delta\varepsilon$~200 K) than the corresponding strength of a homo polystyrene ($T\Delta\varepsilon$~20 K).[28] This suggests a cooperative ZnO relaxation experiencing the local friction of the viscous PS matrix as the origin of the α-process. The effective dipole moment relaxing through the α-process can be obtained from $\mu=(3\varepsilon_f\kappa_B T\Delta\varepsilon/FN)^{1/2}$, where ε_f is the permittivity of free space, F is the local field correction and N is the number density and amounts to about 1.5 Debye. This dipole moment is much smaller than the one reported for CdSe nanorods and the one calculated for other systems (including ZnO) exhibiting the wurtzite structure.[29] We should mention here that an ideal wurtzite structure does not posses a dipole and that the calculated dipole moment is attributed to small crystallographic deviations from the ideal wurtzite structure. In the present case, the strength of the torque experienced by the nanorods within the electric field ($T=\mu xE$, *E:* electric field strength ~ 2x10^4 V/m) is in the order of 10^{-25} J, i.e., much smaller than the thermal energy at room temperature ($\kappa_B T$~4x10^{-21} J) that effectively randomizes the orientation of nanorods. This rules out the possibility that the nanorods can be aligned –

individually- due to a strong dipole moment of the nanoobject. Nevertheless, this dipole moment is sufficient for a cooperative switching in the liquid crystalline phase.

To investigate the switching behavior of the LC-phase formed by the ZnO nanorods, the composite was placed in a liquid crystal test cell with ITO electrodes and an AC electric field was applied. Frequencies above 90 Hz allow it to suppress the movement of ions (electrohydrodynamic effect), which can lead to turbulences in the liquid crystalline phase and counteracts the orientation. This offers the possibility to apply higher voltages in comparison to DC fields. Voltages up to 400 V (p-p) (film thickness of 30 μm) could be applied (higher fields were not stable and led to a short current in all cases). Shearing leads to a homogenous alignment in the field free state with the director (the nanorods) oriented parallel to the substrate. This causes birefringence variations, which can be detected with a polarizing optical microscope (POM). In this context it must be mentioned that the birefringence of the system is relatively small. This is a result of the fact that (i) ZnO has a cubic symmetry (no birefringence if undisturbed) and (ii) the polymeric solvent adds no birefringence. As a result the birefringence of the LC-phase is small and the textures are only black and white. But this is advantageous for the evaluation of the switching process, as the light intensity drops continuously on switching the LC-director from a predominant parallel to a homeotropic (perpendicular) orientation. Figure 3 shows the effect of the electric field and the evaluation of the switching process in a section of the sheared sample at the edge of the electrode area.

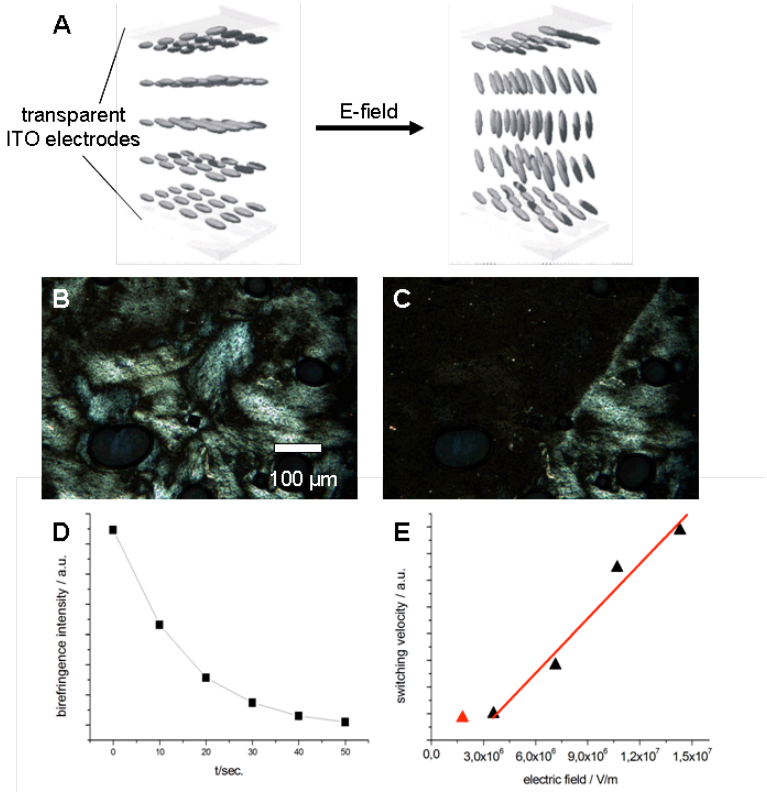

Figure 3.
A) Schematic of the Fredericks transition before and after switching in the electric field; B and C) Polarized microscopy image of a film of PS functionalized ZnO nanorods 60 wt% in 40 wt% PS 980 in a liquid crystal test cell. The image shows the section at the border of the electrode; B) before the AC electric field was switched on; C) after 50 s: texture in the electrode area is completely vanished due to the homeotropic alignment of the rods in the film; D) Intesity loss of the sample at a applied voltage of 400 V(p-p); E) Dependence of the switching velocity on the field strength.

While the texture changes in the left part of the POM image the remaining part of the film maintains its LC texture. The birefringent texture turns gradually black on application of an electric field, showing the transition from a homogeneous to a homeotropic orientation (see movie in Supporting Information). The fact that the sample turns completely black shows that the orientation in the bulk of the sample must be homeotropic. Detailed switching experiments were performed at 50°C (35 °C above the matix T_g) to have a low viscosity of the oligomer melt. The kinetics of nanorod orientation was measured by monitoring the loss of birefringence (see Figure 4D and Supporting Information Figure S1). At high fields exceeding 1.4×10^7 V/m (maximal voltage of 400 V (p-p) at film thickness of 30 µm) the switching to a homeotropic alignment is completed in less than 40 seconds. At fields lower than 10^6 V/m, the applied force on the nanorods is too small to induce the bending deformation of the

director close to the surface) associated with the Fredericks transition. In the range from 50 V(p-p) to 400 v(p-p) the switching velocity increases linearly.

Because of surface alignment (see schematic representation of the Fredericks transition in Figure 3), favoring parallel interaction between the rod and the electrodes, reorientation by the thermal energy is observable, if the field is switched off (it is, however, by many orders of magnitude slower than the switching-on process). This reorientation (reappearance of birefringence) starts from the edges of the film or from air bubbles. Further investigations, such as SEM or TEM were not possible in this setup due to the low viscosity of the oligomer matrix.

These results underline the potential of the LC-phase to orient nanoobjects, even if the individual dipole moment is small. In LC-phases even a small difference in the dielectric constant (ε (PS): 2.6; ε (ZnO nanostructures): up to 71 reported)[30] when coupled with the dielectric anisotropy of the ZnO nanorods suffices to orient the particles.

As the individual mesogens (the nanorods) of the LC-phase are large and possess a sufficient contrast, it was possible to visualize the director orientation after the Fredericks transition on broken cells (see Figure 4). It must, however be mentioned that it is difficult to get such pictures, because the matrix is soft and deforms during breaking. Thus we used high molar mass polystyrene instead of the oligomer to stabilize the matrix. Nevertheless we only succeeded in getting pictures for very thin samples. That is to enable the visual inspection of the orientation of the individual nanorods within the hybrid material we dispersed the ZnO nanorod/poystryrene hybrids (90 wt%) in PS matrix of a higher molar mass (to stabilize the system for SEM-measurements) and diluted this mixture with toluene (10 wt% dispersion of the hybrid polymer composite in toluene) as a volatile solvent to induce mobility. During evaporation of toluene a lyotropic LC-phase is formed,[21] which “freezes” as the solvent evaporates. Toluene was evaporated during 6 h in saturated solvent atmosphere that provide the possibility for a parallel rod orientation with respect to the field (see Experimental Part).

Between the top electrode and the sample, a Kapton® layer was placed to prevent short current in the system. Thus the electro hydrodynamic instabilities that required the use of AC fields in the first experiment were now avoided and a DC electric field of up to 3 x 10^5 V/m (250 V with 800 µm distance (particle film and Kapton® foil) between the electrodes) could now be applied. The particles formed a uniform film with a thickness of about 700 nm between the two electrodes. For such thin films as in Figure 4 the influence of the parallel surface (see Figure 3) is overestimated compared to the bulk orientation (parallel to the electric field). Nevertheless Figure 4 shows clearly that the nanorods in the middle of the cell orient parallel to the electric field. This pattern (mesogens oriented parallel to the substrate at the interfaces and perpendicular in the bulk) is typical for a Fredericks transition known from low molecular liquid crystals.[26, 31] The images in Figure 4 provide thus the first example of a direct visualization of the Fredericks transition on the level of the individual mesogens.

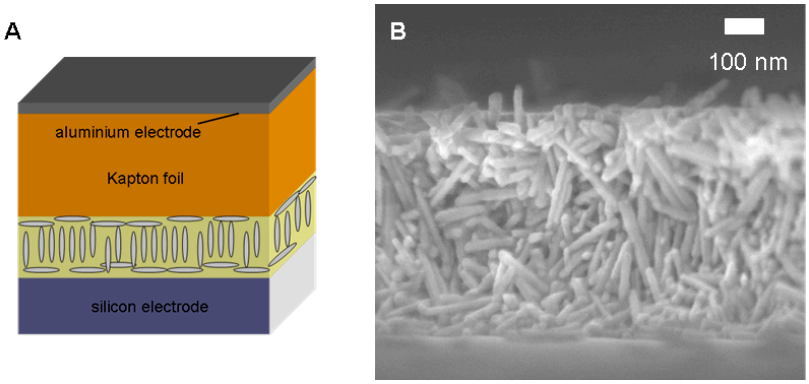

Figure 4.
A) Scheme of the DC Field set up. The Kapton foil is an isolator to prevent short current. B)Cross section SEM image of a ZnO nanorod film (high molar mass polystyrene as matrix) dried between two electrode. In the bulk a preferred orientation perpendicular to the electrodes is observable while the rods are oriented parallel on the interfaces.

Conclusion

The experiments performed with ZnO nanorods forming liquid crystalline phases opens the possibility for bulk alignment of the nanorods in electric fields in full analogy to low molar mass liquid crystals. This allows the transformation of a parallel orientation (shearing) into a

perpendicular one. Dielectric spectroscopy revealed that the ZnO nanorods dispersed in a PS oligomer matrix exhibit a rather small effective dipole moment. Nevertheless, the presence of sufficient form anisotropy when coupled to a small dipole moment suffices to induce the change in orientation. Thus liquid crystallinity offers the potential to align all types of nanostructured material with sufficient form anisotropy. However, it requires a proper coating of the nanorods to improve solubility and mobility in highly concentrated solutions that can be achieved with the block copolymers employed herein.

Acknowledgements

This work was financially supported by the International Research Training Group: Self Organized Materials for Optoelectronics (IRTG 1404) Mainz-Seoul jointly supported by the DFG (stipend for Matthias Zorn) and the Korea Science and Engineering Foundation (KOSEF).Thanks to the Graduate School of Excellence MAINZ - Polymat for support. Thanks to Prof. Kookheon Char, Seoul National University for support and discussions

References

[1] C. Y. Kuo, W. C. Tang, C. Gau, T. F. Guo, D. Z. Jeng, *Appl. Phys. Lett*. **2008**, 93, 033307.

[2] A. Zabet-Khosousi, A.-A. Dhirani, *Chem. Rev*. **2008**, 108 (10), 4072,

[3] W. U. Huynh, J. J. Dittmer, A. P. Alivisatos, *Science* **2002,** *295*, 2425.

[4] X. Wang, C.-J Summers, Z. L. Wang, *Nano Lett*. **2004**, *4(3),* 423.

[5] G. Schmid, Nanoparticles: From Theory to Application, Wiley-VCH, Weinheim, 2004.

[6] S.Ahmed, K. M. Ryan, *Nano Lett.* **2007**, *7*, 2480.

[7] a) S. Gupta, Q. Zhang, T. Emrick, T. P., Russell, *Nano Lett*. **2006**, *6*, 2066.b) K. M. Ryan, A. Matroianni, K. A. Stancil, H. Liu, A .P. Alivisatos, *Nano Lett.* **2006,** *6*, 1479.

[8] B. Cheng, W. Shi, J. M. Russell-Tanner, L. Zhang, E. T. Samulski, *Inorg. Chem*. **2006**, *45*, 1208.

[9] A. Dev, S. Kar, S. Chakrabarti, S. Chaudhuri, *Nanotechnology* **2006**, *17*, 1533.

[10] O.Harnack, C. Pacholski, H. Weller, A. Yasuda, J. M Wessels,. *Nano Lett*., **2003**, *3*, 1097.

[11] K.Jiang, W.Liu, L.Wan, J. Zhang, *Sensor. Actuat. B*, **2008**, *134*, 79.

[12] I. C. Sage in *Handbook of Liquid Crystals, Fundamentals*, (Eds.: D.Demus, J. Goodby, G.W., Gray, H.-W Spiess, V.Vill), Wiley-VCH, Weinheim, New York, **1998.**

[13] M.Schadt in *Liquid Crystals*, H. Stegemeyer Eds., Steinkopf Verlag, Darmstadt, New York, Springer, **1994**.

[14] D. Cochin, M. Passmann, G. Wilbert, R. Zentel, E. Wischerhoff, A. Laschewsky, *Macromolecules* **1997**, 30, 4775.

[15] P. Davidson, J. C. P. Gabriel, *Curr. Opin. Colloid Interface Sci.* **2005**, *9*, 377.

[16] L.-S. Li, A. P. Alivisatos, *Adv. Mater*. **2003**, *15(5),* 408.

[17] J. C. P. Gabriel, P. Davidson, *Adv. Mater*. **2000**, *12(1),* 9.

[18] J. C. P. Gabriel, P. Davidson, *Top. Curr. Chem*. **2003**, *226*, 119.

[19] S. Meuer, K. Fischer, I. Mey, A. Janshoff, M. Schmidt, R. Zentel, *Macromolecules* **2008**, *41*, 7946.

[20] M. Zorn, R. Zentel, *Macromol. Rapid Commun*. **2008,** 29, 922.

[21] M. Zorn, S. Meuer, M. N. Tahir, Y. Khalavka, C. Sönnichsen, W. Tremel, R. Zentel, *J. Mater. Chem*. **2008,** *18*, 3050.

[22] C. Ooi, R. M. Erb, B. B. Yellen, *J. Appl. Phys*. **2008,** *103*, 07E910.

[23] G. Floudas, *Progress Polym. Sci.* **2004**, *29*, 1143.

[24] S. Havriliak, S. Negami , *Polymer* **1967**, *8*, 161.

[25] S. Meuer, P. Oberle, P. Theato, W. Tremel, R. Zentel, *Adv. Mater.* **2007**, 19, 2073.

[26] D.Dunmur, , K.Toriyama in *Handbook of Liquid Crystals Vol. 1* D. Demus, J. Goodby, G.W. Gray, H.-W. Spiess, V. Vill Eds. Wiley VCH, Weinheim, **1998**, p. 265.

[27] C.M. Roland, R. Casalini, *J. Chem. Phys.* **2003**, *119*, 1838.

[28] A.Gitsas, G. Floudas, R. P. White, J. E. G. Lipson, *Macromolecules* **2009**, 42, 5709

[29] a)T. Nann, J. Schneider, *Chem. Phys. Lett.* **2004**, *384*, 150, b) L.- S- Li, A. P. Alivisatos, *Phys. Rev. Lett.* **2003**, 90, 097402

[30] M. K Gupta, N. Sinha, B. K. Singh, K. Kumar, B.Kumar, *Mater. Lett*. **2009**, *63*, 1910.

[31] W.Pisula, M. Zorn, J.Y. Chang, K. Müllen, R. Zentel, *Macromol. Rapid Commun*. **2009**, *30*, 1179.

3.4.

Light Induced Charging of Polymer Functionalized Nanorods: A "Solar Cell" Concept for a Single Particle

Matthias Zorn, Stefan Weber, Mohammad Nawaz Tahir, Wolfgang Tremel, Rüdiger Berger, Rudolf Zentel

Nano Lett. **2010**, submitted.

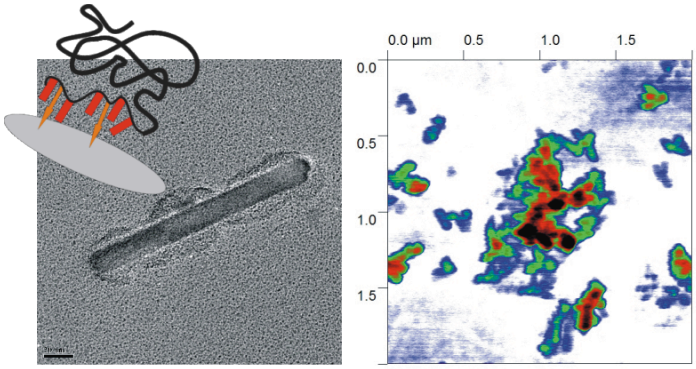

Future applications of the described systems in optoelectronic devices include the use of the functionalized particles in solar cells. In the previous part, the encapsulation of the particles in a hole conducting triphenylamine polymer shell was described. Based on this system, we take advantage from the flexible reactive ester block. An amine containing perylene dye was synthesized and reacted together with dopamine with the reactive ester block. The dye was successfully integrated into the reactive part. By the localisation of the dye in the anchoring part the dye is directly located at the interface between the nanoparticle and the polymer shell. The polymers were synthesized, characterized, and attached to the ZnO nanoparticles according to the described methods. The ZnO nanorods were synthesized by Mohammad Nawaz Tahir.

The system contains all parts necessary for a dye sensitized solar cell, (the metal oxide semi conductor, the dye and the hole transporter) all combined in a single nanoparticle. Energy and charge transfer properties of the system were shown by the decreased photoluminescence,

indicating a quenching due to energy or charge transfer from the excited dye to the nanoparticle.

Charge separation could also be observed by Kelvin probe force microscopy (Stefan Weber), which showed a charging of the nanoparticles upon illumination due to charge separation. A charging of a single particle between 10 and 20 millivolts could be measured.

Introduction

Life on earth would not be possible without light induced charge separation. In photosynthesis this process is responsible for the growth of all plants and the conversion of carbon dioxide and water to carbon hydrates and oxygen. The same concept can also be used to create electricity from sunlight. The system is based on a light absorption by a dye, followed by charge separation and injection of electrons into an inorganic semiconductor. Next to the already commercially established field of silicon photovoltaics these dye sensitized solar cells (DSSC) are an approach to produce –even flexible- photovoltaic cells at low costs. Since Michael Grätzel first reported the concept[1] in 1991 many research groups worldwide try to improve the performance by changing morphology, material, dye[2] and the electrolyte system.[3] In terms of morphology nanoparticles are the favored system due to the high surface area for dye absorption and charge separation.[4] Especially rod shaped particles showed to be promising structures due to an anisotropic, directed percolation way of electrons through the particles.[5]

The dye absorbs light, an exciton is formed and an electron is injected into the inorganic structure. Ruthenium based complexes are the mainly used structures due to good absorption and high efficiency for charge transfer. Promising candidates are perylene based sensitizers.[6] Perylene compounds (see red structure in Figure 1) are cheap industrially available materials with high stability and good light absorption that can be tuned over a broad spectrum (from red to violet) by tailoring substitutents on different positions of the aromatic core. Next to the optical properties, perylene derivatives are used in organic electronic devices due to their redox behaviour and high electron mobility as an electron conducting material.[7] Perylenes were already successfully tested as sensitizers in combination with different semiconducting metal oxides like SnO_2[8] and ZnO.[9]

Furtheron, an electrolyte system is necessary in DSSCs to reduce the dye. The iodine electrolyte mixture used in Grätzels original setup is a weak point of the system that reduces

efficiency and life-time of the devices. Solid electrolytes based on polymeric materials are a promising approach to overcome the liquid electrolyte system[10] and to improve the devices in case of long term stability. Also hole transporting polymers like poly-3-hexylthiophene P3HT are the main focus of interest.[11] In the case of nanoparticle solar cells it is useful to use non-crystalline, glasslike hole conducting materials. Well known examples are triphenylamine based structures that were already applied in OLED and PV applications.[12, 13] They are easy to synthesize and can be produced in large amounts as main and side chain polymer.

The aim of this project is to combine the concept and all of the described materials in one nanometer-sized structure. The hole conducting triphenylamine moiety –as one block- is combined with a light absorbing perylene dye –as the second block- in a single polymer. The formation of a p-n junction in one molecule improves the charge transfer.[14] This block copolymer is then linked to a nanorod of ZnO as the electron acceptor. As a consequence, the perylene dye is attached close to the inorganic-organic interface, while the triarylamine block forms a polymer corona. Mediated by the polymer, the particles should be well soluble, form a stable dispersion and have a better processability.[15] The combination of the polymer with the particle represents a model material for a dye sensitized solar cell on a single particle level operated under open circuit conditions.

Results and Discussion

Triphenylamine (TPA) moiety containing block copolymers can be made by controlled radical polymerization.[16, 17] We chose RAFT polymerization, which is one of the easiest and most straight forward techniques to control a radical polymerization and prepare block copolymers from a huge variety of monomers, without adding transition metal catalysts. As hole conducting block both **TPA** and **TPD** (**polymer 2**: **t**etra**p**henylbiphenyl**d**iamin) macrointiators were synthesized in the first step (see Scheme 1, **M1** and **M2**). While **TPA** has a better match in energy levels for a device structure, **TPD** has a better hole mobility and is

chemically and electrically more stable. To produce an anchoring and light absorbing block copolymer, a post polymerization modification method was applied[18] (see Scheme I). We used pentafluorophenolacrylat as a reactive ester monomer for the second block. This structure is highly reactive towards amines and the polymers are well soluble and characterizable (^{19}F NMR, IR). Homo and block copolymers can be obtained with a low polydispersity and moderate molecular weight (see Scheme 1 and Table 1, Supporting Information S1)). To introduce the light absorbing dye and the anchor an amine group containing perylene derivative (*^{1}N*-(8-pentadecan)-*^{2}N*(2-aminoethyl)perylene-3,4:9,10-tetracarboxdiimide; for details in synthesis see Supporting Information) and dopamine were added in a ratio of 10: 2. This yields the final **polymer1** and **polymer 2**. Dopamine is a strong anchor to oxidic semi conductors[19] and was already applied to anchor dye molecules to TiO_2 surfaces.[20] The post polymerization modification concept offers the possibility to introduce a large variety of functional compounds by a simple reaction.

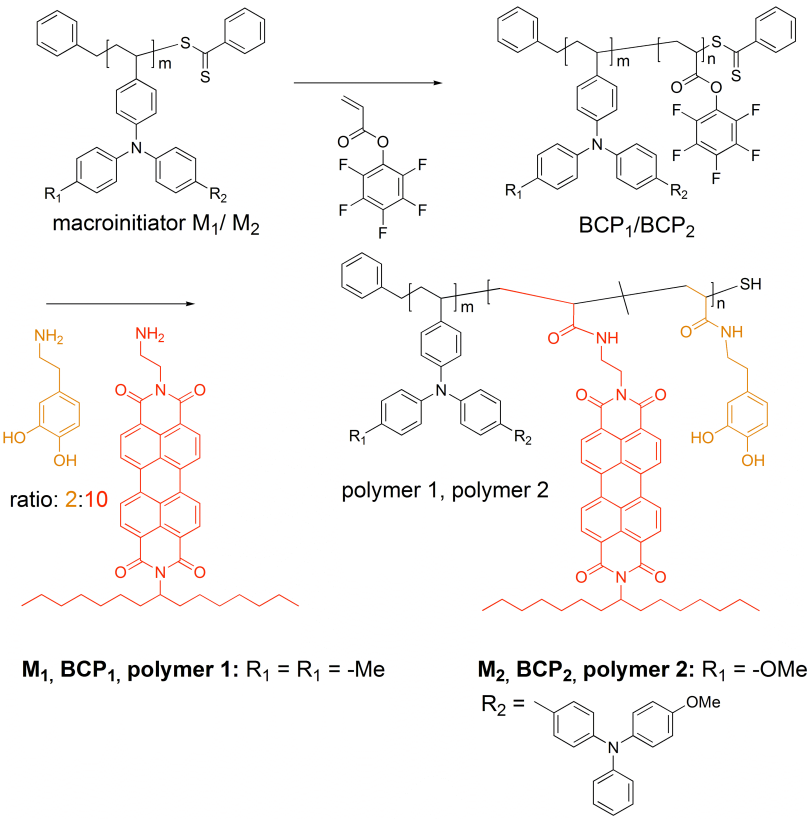

Scheme 1.
Synthetic scheme for the functional block copolymers.

Size exclusion chromatography with UV Vis detection at 520 nm (the maximum absorption of the dye) proves the binding of the dye molecules to the polymer backbone (see Supporting Information). Since the perylene dye is rather bulky it cannot be linked to every reactive ester unit. The dopamine anchor group is less sterically demanding. Thus after conversion with the mixture of dye and anchor group the ^{19}F NMR signal of the reactive ester vanishes. UV vis spectroscopy analysis shows that 30 % (about 10 units) of the reactive ester units have reacted with the dye. The residual reactive ester groups reacted with dopamine. Hence, every polymer chain contains perylene and the dye molecules are located near the surface, which is important for a charge transfer process.

Table 1.
Analytical data of the polymers (see Scheme I).

	M_n /g mol^{-1} (styrene equivalents)	repeating units	PDI
M1(TPA)	2.07 x 10^4	m = 70	1.11
BCP 1 TPA	2.79 x 10^4	n = 30	1.14
M2 (TPD)	3.16 x 104	m = 55	1.10
BCP2 (TPD)	3.87 x 10^4	n = 30	1.24

Cyclovoltammetry measurement of the polymer shows the redox cycles of the hole- and the electron conducting part (see Supporting Information). Reversible cycles can be measured in the positive range for the triphenylamine containing moiety as well as in the negative scanning area (reduction of the perylene containing block). The energy levels of the different moieties were determined by cyclovoltammetry and UV vis spectra. They are as expected. If the dye (HOMO: -6.0 eV) absorbs a photon the promoted electron (LUMO: - 3.6 eV) can be injected into the semiconductor conduction band (in the case of ZnO - 4.4 eV). (see energy diagram Supporting Information S4) The vacant HOMO level of the dye is reduced by the p-type triphenylamine moieties (HOMO (TPA): - 5.1 eV, HOMO (TPD): - 5.0 eV).

To functionalize ZnO nano-particles (nanorods with a length to width of 150 : 20 nm) a dispersion of nanorods in the solution of anchor group containing polymer is sonicated . A slightly scattering, pinkish solution is formed. High Resolution (HR) TEM images of spin coated films show clearly the individually dispersed particles with polymer corona bound to the particle surface (see Figure 2B). The functionalized nanorods are soluble in all solvents of the surrounding polymer corona like toluene and tetrahydrofuran and dispersions of the functionalized ZnO nanorods are stable for many weeks while non-functionalized rods sediment in a few minutes.

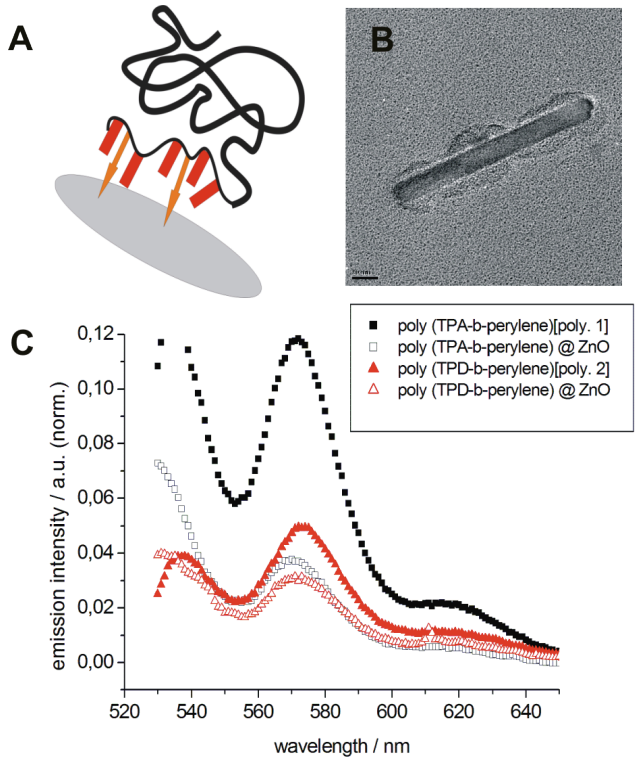

Figure 1.
A) Schematic presentation of the polymer functionalized particles (red squares: perylene, orange arrows: dopamine anchor groups, black chain: hole conducting polymer chain), B) HR TEM of a ZnO nanorod functionalized with polymer; the polymer corona is clearly visible; C) photoluminescence spectra of polymer 1 and 2 (in solution) and polymer 1 and 2 (bound to ZnO). The excitation wavelength is 520 nm. The emission intensity of the pure dye at 565 nm amounts to 1 compared to the values (in a.u.) shown here. (full sized spectrum see Supporting Information S4). Thus fluorescence is quenched in the copolymer and -even more- in the functionalized nanorods.

For perylene dyes it is known that upon photo excitation excitons are created, which are able to dissociate at the donor-acceptor interface.[21] Thus the strong quenching of perylene fluorescence observed for the block copolymer and especially for the block copolymers bound

to the ZnO nanocrystals is not unexpected. After the dye is bound to the hole conducting polymer photoluminescence drops by 88 % in the case of **polymer 1** and 95 % in the case of **polymer 2**. The remaining fluorescence of the block copolymer decreases by nearly 70% for polymer 1 and 40% for polymer 2 upon binding to the nanocrystals (see Figure 1). This fluorescence quenching is high in comparison with similar donor – acceptor systems,[22] because the dye is located near the particle surface between ZnO due to the anchor groups in the same block (see Scheme in Figure 1).

The efficient quenching is a hint for energy or even electron transfer from the dye into the nanorod. In order to elucidate this charge transfer on a single particle level Kelvin probe force microscopy was carried out. This method detects local variations in surface potentials with a lateral resolution[23] in the order of 10 - 50 nm. A sample containing nanoparticles functionalized with **polymer 1** and **polymer 2** was spin coated on a transparent and conductive substrate (ITO). The sample can be illuminated by laser light at a wavelength of $\lambda = 488$ nm and intensity ~1 W/cm² through the ITO substrate (Figure 2a). Upon light absorption charge separation takes place and the internal potentials in the particle-polymer system change. Thus, two different surface potential maps of the functionalized particles were obtained in the dark (Figure 2b) and upon laser illumination (Figure 2c). The potential maps showed several elongated structures of 200 to 400 nm length and 80 to 100 nm width, which can be associated to particles on the surface (topography image: see Figure S6 in the supporting information). For ZnO modified with **polymer 1** in the dark (non illuminated sample) a potential difference of up to 65 mV between the particle and the surrounding polymer corona was observed (Figure 2(b) and blue line in Figure 2(d)). This potential difference can be attributed to the workfunction difference of the respective materials which is in qualitative agreement with the proposed energy diagram (S4 in the supporting information). Upon illumination the potential contrast increased to 100 mV. The line profile across one of the structures demonstrated that the increase in potential contrast originates from a decrease of

the potential in the particle by 10 mV and an increase in the potential in the proximity to the particle by up to 25 mV (Figure 2 (d)). On the right hand side of this line profile, the light induced potential change can be observed even at a distance of 200 nm from the ZnO particle. This behaviour was observed for almost all particles coated with **polymer 1** or **polymer 2** that were investigated by KPFM. We associate this observation to a negative charging of the ZnO particle core and a positive charging of the polymeric corona. Finally, in a control experiment with Polystyrene coated particles no internal potential changes in the nanorod system were observed. In conclusion, the KPFM data showed that light induced charge separation comparable to a dye sensitized solar cell can take place on the level of a single nanoparticle.

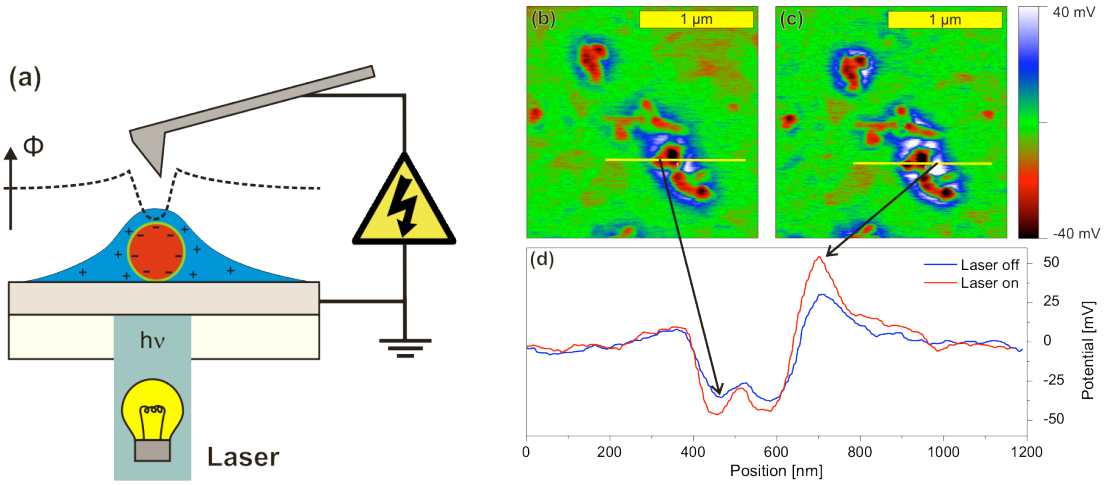

Figure 2.
(a) Schematic view of the Kelvin probe force microscope (KPFM) on top of a of a polymer functionalized nanorod upon irradiation with light. (b, c) Surface Potential maps (Kelvin probe force microscopy) in the dark (b) and (c) under illumination. The minimum in surface potential is associated to the ZnO nanorod (black to red). In surrounding of these nanorods the surface potential increases (colour blue to white). The latter potential is attributed to the patchy polymer corona in agreement with the TEM results provided in Fig 1b. At distance > 200 nm from the ZnO nanorod no surface potential changes were observed. (d) line profiles of the measured surface potential across a polymer functionalized nanorod (red corresponds to laser on, blue to laser off).

These results show that the combination of a block copolymer containing a sensitizer and hole transporter with a semiconducting oxide creates a p-n junction, that allows to separate charges and induce a charging of single particles. The system creates a solar cell like structure in each single particle, inducing potential differences of some tens of millivolts. The flexible

synthesis concept with functionalization by post polymerization modification allows introducing various dyes for sensitisation at different wavelength and introduction of various anchor groups for anchoring on different particles. The hybrid materials are an interesting approach to create and investigate processes in a dye sensitized solar cell on a single particle level.

Experimental Section

Generals: All raw materials were purchased by Aldrich. α,α'-azoisobutyronitrile (AIBN, from Fluka) was recrystallized from diethyl ether, dopamine hydrochloride and cysteamine (3-hydroxy tyramine hydrochloride, from Acros) were used as purchased. ZnO nanorods were synthesized according to literature.[24] Solvents used to prepare nanoparticle dispersions all were distilled before usage. Tetrahydrofuran used for polymerization was dried over Na/K and distilled. TPA monomer and TPD monomer and the chain transfer agent were synthesized according to literature.[25]

Gel permeation chromatography (GPC) was carried out in THF as solvent and the detector system contained refractive index (Jasco), UV-Vis (Jasco) and light scattering (Wyatt) detectors.

NMR spectra were obtained in a Bruker AC 300. Infrared spectroscopy was done in a Bruker Vector 22, UV-Vis spectroscopy was measured in a Shimadzu UV 2102 PC UV-Vis Scanning Spectrophotometer.

Cyclovoltammograms were obtained with an Autolab P30 potentiostat. We used an undivided cell and three electrode configurations with a platinum mesh as counter electrode. As reference electrode an Ag/AgCl electrode was chosen. We used THF as a solvent containing 0.1 M tetrabutylammonium tetrafluoroborate (Aldrich) as a conducting salt. The samples were measured in solution. The system was calibrated against a ferrocene standard.

High Resolution Transmission Electron Microscopy was carried out with a JEOL JSM-890 operated at 200 kV. Photoluminescence spectroscopy was measured with

Scanning Electron Microscopy was measured with a FEI Nova 600, dual beam setup at an electron energy of 5 keV.

Kelvin Probe Force Microscopy was done using a modified MFP-3D standalone setup (Asylum Research, Santa Barbara). The cantilevers with a nominal resonance frequency of 70 kHz and a backside Al-coating were from Olympus (OLYMPUS OMCL-AC240TS). The setup was equipped with a sample illumination optics using a diode laser (Point Source) with a wavelength of 488 nm, power of 12 mW and intensity on the sample of ~ 1 Wcm^{-1}. The SFM is placed in an acoustic chamber that shields the measurement from scattered ambient light and in a glove box under low humidity (<0.1%) and low oxygen (<0,01%) conditions. The laser needed for the detection of the cantilever deflection has a wavelength of 860 nm (power < 1mW) which is uncritical for the measurement, as the system shows no absorption in this spectral region (see Supporting Information S2).

Synthesis of dye and anchor group functionalized polymers: 3 g monomer (150 eq), 15.1 mg 2-phenylpropan-2-ylbenzodithioate/chain transfer agent (0.06 mmol, 1eq) and 0.9 mg AIBN (0.006 mmol, 0.1 eq) were dissolved in THF in a Schlenck tube. Oxygen was exchanged by nitrogen in three freeze-pump-thaw cycles and polymerisation was carried out at 63 °C for 24 h. The polymer was purified by repeated precipitation in methanol and petrolether to yield the desired yellow-orange polymer.

To synthesize the reactive block copolymer, the macroinitiator and 50 eq pentafluorophenylacrylate per polymer chain were dissolved in THF and oxygen was exchanged by nitrogen in three freeze-pump-thaw cycles. Polymerization was carried out at 63°C for 3 d. The polymer was purified by repeated precipitation in methanol to yield the reactive blockcopolymer.

The reactive block copolymers were dissolved in THF together with H, dopamine hydrochlorid (10:2) and NEt_3 and stirred over night. The polymer was precipitated in methanol and petrolether for several times to get the functionalized deep red polymer quantitatively.

Poly(TPA-b-perylene): ^{1}H NMR (d^8-THF, 300 MHz): 8.64 (m, 0.1 H, perylene), 7.0-6.30 (m, 12 H, TPA-Ar-H), signal of perylene dye can not be distinguished from the noise, 2.12 (bs, 6H, -Me), 1.75-0.43 (m,~ 5H, assignment not possible)

Poly(TPD-b-perylene): ^{1}H NMR (d^8-THF, 300 MHz): 8.64 (m, 0.05 H, perylene), 6.84 (m, 25H, ArH), 3.73 (m, 6H, -OMe), 2.54 – 1.19(m, 7H, assignment not possible).

Acknowledgement

This work was financially supported by the International Research Training Group: Self Organized Materials for Optoelectronics Mainz-Seoul jointly supported by the DFG (stipend for M. Zorn and S. Weber), the Korea Science and Engineering Foundation (KOSEF) and BMBF "OPV-Stabilität" (FKZ 03SF0334C). Thanks to K.S. Kim and Prof. B. H. Sohn (Seoul National University) for help with photoluminescence spectroscopy.

References

1 O´Regan, B.; Grätzel, M.*Nature* **1991**, 353, 737.

2 Grätzel, M. *J. Photochem. Photobiol., C* **2003**, 4, 145.

3 Kubo, W.; Kambe, S.; Nakade, S.; Kitamura, T.; Hanabusa, K.; Wada, Y.; Yanagida, S. *J. Phys. Chem. B* **2003**, 107, 4374–4381.

4 Beek, W. J. E.; Wienk, M. W.; Janssen, R. A. J. *Adv. Mater.* **2004**, 16, 1009.

5 Huynh, W. U., Dittmer, J. J., Alivisatos, A. P., *Science* **2002,** 295, 2425.

6 Li, C.; Liu, Z.; Schöneboom, J.; Eckemeyer, F.; Pschirer, N. G.; Erk, P.; Herrmann, A.; Müllen, K. *J. Mater. Chem*. **2009**, 19, 5405.

[7] Sommer, M.; Lindner, S. M.; Thelakkat, M. *Adv. Funct. Mater*. **2007**, 17, 1493.

[8] Ferrere, S.; Zaban, A.; Gregg, B. A. *J. Phys. Chem. B* **1997**, *101,* 4490-4493.

[9] Wang, M.; Wang, X. *Sol Energ. Mat. Sol. C*. **2008**, 92, 766-771.

[10] Bach, U.; Lupo, D.; Comte, P.; Moser, J. E.; Weissörtel, F.; Salbeck, J.; Spreitzer, H.; Grätzel, *Nature* **1998**, 395, 583.

[11] Kwong, C.Y.; Choy, W.C.H.; Djurisic, A. B.; Chui, P. C.; Cheng, K. W.; Chan, W. K.; *Nanotechnology* **2004**, 15, 1156

[12] Schmitz, C.; Thelakkat, M.; Schmidt, H.-W. *Adv. Mater*. **1999**, 11, 821-826.

[13] Wang, H.; Klubek, K. P.; Tang, C. W. *Appl. Phys. Lett*., **2008**, 93, 093306.

[14] Jang, S.-R.; Lee, C.; Choi, H.; Ko, J.J.; Lee, J.; Vittal, R.; Kim, K.-J. *Chem. Mater*. **2006**, 18, 5604-5608.

[15] Zorn, M.; Bae, W. K.; Kwak, J.; Lee, H.; Lee, C.; Zentel, R.; Char, K. *ACS Nano* **2009**, 3, 1063-1068.

[16] Behl, M.; Zentel, R. *Macromol. Chem. Phys*. **2004**, 205, 1633.

[17] Behl, M.; Hattemer, E.; Brehmer, M.; Zentel, R. *Macromol. Chem. Phys*. **2002**, 203, 50.

[18] Zorn, M.; Zentel, R.; *Macromol. Rapid. Commun*. **2008**, 29, 922 - 927.

[19] Zorn, M., Meuer, S., Tahir, M.N., Khalavka, Y., Sönnichsen, C., Tremel, W., Zentel, R. *J. Mater. Chem*. **2008,** 18, 3050

[20] Rice, C. R.; Ward, M. D. ; Nazeeruddin, M. K.; Grätzel, M. *New. J. Chem*. **2000**, 24, 651.

[21] Planells, M.; Cespedes-Guirao, F. J.; Forneli, A.; Sastre-Santos, A.; Fernandez-Lazaro, F.; Palomares, E. *J. Mater. Chem*. **2008**, 18, 5802.

[22] Ravichandar, R.; Thelakkat, M.; Somanathan, N. *J. Fluoresc*. **2008**, 18, 891 – 898.

[23] Berger, R., Butt, H.-J., Retschke, M. B., Weber, S. A. L. *Macromol. Rapid Commun*. **2009**, 30, 1167

[24] Cheng, B.; Shi, W.;. Russell-Tanner, J.M ; Zhang, L.; Samulski, E.T. *Inorg. Chem*. **2006**, 45, 1208.

[25] Kido, J. Hurada, G.; Nagai, K. *Chem. Lett*. **1996**, 161.

3.5.

Quantum Dot-Block Copolymer Hybrids with Improved Properties and Their Application to Quantum Dot Light-Emitting Devices

Matthias Zorn, Wan Ki Bae, Jeonghun Kwak, Hyemin Lee, Changhee Lee, Rudolf Zentel, Kookheon Char

ACS Nano, **2009**, 3, 1063-1068.

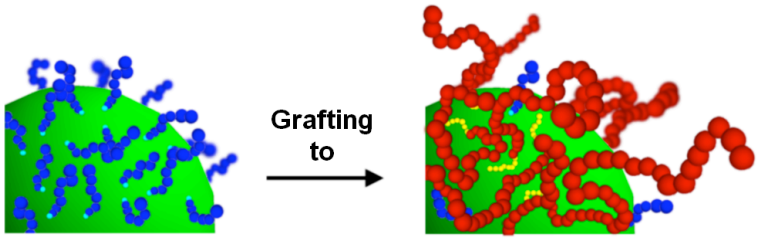

As another important kind of nanoparticles we modified the surface of quantum dots (synthesized by Wan Ki Bae) with a polymer. Quantum dots (CdSe@ZnS) as strongly luminescent particles with a very sharp luminescence wavelength can be applied in light emitting devices. For this application of QDs we used a triphenylamine block copolymer. As an anchor the reactive block was reacted with cysteamine (poly(*para*-methyl triphenylamine-*b*-cysteamine acrylamide)). The modification is performed by a phase transfer which allows the assumption that the particles are completely functionalized. Due to the polymer functionalization the particles are sterically stabilized and show an increased stability upon UV illumination.

Also in terms of processing the particles show an improvement. Due to the polymer corona it is possible to create free standing films from the functionalized particles, due to polymer entanglement. This is especially important for the preparation of devices.

Due to the hole conducting shell light emitting devices can be prepared with the hybrid combining the hole conducting and the emitting layer (device preparation and analysis:

Jeounghun Kwak).The devices containing the hybridized emitting layer, show even without optimization of the device setup an improved efficiency. The devices were optimized and published separately.** The optimized and well characterized devices showed efficiencies higher than 1.5 %.

* This work was mainly conducted in the laboratory of Prof. Kookheon Char and Prof. Changhee Lee, Seoul National University

** J. Kwak, W. K. Bae, **M. Zorn**, H. Woo, H. Yoon, J. Lim, S. W. Kang, S. Weber, H.-J. Butt, R. Zentel, S. Lee, K. Char, C. Lee; Characterization of Quantum Dot/Conducting Polymer Hybrid Films and Their Application to Light-Emitting Diodes, *Adv. Mater*, **2009**, 21, 5022- 5026.

Introduction

Due to their size in the nanometer range, quantum dots (QD) show an interesting physical behavior that is totally different from the properties exhibited by bulk material. This effect is known as the quantum confinement effect. For semiconducting QDs such as CdSe or CdTe, fluorescence and emission properties can be varied over a broad range in the electromagnetic spectra simply by tuning the particle size. High fluorescence quantum yield and high optical stability make the quantum dots potentially important nanomaterials for photovoltaic cells,[1] bio sensors[2] or light-emitting diodes.[3] Compared with their counterparts such as organic fluorescent small molecules and polymers, quantum dots offer the combination of solution processing with the high efficiency of fluorescent inorganic materials. However, quantum dots do not yet show additional desired properties known from polymers, such as film formation and the possibility for inkjet printing.[4]

Inorganic-organic hybrid materials that combine the unique properties of inorganic and quantum-confined particles with that of polymers are therefore interesting candidates for combining the two desired properties in a synergistic way. Polymers can provide various properties such as solubility in different solvents and film formation. Recently we could show that the solubility of inorganic nanoparticles can be strongly improved with suitable block copolymers.[5] In these block copolymers a short anchor block binds strongly to the nanoparticle, while the second block creates a soft shell and acts as a steric stabilisation for the inorganic nanoparticle. In addition properties like a stimuli-responsive behaviour, e.g. for switchable dispersions,[5] gets possible. Further, surface functionalization with polymers allows the direct linkage of organic and semi conducting materials[6] to an inorganic core as described in this article. This might improve the injection of electrons and holes into the quantum dot. Like surfactants polymer chains grafted onto the surface of inorganic nanomaterials protect the inorganic nanomaterials from aggregation, and increase the solubility and miscibility of such inorganic nanomaterials in an organic host. In addition they might improve film formation, an important property that influences the device characteristics of optoelectronic components.

Generally polymer chains can be introduced by two methods. One is a polymerization from the nanoparticle surface (grafting-from approach). For this purpose, an initator like a radical

or ROMP starter,[7] a dithioester for RAFT polymerization,[8, 9] or a halogen containing surfactant for ATRP[10] has to be linked to the particle surface. It is also possible to anchor pre-made polymers containing anchor groups at the chain end(s)[11] or an anchor block by simple ligand exchange. This grafting-to approach will be used here. It has the advantage that the polymer for surface modification can be characterized very well before grafting.

In this article, we describe the synthesis of a block copolymer (BCP) containing a semiconducting block based on triphenylamine (TPA) moieties and a short reactive ester block, which allows to introduce the desired anchor groups.[12] Triphenylamine polymers and small molecule TPA derivatives are known to show good hole conducting properties in the bulk state. They are easy to process and relatively well known materials for applications in OLEDs[13] and photovoltaics.[14] The short multidentate anchoring block binds to the particle surfaces effectively. In this case we used thiol-based anchor groups to bind to Zn-chalcogenide based QDs (i.e., CdSe@ZnS QDs). The resulting inorganic-organic hybrid materials consist of the inorganic core, wrapped by the short anchoring block and surrounded by a shell of triphenylamine polymers. With regard to light emitting devices, the semiconducting polymer brushes also improve the hole injection into the quantum dots. By the simultaneous injection of electrons from a counter electrode, excitons will be formed within QDs and photons with a characteristic wavelength relevant to the QDs will be emitted. By testing such hybrid materials for QLED devices, we could demonstrate that the turn-on-voltage and the efficiency of QLEDs could be improved by employing such QD/polymer hybrid materials in multilayered devices.

Results and Discussion

To prepare semiconducting block copolymers with anchor groups for CdSe@ZnS QDs, RAFT polymerization was chosen for the controlled radical polymerization, as this method can be applied to many radically polymerizable monomers. *Para*-methylated vinyltriphenylamine (TPA) was used as a hole conducting species. It can be polymerized in a controlled radical way by NMP and RAFT polymerization.[6,15] We used 2-phenylpropan-2-yl benzodithioate as a chain transfer agent, as already described in previous work.[16] By using pentafluorophenylacrylate as a monomer for the second block, it is possible to introduce

various types of anchor groups for inorganic materials (see Figure 1). The reactive ester blocks can be converted with any kind of primary amines to introduce functionality to such blocks.[6] For binding to the QD surfaces, the reactive esters were treated with cysteamine and thus transformed into poly(*para*-methyl triphenylamine-*b*-cysteamine acrylamide) (PTPA-*b*-CAA) block copolymers. Because of the thiol-containing anchor blocks with multiple binding sites, the adsorption of such BCPs at QD surfaces is much more efficient than the adsorption efficiency of end-functionalized polymers or monodentate surfactants often used for the synthesis of well-defined nanoparticles.

The block copolymerization can be monitored by GPC and NMR. The conversion of the reactive ester block can be followed by ^{19}F NMR and IR spectroscopy, showing the split-off of pentafluorophenole moieties followed by the appearance of the absorption characteristic for amides at 1680 cm^{-1} after the reaction with cysteamine. Both methods demonstrate the conversion to be quantitative.[17] Due to the controlled radical polymerization, block copolymer **P2** could be prepared with a low polydispersity (PDI ~1.2). (see Supporting Information **S1**). We prepared two block copolymers with different molecular weights. Table 1 gives the analytical data of GPC analysis (PS equivalents). The GPC traces of the BCP show a shoulder at higher molecular weights due to oxidative disulfide bridges between the thiol groups in the anchor block. The tested polymers (50 and 100 repeating units of TPA, see Table 1) showed similar properties in the hybrid case.

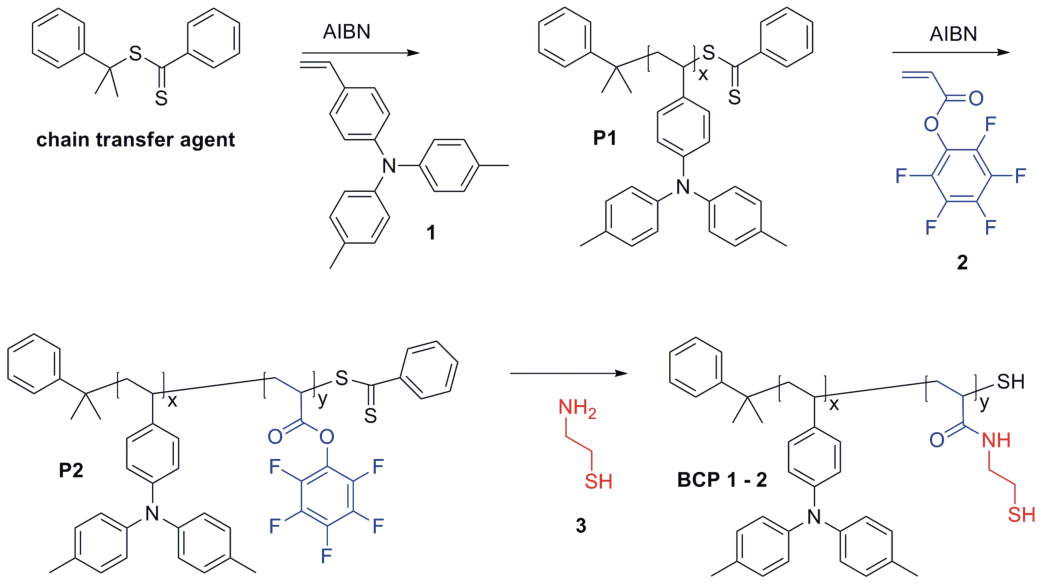

Figure 1.

Synthetic scheme for poly(*para*-methyl triphenylamine-*b*-cysteamine acrylamide) (PTPA-*b*-CAA) (P3) derived from triphenylamine (1) and pentafluorophenylacrylate (PFA) (2) through RAFT polymerization followed by the polymer analogous conversion with cysteamine (3) (P1: poly-TPA, P2: poly-TPA-b-PFA).

Table 1. Analytical data for the prepared block copolymers (based on GPC data (PS equivalents))

	M_n (P1)	x	M_n (P2)	y	PDI (P2)
BCP 1	$1.5x10^4$	50	$1.7 x10^4$	10	1.16
BCP 2	$3.0 x10^4$	100	$3,2 x10^4$	10	1.23

For the hybridization with inorganic nanomaterials, CdSe@ZnS quantum dots were employed, which were prepared by the one-pot synthesis from our laboratory[18] and already investigated in QLEDs.[19] Since oleic acid was used as a surfactant for the QDs, oleic acid chains are bound to the QD surface during the synthesis. By variation of the size and the composition of the core, the emission colors can be varied over a wide range of the spectrum.[18] The results presented here were obtained with green emitting QDs while stability tests were performed with blue emitting QDs.

The quantum dots were functionalized with the block copolymers **(BCP1 and 2)** by the ligand exchange procedure, which is driven by the strong enthalpic binding of multiple thiols in the anchoring blocks, displacing the weakly bound carboxylic acid groups derived from oleic acid. The exchange reaction was performed under phase transfer conditions. The oleic acid-capped QDs are soluble in chloroform, tetrahydrofurane, and hexane, while insoluble in dimethylformamide (DMF) and water. An immiscible solvent pair of hexane (a good solvent for QDs) and DMF (a good solvent for TPA polymer) was chosen for monitoring the phase transfer of QDs from hexane to DMF as a proof for the functionalization of QD surfaces (see Figures 2(a) and 2(b)).

To cover the QD surfaces with semiconducting triphenylamine polymers, 6 mg of PTPA-*b*-CAA (P3) was dissolved in 1 mL DMF and 20 mg of green QDs was dissolved in 1 mL of hexane. Due to the immiscibility between hexane and DMF as well as the insolubility of QDs in DMF and of the block copolymers in hexane, this combination gives a two-phase system. By ultrasonication, it is possible to transfer the QDs to the DMF phase by displacing oleic acids with the block copolymer brushes. Due to the excess amount of QDs in the two phase

mixture, all the block copolymer chains in the DMF phase should be bound to the QD surfaces while residual unmodified QDs remain in hexane after surface modification procedure. The hexane phase can be thus separated and the QDs transferred to the DMF phase can be purified for further experiments. The QDs functionalized with the block copolymers show the same solubility behaviour as the block copolymer itself, providing the evidence for sufficient surface modification of QDs (see Figure 2). The functionalized QDs were then precipitated in methanol three times to remove displaced oleic acids and were washed with hexane to eliminate unmodified QDs (capped with oleic acid) which might be accidentally transferred to the DMF phase during the ultrasonication process.

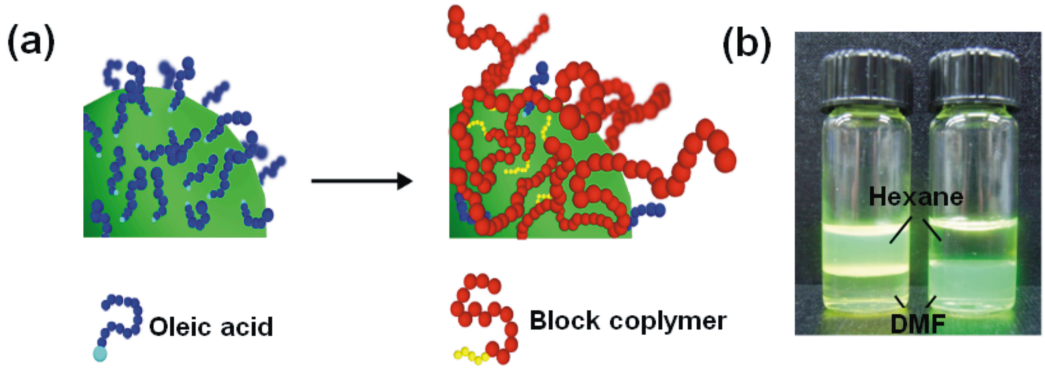

Figure 2. (a) A schematic presentation of QD functionalization and (b) a photograph showing the hybridization of QDs with PTPA-*b*-CAA through the phase-transfer method (hexane on top and DMF at the bottom in immiscible mixture). Left vial: QDs dissolved in hexane over DMF, Right vial: QDs functionalized with BCP in DMF.

In order to determine the degree of substitution of oleic acid with block copolymer, NMR spectroscopy and thermal gravimetric analysis (TGA) were used. NMR spectra reveal that the QDs still retain oleic acid on the surface to some extent. Comparing the signals of the oleic acid double bond with the aromatic protons from triphenylamine, a relative ratio of 1: 5 was estimated (one oleic acid to 5 triphenylamine moieties). Consequently, a complete exchange of oleic acids was not possible, but the majority of the bound organic material is now polymeric. Therefore block copolymers anchoring to the QDs mostly influence the solubility and the properties of the hybrid materials.

TGA analysis could also be used to determine the content of organic species attached to the QD surface. Data were taken at a heating rate of 20 K/min in nitrogen atmosphere. For

the oleic acid-capped QDs, the degradation temperature, which is defined as the temperature at which 5 wt% of organic species is burned off, is determined to be 388 °C. The weight loss shows that about 20 wt% of the oleic acid-coated QDs consist of the organic surfactants. For the triphenylamine-containing block copolymer, the degradation temperature was found to be 350 °C and we also found that the block copolymer depolymerises almost completely (~ 4 wt% solid content left). The organic species in the QD/polymer hybrid material shows the degradation temperature at 350 °C, which is the same as the temperature found for the BCP. A second step around 388 °C was not observed. In the hybridized QDs 30 - 40 wt% is organic material, composed of a mixture of the semiconducting block copolymer and oleic acid. The increase in the organic materials attached to the QD surface and the reduced degradation temperature indicates that the QD surfaces are covered mainly by block copolymer chains (see Supporting Information Figure **S2**).

A photoluminescence spectrum of the QD/polymer hybrid material shows that 80 % of the PL intensity remains after grafting the QD surfaces with block copolymer. This is a high intensity value compared with other functional QDs in which fluorescence drops mostly after surface modification. (see Supporting Information Figure **S3**).

The hybridized QDs consist -in analogy to earlier work[5]- of an inorganic core (CdSe@ZnS) around which the short anchor block is wrapped, while the triphenylamine polymer acts as a polymeric shell. To determine the nature of colloidal state of the hybridized QDs dynamic light scattering and AFM measurements were performed. AFM measurements show mostly individual QDs in combination with small aggregates. Dynamic light scattering gives an z – averaged hydrodynamic radius $\langle R_h \rangle_z$ of the hybridized QDs of 18 nm, which is a bit larger than the one of the pristine QDs (6 nm). As the z-averaged weighs aggregates much stronger than the individual QDs this result is coincident with the AFM-measurements (number majority of individual QDs plus small aggregates, see Supporting Information Figure **S4**)

Experiments to test the colloidal stability of QDs demonstrate the improved stability of the QD/polymer hybrids in comparison with pristine QDs with oleic acids bound to the surface or QDs covered with hexadecylthiol (prepared by ligand exchange).[19] We used blue emitting QDs which are instable under continuous UV illumination. It was noted that QDs covered with small molecules massively agglomerate under UV illumination (@ 365 nm with

2 mW/cm^2) for two hours, while QD/polymer hybrids show extended stability under the continuous illumination for more than 30 hours in chloroform (see Figure 3). The improved colloidal stability is due to two reasons: at first, longer polymer brushes attached to QD surfaces provide the enhanced steric stabilisation of the colloidal QD dispersions, preventing agglomeration of QD particles. Secondly, we can also assume that the UV illumination breaks the bonds between small molecule surfactants and the QD surfaces. The unprotected QDs tend to agglomerate massively. In the case of the multidentate ligands, the probability that all the anchoring bonds are broken is quite unlikely. As a result, the QD/polymer hybrids are quite stable in dispersion due to the strongly bound steric stabilization layers.

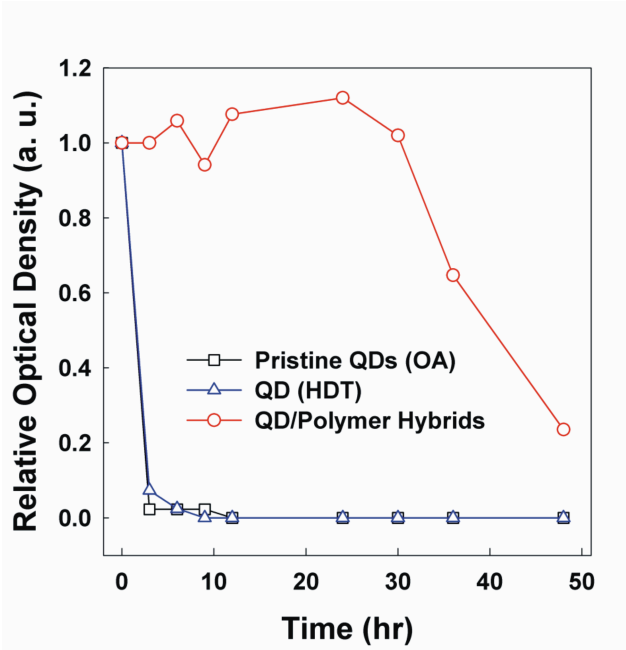

Figure 3.
Test for colloidal stability of the QD/polymer hybrid (blue emitting QDs) under illumination in comparison with oleic acid and hexandecanthiol (HDT) coated QDs in $CHCl_3$. While pristine QDs and HDT coated agglomerate during illumination (365 nm, 2 mW/cm^2) QD/polymer hybrids are stable for more than 30 hours.

The QD/polymer hybrids show, due to the polymer brushes (~ 40 wt%) attached to QD surfaces, good film formation properties, similar to QDs carrying crosslinkable ligands.[20] The surface morphology of thin films was tested by AFM measurements with regard to the chain length of the grafted polymer. The RMS roughness varies slightly with the molecular weight. While films of QD functionalized with **BCP 1** (50 TPA units) exhibit a roughness of 2.7 nm **BCP 2** grafted QD have a slightly higher RMS roughness of 4.1 nm, due to the increased radius with higher molecular weight soluble blocks added to the QD surface. Also thin layers

of QD/polymer hybrids spun coated on a mica substrate can be floated on water surface yielding a free standing film of the quantum dots. From thicker layers (around 500 nm) large films can be floated off intact (Figure 4). By varying solution concentration thin free standing films from polymer hybridized QDs could be prepared. Thin layers (< 100 nm) allow the direct visualisation by TEM (Figure 4). This is not possible with pristine QDs capped only with oleic acids. Ellipsometric measurement of the film deposited on a silicon wafer shows the average film thickness of about 60 nm from 0.5 wt% solution of the QD/polymer hybrids dissolved in toluene and spun at 4000 rpm. This value showed to be the best for device application in terms of low turn-on voltage and EQE at moderate current density as experiments with different concentrations for device preparation demonstrated. This value was taken as an ideal standard film thickness for the preparation of light emitting devices.

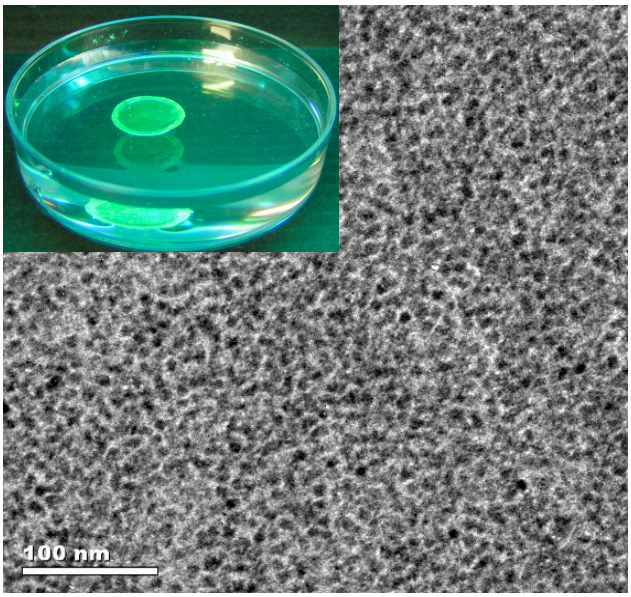

Figure 4. (Upper left picture) QD/ PTPA-*b*-CAA hybrid film (size about 1 cm) floated on water surface (from KBr pellet; optical picture) and a TEM image of the corresponding thin free standing film.

QLEDs with a multilayer structure of ITO / PEDOT:PSS (40 nm) / QDs or QD/PTPA-*b*-CAA hybrids / TPBI (40 nm) / LiF (0.5 nm) / Al (1000 nm) were prepared as test devices (Figure 5(a) and Figure 5(b) for the corresponding band diagram). The QLED based on QD/PTPA-*b*-CAA hybrids for the emitting layer shows improved device performance in terms of device efficiency compared with the QLED based on pristine (or unmodified) QDs (Figures 5(c) and 5(d)). These improvements in device performance are mainly attributed to the electrical and

physical properties of PTPA-*b*-CAA encapsulating the QDs. The HOMO energy level of PTPA-*b*-CAA resides between the valence band edge energy level of QDs (~ 6.8 eV) and the HOMO energy level of PEDOT:PSS (5.0 eV). Consequently, the block copolymer shell facilitates the hole injection from PEDOT:PSS into the QDs, increasing the possibility of exciton formation within (or exciton migration to) the QDs. Moreover, the PTPA-*b*-CAA brushes guarantee the uniform coating of the QD emitting layer, filling up voids between adjacent QDs due to the spherical geometry of QDs or the imperfection of QD layering process (as discussed in Figure 3). In addition, this uniform coating of the emitting hybrid layer suppress the current leakage, which can result from the direct contact between TPBI and PEDOT:PSS layers through interstitial voids or defects in the case of pristine QD layers. Owing to these combined effects (i.e. facilitated carrier injection as well as the uniform film formation), the QLED with an emitting layer based on QD/PTPA-*b*-CAA hybrids exhibits 3 folds higher device efficiency despite the comparable photoluminescent quantum efficiency (or slightly lower PL QY) of the hybrid materials when compared with unmodified QDs used as an emitting layer.

The EL spectra, shown in Figure 5(c), represent the enhanced emission from the QLED based on QD/polymer hybrids. The QLED containing QD/polymer hybrids exhibits a weak parasitic shoulder below 460 nm (presumably originating from the emission from PTPA-*b*-CAA itself - also see Supporting Information Figure **S5**) on top of a strong emission from the QDs. However the contribution to the emission from PTPA-*b*-CAA remains still quite low (less than 10 % of the total EL emission) and the enhancement of QD band edge emission is truly remarkable (increased by three times in the EL intensity). This underlines the benefits and advantages of QD/PTPA-*b*-CAA hybrids as an emitting layer for efficient QLEDs. We are confident that the QLED device can be even further improved in terms of device efficiency and color purity by introducing both hole-transporting moieties and electron- transporting moieties to copolymers (with either random or block copolymer structure) bound to QD surfaces (Further QLED characteristics : see Supporting Information Figure **S6**).

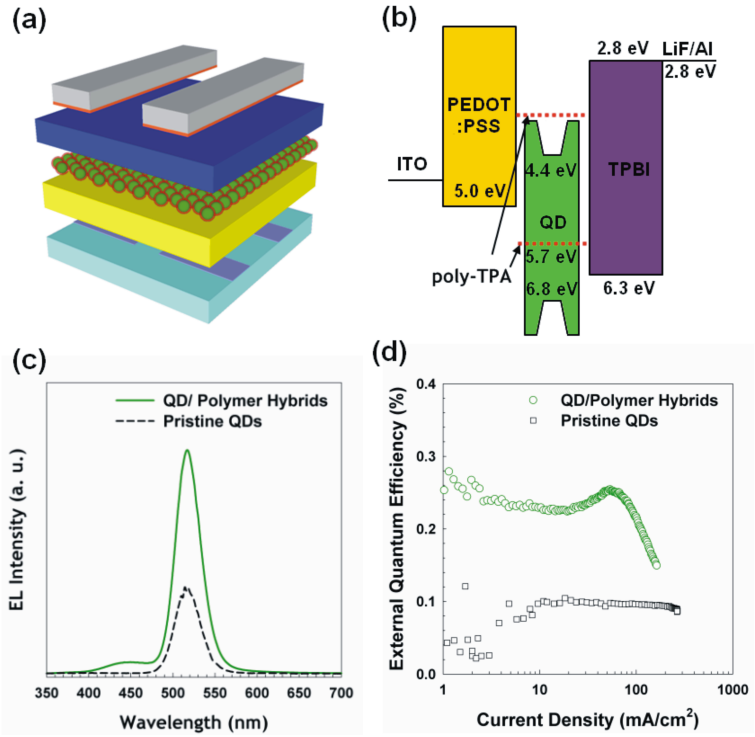

Figure 5.
(a) Schematic for the test QLED device structure and (b) the energy band diagram of QLEDs prepared, and (c) electroluminescence spectra (inset: a picture of a QLED with a pixel size of 1.4 x 3.65 mm^2) and (d) external quantum efficiencies of QLEDs based on pristine QDs (black open squares) and QD/PTPA-*b*-CAA hybrids (green open squares).

Conclusion

We have presented QD/polymer hybrids by grafting a block copolymer containing thiol anchoring groups (poly(*para* methyl triphenylamine-*b*-cysteamine acrylamide)) onto the surfaces of CdSe@ZnS QDs through the ligand exchange procedure. The QD/polymer hybrids possess both optical properties of QDs (i.e. high photoluminescence with narrow spectral bandwidth) as well as good processability based on the grafted block copolymers (i.e. enhanced solubility in typical organic solvents as well as good film forming property) along with improved colloidal stability compared with unmodified QDs (capped with oleic acid). We have also fabricated light-emitting diodes based on the new QD/polymer hybrid material, exhibiting the improved device performance (increased EL intensity at 50 mA/cm^2 and 3-fold increase in EQE) compared with the QLED device based on unmodified QDs due to the uniform deposition of QD/polymer hybrid layer for the emitting layer as well as the facilitated hole injection into the QDs. Since the approaches taken and results presented here prove positive process capability along with new functionality on QDs, these approaches can be

extended to other functional nanomaterials (such as rod, wires, tubes, and sheets) for further practical applications.

Experimental Methods

Solvents and chemicals for preparation of the hybrids and film preparation were purchased from Sigma-Aldrich and Fisher Scientific in analytical grade and used without further purification. TPA monomer and PTPA-*b*-CAA were synthesized as described in previous work,[6] and cysteamine (Sigma-Aldrich) was used as a reagent for the conversion of the reactive ester. QDs were synthesized in a one pot method as described in previous work.[18] Thermo gravimetry was carried out in a TGA 2050 instrument (TA instruments Inc.) under nitrogen atmosphere. NMR spectra were obtained in a Bruker AC 400. Transmission Electron Microscopy was performed on a CM-20, Philipps, operated at 200 kV. QD/polymer hybrid films for TEM investigations were spin coated on Mica from a 0.5 wt % solution in toluene at 4000 rpm, floated on a water surface and investigated on a TEM grid without additional layer. Thicker films were prepared by spin coating a 10 wt% solution on a KBr pellet, which was afterwards dissolved in water. A variable-angle multi-wavelength ellipsometer (Gaertner L2W16C830) was used to measure the thickness of the films.

Colloidal stability test: For the investigation of the stability of QD/polymer hybrid against UV, blue QDs were used, which are less stable against external environment. Three samples were prepared with different ligands (QDs capped with oleic acids, hexadecane thiol, QDs , **BCP**). All samples were dissolved in $CHCl_3$ and were irradiated by UV light with λ=356 nm continuously. UV-Vis spectra were measured every 3 hours. The stability of QDs against UV irradiation was characterized by analyzing the transmission of the UV-Vis spectra after exposure of UV irradiation.

Device preparation: A QD-polymer hybrid LED was fabricated by the following sequence: The ITO substrate (sheet resistance of about 10Ω/□) was cleaned ultrasonically in organic solvents (isopropyl alcohol, acetone, and methanol), rinsed in deionized water, and dried in an oven at 120 ºC for more than an hour. The substrate was cleaned with a UV-ozone cleaner prior to spin-coating PEDOT:PSS (CLEVIOS™ P VP AI 4083, H.C. Starck) and QD-hybrid material. TPBI, LiF and Al electrodes were deposited under a base pressure of 3×10^{-6} Torr by

thermal evaporation, and the evaporation speed was 1–1.5 Å/s for TPBI and 4–5 Å/s for the metals. The current-voltage (I-V) and electroluminescence (EL) characteristics were measured by using a Keithley-236 source measurement unit, Si photo-diode (Hamamatsu) and a photomultiplier-tube combined with a monochromator (Acton Spectropro-275). The measurement of EL device was conducted under vacuum.

Acknowledgements

This work was financially supported by the International Research Training Group: Self Organized Materials for Optoelectronics Mainz-Seoul jointly supported by the DFG (stipend for M. Zorn) and the Korea Science and Engineering Foundation (KOSEF). This work was also supported in part by the KOSEF through the Acceleration Research Program (R17-2007-059-01000-0), the NANO Systems Institute-National Core Research Program (NSI-NCRC) (R15-2003-032-02002-0), World Class University (WCU) Program (400-2008-0230) and the National Research Laboratory (NRL) Program grant (R0A-2008-000-20108-0). Thanks to J. Lim for his help with the graphical work and Dr K. Fischer and S. Muth (group of Prof. M. Schmidt, Mainz) for DLS and AFM measurements.

References

[1] Johnston, K. W.; Pattantyus-Abraham, A. G.; Clifford, J. P.; Myrskog, S. H.; Mac Neil, D. D.; Levina, L.; Sargent, E. H. Schottky-quantum dot photovoltaics for efficient infrared power conversion. *Appl. Phys. Lett.* **2008**, *92*, 151115.

[2] Medintz, I. L.; Clapp, A. R.; Mattoussi, H.; Goldman, E. R.; Fisher, B.; Mauro, J. M. Self-assembled nanoscale biosensors based on quantum dot FRET donors. *Nat. Mater.* **2003**, *2*, 630-638.

[3] Coe, S.; Woo, W. K.; Bawendi, M.; Bulovic, V. Electroluminescence from single monolayers of nanocrystals in molecular organic devices. *Nature* **2002**, *420*, 800-803.

[4] Tekin, E.; Smith, P. J.; Hoeppener, S.; van den Berg, A. M. J; Sasha, A. S.; Rogach, A. L.; Feldmann, J.; Schubert, U. S. Inkjet Printing of Luminescent CdTe Nanocrystal-Polymer Composites. *Adv. Funct. Mater.* **2007**, *17*, 23-28.

[5] Meuer, S.; Fischer, K.; Mey, I.; Janshoff, A.; Schmidt, M.; Zentel, R. Liquid Crystals from Polymer-Functionalized TiO_2 Nanorod Mesogens. *Macromolecules* **2008**, *41*, 7946-7952.

[6] Zorn, M.; Zentel, R. Liquid Crystalline Orientation of Semiconducting Nanorods in a Semiconducting Matrix. *Macromol. Rapid Commun.* **2008**, *29*, 922-927.

[7] Fogg, D. E.; Radzilowski, L. H.; Dabbousi, B. O.; Schrock, R. R.; Thomas, E. L.; Bawendi, M. G. Fabrication of Qunatum Dot-Polymer Composites: Semiconductor Nanoclusters in Dual-Function Polymer Matrices with Electron-Transporting and Cluster-Pssivating Properties. *Macromolecules* **1997**, *30*, 8433-8439.

[8] Roth, P. J.; Theato, P. Versatile Synthesis of Functional Gold Nanoparticles: Grafting Polymers From and Onto. *Chem. Mater.* **2008**, *20*, 1614-1621.

[9] Li, C.; Han, J.; Ryu, C. Y.; Benicewicz, B. C. A Versatile Method To Prepare RAFT Agent Anchored Substrates and the Preparation of PMMA Grafted Nanoparticles. *Macromolecules* **2006**, *39*, 3175-3183.

[10] Skaff, H.; Sill, K.; Emrick, T. Quantum Dots Tailored with Poly(*para*-phenylene vinylene). *J. Am. Chem. Soc.* **2004**, *126*, 11322-11325.

[11] Zhang, Q. L.; Gupta, S.; Emrick, T.; Russell. T. P, Surface-Functionalized CdSe Nanorods for Assembly in Diblock Copolymer Templates. *J. Am. Chem. Soc.* **2006**, *128*, 3898-3899.

[12] Eberhardt, M.; Theato, P. RAFT Polymerization of Pentafluorophenyl Methacrylate: Preparation of Reactive Linear Diblock Copolymers. *Macromol. Rapid Commun.* **2005**, *26*, 1488-1493.

[13] Wang, H.; Klubek, K. P.; Tang, C. W. Current efficiency in organic light-emitting diodes with a hole-injection layer. *Appl. Phys. Lett.* **2008**, *93*, 093306.

[14] Sommer, M.; Lindner, S. M.; Thelakkat, M. Microphase-Separated Donor-Acceptor Diblock Copolymers: Influence of HOMO Energy Levels and Morphology on Polymer Solar Cells. *Adv. Funct. Mater.* **2007**, *17*, 1493-1500.

[15] Behl, M.; Hattemer, E.; Brehmer, M.; Zentel, R. Tailored semiconducting polymers: Living radical polymerization and NLO-functionalization of triphenylamines. *Macromol. Chem. Phys.* **2002**, *203*, 503-510.

[16] Zorn, M.; Meuer, S.; Khalavka, Y.; Tahir, M. N.; Sönnichsen, C.; Tremel, W.; Zentel, R. Liquid crystalline phases from polymer functionalised semiconducting nanorods. *J. Mater. Chem.* **2008**, *18*, 3050-3058.

[17] Eberhartdt, M.; Mruk, R.; Zentel, R.; Theato, P. Synthesis of pentafluorophenyl(meth)acrylate polymers: New precursor polymers for the synthesis of multifunctional materials. *Eur. Polym. J.* **2005**, *41*, 1569-1575.

[18] Bae, W. K.; Char, K.; Hur, H.; Lee, S. Single Step Synthesis of Quantum Dots with Chemical Composition Gradients. *Chem. Mater.* **2008**, *20*, 531-539.

[19] Bae, W. K.; Kwak, J.; Park, J. W.; Char, K.; Lee, C.; Lee, S. Highly Efficient Green Light-Emitting Diodes Based on CdSe@ZnS Quantum Dots with Chemical Composition Gradient. *Adv. Mater.* **2008**, *in press*.

[20] Lin, Y.; Skaff, H.; Boker, A.; Dinsmore, A. D.; Emrick, T.; Russell, T. P. Ultrathin Crosslinked Nanoparticle Membranes. *J. Am. Chem. Soc.* **2003**, *125*, 12690-12691.

3.6.

Reduced Efficiency Roll-Off in Light-Emitting Diodes Based on Quantum Dot-Conducting Polymer Hybrids

Wan Ki Bae, Jeonghun Kwak, Matthias Zorn, Bongjun Yeom, Heeje Woo, Donggu Lee, Jaehoon Lim, Seonghoon Lee, Rudolf Zentel, Kookheon Char, Changhee Lee

Angew. Chem., **2010**, submitted

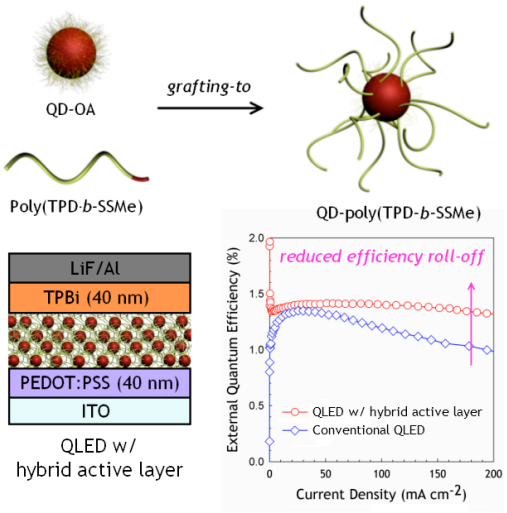

This paper shows the power and possibilities of the concept using polymer nanoparticle composites in quantum dot based light emitting diodes. We substituted the unstable hole conducting triphenylamine polymer against the more stable and already in OLED approved TPD block copolymer (poly(*N*,*N*′′-bis(4-methoxyphenyl)-*N*-phenyl-*N*-4-vinylphenyl(1,1′-biphenyl)-4,4 diamine-*b*-(2-methyldisulfanyl)ethylacrylamide). The anchor moiety was exchanged from a thiol to a disulfide group. This anchor group suppresses the cross linking of the functional block copolymer due to oxidative interchain disulfide bridge formation. The chemically and electrically stable polymer improves the injection of charge carriers into the QD. At higher current densities excitons are quenched in a standard device set up. If the luminescent particles are well distributed in the semiconducting matrix, this quenching, macroscopically seen as a roll-off in efficiency, can be avoided. The synthetic part and the

hybridization were done by Matthias Zorn, while device analysis was performed mainly by Wan Ki Bae and Jeounghun Kwak.

* This work was mainly conducted in the group of Prof. Kookheon Char and Prof. Changhee Lee, Seoul National University

Introduction

Great efforts have been devoted for the application of colloidal quantum dots (QDs) as a new type of emitting materials in next generation electroluminescent (EL) or photoluminescent (PL) devices due to their superb and unique properties, for instances, broad absorption, narrow emission (full width at half maximum (FWHM) below 35 nm) and easy color tunability over the wide range in visible region, as well as the solution process capability.[1] Since the first quantum dot based light-emitting diodes (QLEDs) were demonstrated,[2] rapid advances have been achieved in QLEDs with multilateral approaches, and recently QLEDs are realized over wide emission wavelengths in the visible region with improved device performances (i.e., maximum external quantum efficiency (EQE) above 2 % and maximum brightness above 10,000 cd m^{-2}).[3-11]

Despite the recent progress, there still are remaining issues to be resolved in QLEDs. Particularly the drastic efficiency roll-off in the range of practically applicable brightness is considered as one of the most significant problems, which restricts the practical application of QLEDs as displays or lightings. The reasons for the drastic efficiency roll-off in QLEDs at high current density and brightness, in contrast to organic light-emitting diodes (OLEDs) with similar device structure (*p*-i-*n* structure) and materials,[12] can be traced as follows: the material instability of QDs, or the narrow QD emitting layer (typically QD monolayer) which leads to the exciton quenching as a result of concentrated exciton and carrier distribution within QDs. While the stability of QDs has been improved with help of the advances in material chemistry,[13] the thickness of QD active layer is still remained as at most two QD monolayers due to the poor carrier (electron or hole) transport property between core/shell structured QDs stabilized with insulating organic surfactants (typically 1 nm length).

Recently various approaches have been introduced to improve carrier transport property within the QD multilayer films either by removing the surfactants or by replacing them with the short hydrocarbon chains or conductive organic/inorganic moieties.[14, 15] Among these

previous attempts, the hybridization of QDs with conducting polymers is regarded as one of the most advantageous and practicable methods, not only because of the enhanced carrier transport through the conducting polymer brushes and the facilitated carrier injection/separation at the interface between QDs and conducting polymer brushes, but also because of the improved colloidal stability as well as the extensive process capability of hybrids with help of the chemically grafted polymer brushes.[15]

Results and Discussion

Herein, we present QLEDs with a reduced efficiency roll-off at high current density and brightness by introducing the QD-conducting polymer hybrid active layer with broad QD distribution within the hybrid matrix. For the correlation study between QD morphology within the active layer and device characteristics, a block copolymer with chemical and electrical stability (poly(*N*,*N*′′-bis(4-methoxyphenyl)-*N*-phenyl-*N*-4-vinylphenyl(1,1′-biphenyl)-4,4diamine-*b*-(2-methyldisulfanyl)ethylacrylamide, poly(TPD-*b*-SSMe)) was newly synthesized through Reversible Addition-Fragmentation chain Transfer (RAFT) polymerization and hybridized with QDs through the *grafting-to* method. The comparison of device performances between QLEDs employing active layers with different QD morphologies reveals that the broad distribution of QDs within the active layer leads to the reduced efficiency roll-off at high current density when compared with the narrow QD distribution embedded within the carrier transport layers (conventional QLED structure), which indicates the suppressed exciton quenching within QDs at high current density due to the sufficient exciton and carrier distribution over the active layer with the broad QD distribution as well as the improved carrier balance within the organic-inorganic hybrid active layer. As a result, the QLED exhibiting the stable device efficiency of 1.38 % (Std. = ± 0.03) over the wide range of current density (1 ~ 200 mA cm^{-2}) as well as color-saturated EL emission (FWHM = 28 nm) with a maximum brightness above 7,000 cd m^{-2} can be realized.

The approaches and results in the present study address, for the first time, the reduced efficiency roll-off in QLEDs in correlation with the nanoscopic morphology of QDs, and also suggest reasonable guidelines in designing materials and device architectures of QLEDs toward the practical application as full color displays and lightings.

For the QLED fabrication, QDs with chemical composition gradient (a diameter of 8 nm, stabilized with oleic acid) were synthesized as previously reported methods (Figure S1).[13a] To disperse QDs within the hole transport layer (HTL), block copolymers with a hole transport molecule (i.e., TPD) as the side chain of the major block (~ 55 repeat units) and an anchoring moiety (SSMe) as the side chain in the minor block (~ 30 repeat units) were prepared by RAFT polymerization and a subsequent post polymerization modification of a reactive ester (Figure 1, see also Figure S2) and hybridized with QDs by the *grafting-to* method.[15] TPD, which is widely used in OLEDs or QLEDs as the HTL, was chosen as the conducting moiety due to its chemical and electrical stability. SSMe with the dithiol (-S-S-) group was introduced as the anchoring moiety in order to prevent possible cross-linking problem which has been frequently observed in the case of monothiol (SH) anchoring moiety. The HOMO and LUMO energy level of the synthesized poly(TPD-*b*-SSMe) were determined as 5.6 eV and 2.6 eV, respectively, based on ultraviolet photoelectron spectroscopy (UPS) measurements and UV-visible spectra (see Figure S3). Throughout the hybridization, QDs maintained their optical properties, for example, Gaussian photoluminescent (PL) emission spectra ($\lambda_{max.}$ = 508 nm, FWHM = 28 nm) as well as the PL quantum efficiency of 80 % (excited at 420 nm) (Figure S4).

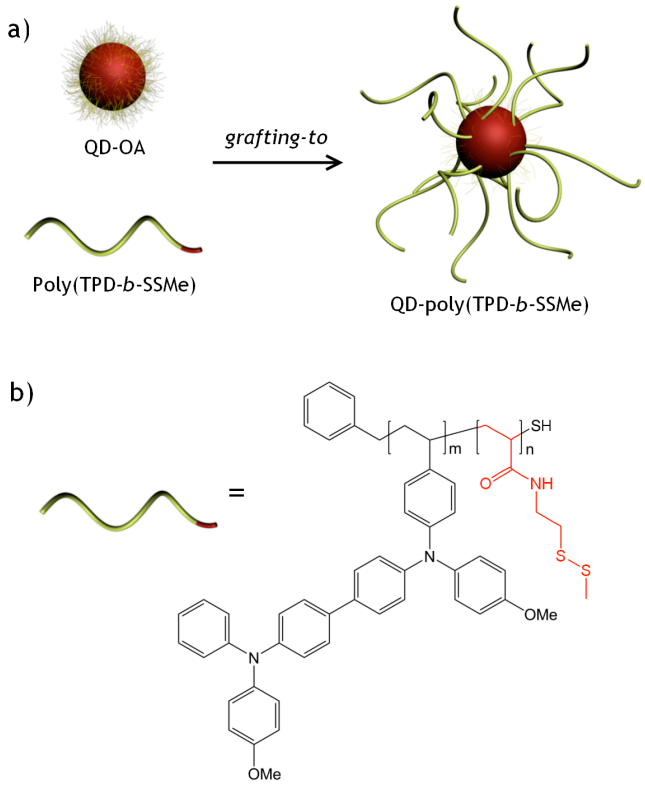

Figure 1.
(a) Schematics on the hybridization of QDs (stabiliazed with oleic acid, QD-OA) with poly(TPD-b-SSMe) through the grafting-to method, and (b) the chemical structure of poly(TPD-b-SSMe) (m = 55, n = 30).

To explore the correlation between the QD morphology within the active layer and the device characteristics, QLED employing the QD-poly(TPD-*b*-SSMe) hybrid film with broad QD distribution within the active layer (Device I, Figure 2a) was characterized and compared with the conventional QLED employing narrow QD layer embedded within the charge transport layer (Device II, Figure 2b). Both devices are built with the common device structure of ITO (anode) // poly(3,4-ethylenedioxythiophene):poly(styrenesulfonate) (PEDOT:PSS) (40 nm) // active layer (QD-poly(TPD-*b*-SSMe) hybrid layer (40 nm) (Device I) or poly-(N,N'-bis(4-butylphenyl)-N,N'-bis(phenyl)benzidine) (polyTPD, 40 nm)/QD (1.5 monolayers) (Device II) // 1,3,5-tris(N-phenylbenzimidazol-2,yl) benzene (TPBi) (40 nm) // LiF (0.5 nm) // Al (100 nm) (cathode). PEDOT:PSS was used to facilitate hole injection from ITO to the active layer, and TPBi was chosen as the electron transporting layer (ETL) and the hole blocking layer. The TEM images in Figure 2 apparently reveal that Device I possesses the hybrid active layer

(40 nm) with uniform QD distribution within the poly(TPD-*b*-SSMe) matrix due to the favorable attraction between QDs and the SSMe anchor block, while Device II possesses a narrow QD emitting layer embedded between polyTPD and TPBi. Among Device II comprising various QD thickness, a QLED (Device II) comprising 1.5 QD monolyaers was chosen for comparison, which exhibits the best performance in terms of turn-on voltage, brightness and device efficiency (Figure S5, S6).

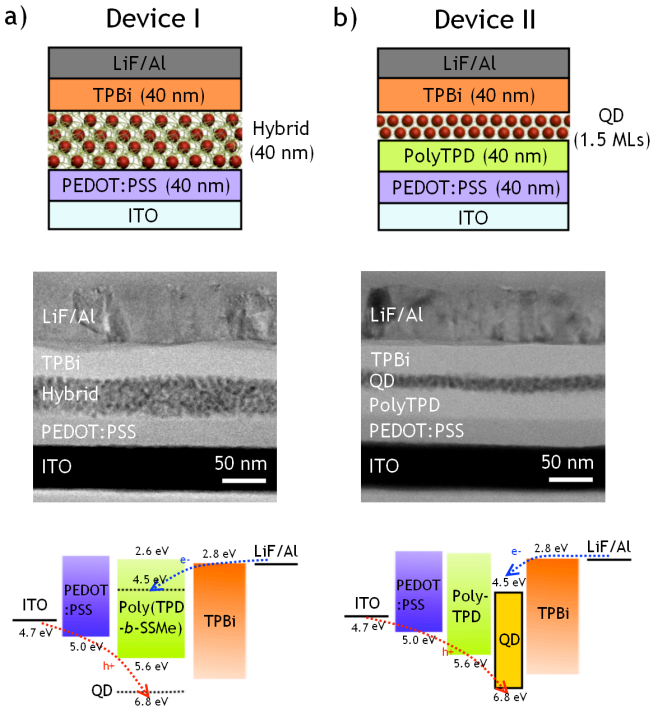

Figure 2.
Schematic illustration of the device structure (top), TEM image (cross-section view) (middle) and the energy band diagram (bottom) of (a) QLED employing QD-poly(TPD-b-SSMe) hybrid layer as the active layer (Device I) and (b) QLED employing polyTPD/QD bilayer as the active layer (Device II).

Figure 3 shows the device characteristics (i.e., current (J) – voltage (V) – luminance (L), EL spectra and efficiency) of Device I and Device II. Both QLEDs exhibit narrow EL spectra with a Gaussian shape ($\lambda_{max.}$ = 510 nm, FWHM = 28 nm) (Figure 3b), which indicates that QDs are the emitting centers within the active layer in both types of QLEDs. In contrast to the previous report (in the case of QLED with the QD monolayer embedded within the HTL (i.e., TPD)),[11] the parasitic emission from the embedding matrix was not observed in Device I,

which represents the efficient exciton generation within QDs with help of the facilitated carrier (electron and hole) injection from poly(TPD-*b*-SSMe) into QDs as well as the sufficient exciton transfer from poly(TPD-*b*-SSMe) to QDs. Although both devices show similar luminance profile as a function of the applied voltage, obvious difference is observed in the device efficiency as a function of the current density (Figure 3c): Device I shows stable device efficiency (Avg. EQE = 1.38 %, Std.(σ) = ± 0.03) in the wide range of the current density from 1to 200 mA cm^{-2}, while Device II shows the large variation in the device efficiency (Avg. EQE = 1.20 %, Std.(σ) = ± 0.11) and the drastic efficiency roll-off at the current density above 50 mA cm^{-2}. The increase in the thickness of QD emitting layer in Device II above 2 QD monolayers does not improve the efficiency roll-off at high current density, but leads to the decrease in the current density and the luminance as well as the dramatic efficiency roll-off at the current density due to the insufficient carrier transport within the QD multilayer films (Figure S6).

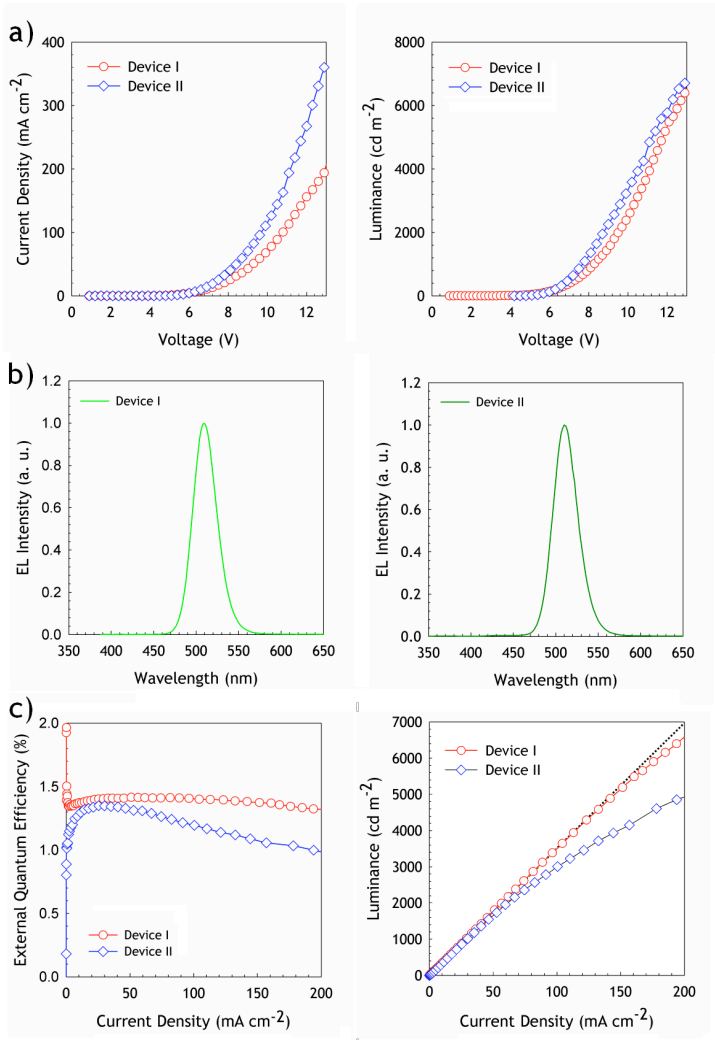

Figure 3.
(a) Current (J) – voltage (V) – luminance (L) characteristics, (b) EL spectra, and (c) external quantum efficiency (EQE) – current (J) – luminance (L) characteristics of both QLEDs (Device I and Device II). The guideline (---) in Figure 3c (right) plots the linear increase of the luminance versus the current density. Device I exhibits stable device efficiency (Avg. 1.38 %) over wide current density (1 ~ 200 mA cm^{-2}) while the Device II shows the drastic efficiency roll-off above the current density of 50 mA cm^{-2}.

The reduced efficiency roll-off in Device I at the current density above 50 mA cm^{-2} is seemingly attributed to the morphology of QDs: broad distribution of QDs within the hole transport layer (i.e., poly(TPD-b-SSMe)). Since the QDs possess lower conduction or valence band edge energy levels compared with the LUMO or HOMO energy level of typical conjugated organic molecules or polymers, electrons migrate into QDs spontaneously from the adjacent organic layer (i.e., TPD or TPBi) while holes require external energies to overcome the injection barrier (above 1 eV), which brings about the charge imbalance within QDs. It seems that, in the case of the conventional structured QLED with a narrow active

layer composed of at most 2 QD monolayers, excitons and carriers (preferentially electrons) are accumulated within QDs in high concentration when devices are operated at higher current density, which leads to the exciton dissociation within QDs by the Auger recombination process.[11, 16] By contrast, the QLED with the hybrid active layer (Device I) possesses a broad QD distribution within the hole transport layer, which can sufficiently distribute the excitons or carriers concentration over the active layer and also improve the charge balance within the active layer, and, therefore, the device exhibits stable efficiency even at the high current density as a result of the suppressed exciton quenching.

Although the QLED in the present study shows improved device characteristics (i.e., reduced efficiency roll-off at high brightness) with the moderate device efficiency (EQE ~ 1.38 %) when compared with the conventional QLEDs, the device characteristics, in terms of the efficiency, brightness and stability, are still required to be improved for the practical applications. However, we believe that the performances can be further improved through the design and synthesis of the carrier transport layers with better electrical properties as well as QDs with improved stability and efficiency, the optimization of the device structure, and the fundamental understanding on the device operation or degradation mechanism.

In summary, we have presented QLED with reduced efficiency roll-off at high current density and brightness based on QD-conducting polymer hybrids (QD-poly(TPD-*b*-SSMe)). In contrast to QLED with the conventional device structure employing narrow QD emitting layer (i.e., at most two QD monolayers) embedded between HTL and ETL, QLED employing the QD-poly(TPD-*b*-SSMe) hybrid active layer with a broad QD distribution within HTL exhibited stable device efficiency roll-off in a wide range of current density, indicating a suppressed exciton quenching within QDs even at higher current density due to a sufficient distribution of exciton and carrier concentration over the broad active layer as well as an improved charge balance within the active layer. As a result, the QLED possessing stable device efficiency of 1.38 % (Std. = ± 0.03) in the wide range of current density (1 ~ 200 mA

cm^{-2}) as well as the color-saturated EL emission (FWHM = 28 nm) with the maximum brightness above 7,000 cd m^{-2} was realized. The approaches and results in the present study firstly address the reduced efficiency roll-off in QLEDs in correlation with the nanoscopic morphology of QDs within the devices, and also suggest reasonable guidelines in designing materials or device architectures of QLEDs toward the practical application as full color displays and lightings.

Experimental Section

Materials: CdSe@ZnS QDs (diameter of 8 nm) stabilized with oleic acid were synthesized as previously reported.[13a] QDs were purified repeatedly (5 times) and dispersed in toluene for further experiment. Poly(TPD-*b*-SSMe) was obtained by conversing pentafluorophenol groups in poly(TPD-*b*-PFP) with 2-(2-ethyldisulfanyl)ethanamine as a previously reported method.[15] The QD-poly(TPD-*b*-SSMe) hybrid solution was prepared by mixing 0.5 ml of QD dispersion (6 wt% in toluene) with 0.5 ml of poly(TPD-*b*-SSMe) solution (3 wt% in toluene). Detailed experimental procedures and results are described in Supporting Information.

Device fabrication and characterization: PEDOT:PSS was spin-casted on patterned ITO substrates with a spin-rate of 4000 rpm for 30 min and baked in a vacuum oven at 120 ^{o}C for 30 min. QD-poly(TPD-*b*-SSMe) hybrid film was spun-casted with a rate of 4000 rpm for 30 sec and cured at 80 ^{o}C under N_2 atmosphere for 30 min to remove residual solvent. PolyTPD/QD bilayer film was prepared by spin-casting each solution (polyTPD in chlorobenzene (1.5 wt%) and QD in toluene (2 wt%)) consecutively with a rate of 4000 rpm for 30 sec. TPBi, LiF and Al were thermally evaporated with the deposition rate (monitored with a quartz-oscillator) of 1–2 Å sec^{-1}, 0.1 Å sec^{-1}, and 4–5 Å sec^{-1}, respectively. The current (J) – voltage (V) – luminance (L) characteristics were measured using a Keithley 236 source-

measure unit and a Keithley 2000 multimeter coupled with a calibrated Si photodiode. EL spectra of the devices were obtained using a Konica-Minolta CS-1000A spectroradiometer.

References

[1] a) L. Brus, *J. Phys. Chem.* **1986**, 90, 2555-2560; b) C. B. Murray, C. R. Kagan, M. G. Bawendi, *Annu. Rev. Mater. Sci*. **2000**, 30, 545-610; c) A. P. Alivisatos, *Science* **1996**, 271, 933-937.

[2] V. L. Colvin, M. C. Schlamp, A. P. Alivisatos, *Nature* **1994**, 370, 354-357.

[3] S. Coe, W. K. Woo, M. G. Bawendi, V. Bulovic, *Nature* **2002**, 420, 800-803.

[4] M. Achermann, M. A. Petruska, S. Kos, D. L. Smith, D. D. Koleske, V. I. Klimov, *Nature* **2004**, 429, 642-646.

[5] J. M. Caruge, J. E. Halpert, V. Wood, V. Bulovic, M. G. Bawendi, *Nat. Photonics* **2008**, 2, 247-250.

[6] Q. Sun, Y. A. Wang, L. S. Li, D. Wang, T. Zhu, J. Xu, C. Yang, Y. Li, *Nat. Photonics* **2007**, 1, 717-722.

[7] Y. Li, A. Rizzo, R. Cingolani, G. Gigli, *Adv. Mater*. **2006**, 18, 2545-2548.

[8] K. Cho, E. K. Lee, W. Joo, E. Jang, T. Kim, S. J. Lee, S. Kwon, J. Y. Han, B. Kim, B. L. Choi, J. M. Kim, *Nat. Photonics* **2009**, 3, 341-345.

[9] a) W. K. Bae, J. Kwak, J. W. Park, K. Char, C. Lee, S. Lee, *Adv. Mater*. **2009**, 21, 1690-1694; b) W. K. Bae, J. Kwak, J. Lim, D. Lee, M. K. Nam, K. Char, C. Lee, S. Lee, *Nanotechnology* **2009**, 20, 075202.

[10] Z. Tan, F. Zhang, T. Zhu, J. Xu, A. Y. Wang, J. D. Dixon, L. Li, Q. Zhang, S. E. Mohney, J. Ruzyllo, *Nano Lett*. **2007**, 7, 3803-3807.

[11] P. O. Anikeeva, C. F. Madigan, J. E. Halpert, M. G. Bawendi, V. Bulovic, *Phys. Rev. B* **2008**, 78, 085434.

[12] a) S. Jeon, K. S. Yook, C. W. Joo, J. Y. Lee, K. Ko, J. Park, Y. G. Baek, *Appl. Phys. Lett.* **2008**, 93, 063306; b) J. Kang, S. Lee, H. Park, W. Jeong, K. Yoo, Y. Park, J. Kim, *Appl. Phys. Lett.* **2007**, 90, 223508; c) J. Wang, J. Yu, L. Li, T. Kang, K. Yuan, Y. Jiang, *Appl. Phys. Lett.* **2008**, 92, 133308.

[13] a) W. K. Bae, K. Char, H. Hur, S. Lee, *Chem. Mater.* **2008**, 20, 531-539; b) J. Lim, S. Jun, E. Jang, H. Baik, H. Kim, J. Cho, *Adv. Mater*. **2007**, 19, 1927-1932; c) R. Xie, U. Kolb, J. Li, T. Basche, A. Mews, *J. Am. Chem. Soc*. **2005**, 127, 7480-7488.

[14] a) Y. Niu, A. M. Munro, Y. Cheng, Y. Tian, M. S. Liu, J. Zhao, J. A. Bardecker, I. J. Plante, D. S. Ginger, A. K. –Y. Jen, *Adv. Mater*. **2007**, 19, 3371-3376; b) M. V. Kovalenko, M. Scheele, D. V. Talapin, *Science* **2009**, 324, 1417-1420; c) S. A. Mcdonald, G. K. Konstantatos, S. Zhang, P. W. Cyr, E. J. D. Klem, L. Levina, E. H. Sargent, *Nat. Mater.* **2005**, 4, 138-142.

[15] a) J. Kwak, W. K. Bae, M. Zorn, H. Woo, H. Yoon, J. Lim, S. W. Kang, S. Weber, H. Butt, R. Zentel, S. Lee, K. Char, C. Lee *Adv. Mater*. **2009**, 21, 5022-5026; b) M. Zorn, W. K. Bae, J. Kwak, H. Lee, C. Lee, R. Zentel, K. Char *ACS Nano* **2009**, 3, 1063-1068.

[16] a) V. I. Klimov, A. A. Mikhailovsky, D. W. McBranch, C. A. Leatherdale, M. B. Bawendi, *Science* **2000**, 287, 1011-1013; b) A. K. Goodling, D. E. Gomez, P. Mulvaney, *ACS Nano* **2008**, 2, 669-676.

4. Summary

The work shows a spectrum of applications of polymer functionalized nanoparticles from orientation phenomena, improved properties and applications in optoelectronic devices.

Based on RAFT polymerization we prepared several functional block copolymers from various monomers, containing a longer soluble and functional block and a shorter anchor block. As a second block we used the reactive pentafluorophenylacrylate monomer. With the controlled radical poymerisation technique we were able to create various polymers with a low polydispersity. This activated ester monomer was converted with several primary amines to integrate anchor units for inorganic nanoparticles. For particles based on metal oxides dopamine was used as an anchor moiety. For nanoparticles based on cadmium thiol anchoring moieties were integrated. The block copolymer binds efficiently to nanoparticles. The ratio between the soluble block and the reactive block is variable, but a ratio of 100: 10 was found to give the best surface coverage. By modification by TiO_2, SnO_2, ZnO and CdTe nanorods the universality of the approach was shown. Due to the steric stabilization the particles with a modified surface form stable dispersion, with most of the nanorods individually solubilized. The grafting density was analyzed by TGA measurements. The hybrid materials are soluble in all solvents appropriate for the polymer corona. Further on, the particles can be dispersed in polymers of the same chemical composition as the functionalization polymer.

We distributed the particles uniformly in a styrene oligomer (M_n: 580 g/mol). The oligomers glass transition temperature is below room temperature. Hence, the matrix has a low viscosity and can be sheared. In such a matrix liquid crystalline phases could be observed for all described anisotropic nanoparticles. These phases can be sheared to orient the particles uniformly in the matrix.

In analogy to low molecular or polymeric liquid crystals the phases clear reversibly at distinct temperatures. These temperatures increase with the nanorod length. While shorter nanorods (TiO_2, SnO_2, CdTe : 20 to 30 nm) clear in the range from 60-90 °C, the clearing of phases

formed by the longer ZnO nanorods (Ca. 120 nm) could not be observed at temperatures lower than 230°C.

Working towards optoelectronic applications triphenylamine based monomers as a hole conducting material were polymerized in a controlled manner by RAFT polymerization. Modification of electron conducting semiconductors gives rise to p-n junctions of a single particle level. For these functional polymers also narrowly distributed polymers with a short reactive block were prepared that can be modified to anchor to various inorganic materials. TiO_2, SnO_2 and ZnO were functionalized with the TPA polymers. Analogously to LC phases in styrene, birefringent structures can also be observed, if the particles are dispersed in TPA oligomers. These phases also show reversible clearing phase transitions.

To achieve the ideal morphology for the charge percolation with nanorods oriented perpendicular to the electrode we took advantage of the liquid crystalline behaviour of the rods in a matrix. By applying an electric field to the LC phases, a disappearance of the birefringent areas was observed. This is an evidence for a homeotropic orientation of the nanorods.Electron microscopy showed orientations that remember of a Fredericks transition know from low molecular liquid crystal in display applications. As shown by dielectric relaxation spectroscopy, which observes a low effective dipole moment, this switching behaviour is only possible due to the cooperative behaviour in a LC phase.

We also used the flexibility of the reactive block to integrate further functionality in the anchoring part of the block copolymer. Looking towards application in dye sensitized solar cell model materials, a perylene dye was synthesized that can be converted with the reactive ester. The dye was successfully intregrated into the polymer and could be linked directly at the interface between the nanoparticle and hole conducting polymer. The quenched luminescence of the dye shows the energy transfer due to the ideally fixed location. By Kelvin probe force microscopy we could show that upon illumination particles are charged up to 20 mV /particle due to a charge transfer from the dye to the ZnO nanoparticle and subsequent

reduction of the dye by the p-type TPA polymer. Hence, the system behaves like a solar cell in a single particle.

With TPA block copolymer with thiol anchor groups we could also modify the surface of luminescent CdSe@ZnS quantum dots. The modification improves several properties of the quantum dots: the stability of QD upon UV illumination is increased by stabilization with the multi dentate anchor block. At the same time the photoluminescence characteristics are only slightly changed. The hybrids show advantages in terms of processability like film formation properties. The functional corona can be used to improve charge injection, if the particles are used in electroluminescent devices. Due to the well dispersed particles and the hole conducting polymer shell, the hole-conductor and emitter can be deposited at the same time, reducing device preparation by one step. Compared with the same device structure with non hybridized QDs the device efficiency could be improved three times. Later experiments yielded very high and stable efficiencies of up 2.5 % EQE.

By changing the TPA side chains to more stable TPD derivatives we could prepare very stable devices, where the roll-off in efficiency could be suppressed. This is explained by the fact that the emitting nanoparticles are well dispersed in the hole conducting matrix and the exciton quenching, which occurs at high current densities, when the particles are in close contact, vanishes.

As a result this work demonstrates that properly designed polymer nanoparticle composites offer the potential to improve optoelectronic devices with regard to orientation and luminescence.

5. Supporting Information

Supporting Information to 3.3

Orientation and Dynamics of ZnO Nanorod Liquid Crystals in Electric Fields (p. 76-93)

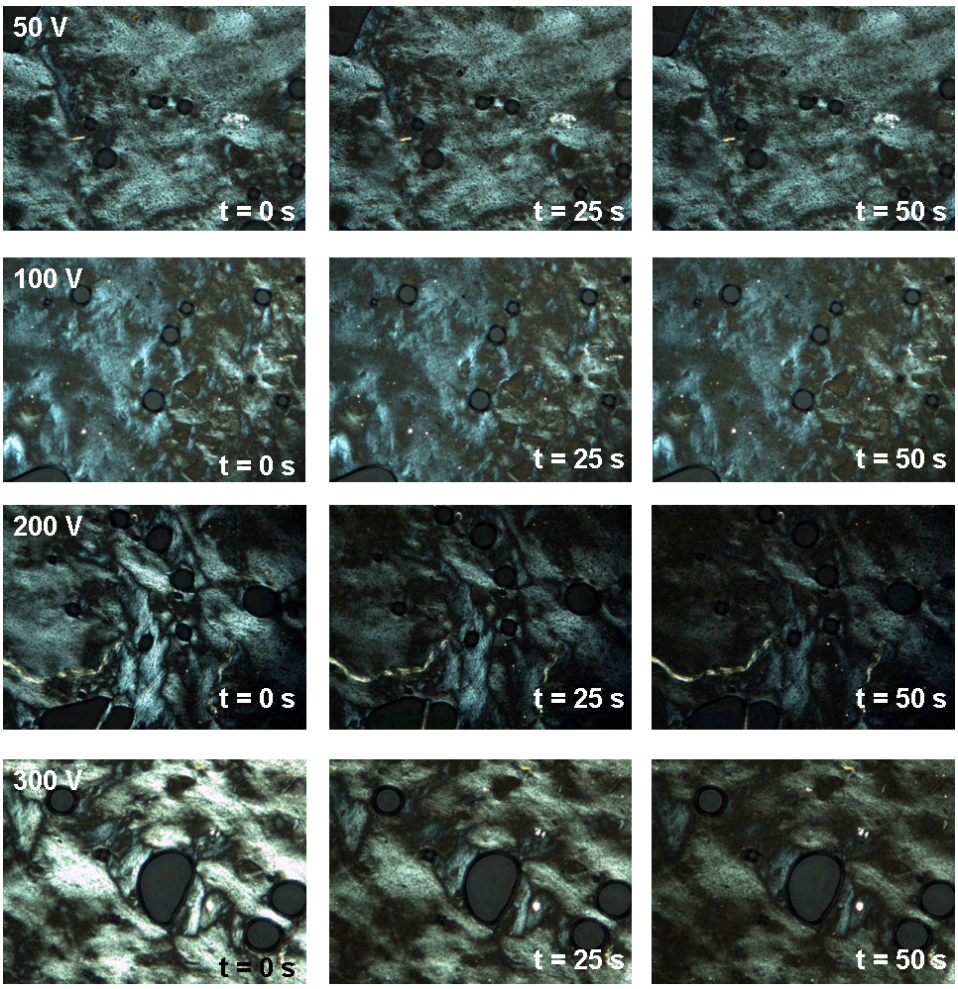

Figure S1.
POM images of the LC textures at different AC field strength at t = 0s, t = 25s and t = 50s. The difference in the loss of birefringence with field strength is plotted in Figure 4.

Supporting Information to 3.4

Light Induced Charging of Polymer Functionalized Nanorods: A "Solar Cell" Concept for a Single Particle (p. 94-106)

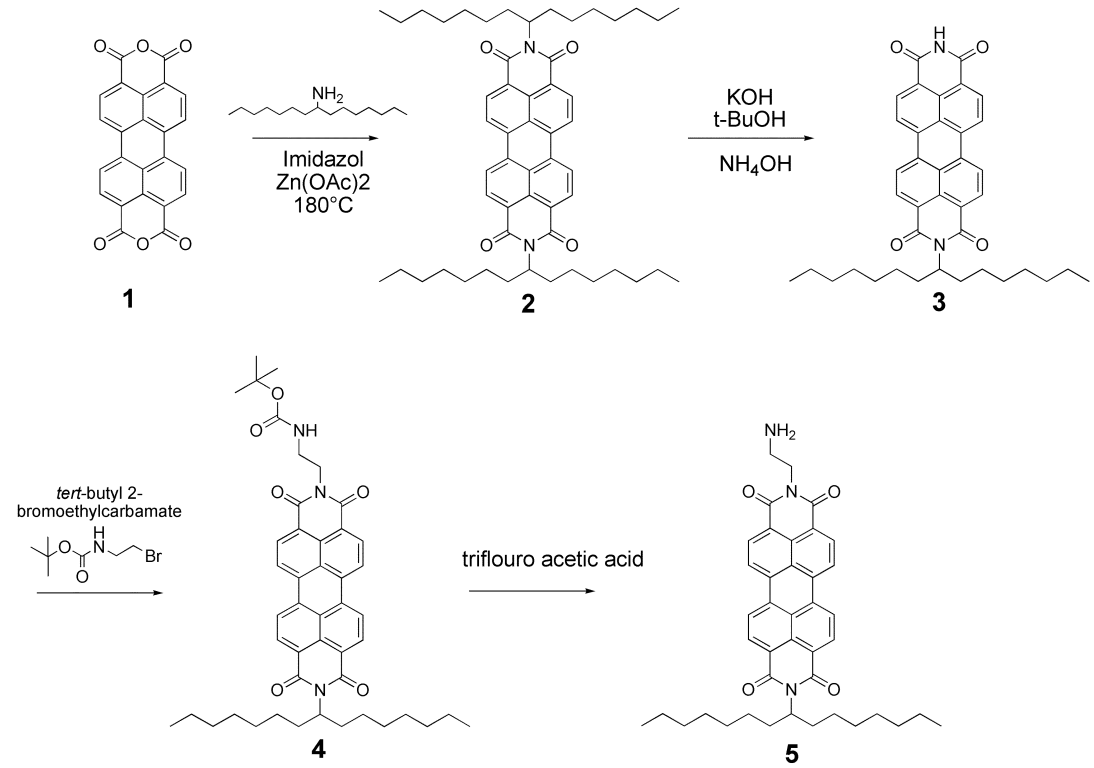

Scheme S1:
Synthetic details for the amine functionalized dye

Synthesis of [1]N- (8-pentadecan)-[2]N (ethyl-2-amine) perylene-3,4:9,10-tetracarboxdiimides

30.6 g perylene-3,4:9,10-tetracarboxdianhydride **1** (1 eq, 78 mmol) were mixed with 13.7 g Zn(OAc)2 (62 mmol, 0.8 eq), 42 g of pentadecan-8-amine (172 mmol, 2.2 eq) and 106 g imidazole (20 eq) as solvent, The mixture was heated to 160 °C for under a N_2 atmosphere. After 4 h the reaction mixture was poured to a cooled 4N HCl to precipitate the product. The product was filtered, washed with water and purified by column chromatography with as an eluent. The product could be isolated as a red solid **2** (50.7 g, 70 %).

6 g of the red solid **2** were suspended in 135 mL *tert*. butanol, heated to 120°C and 1.2 g KOH were added. After 12 min the reaction was poured into acetic acid to stop the reaction. The

precipitate was filtered and cooked at 90°C in 390 mL 3 % NH_4OH. After 1 h a solution of 2.2 g K_2CO_3 in 5 mL was added and cooked for one more hour. The reaction mixture was poured into 1 N HCl and extracted with $CHCl_3$. The product was purified by column chromatography ($CHCl_3$:EtOH, 20:1) to 2.9 g (65 %) of the desired product **3**.

2.9 g of 3 (1 eq) were dissolved in 10 mL DMF with 2.3 g *tert*-butyl 2-bromoethylcarbamate, 15 mg K_2CO_3 and refluxed at 120° for 6 h. Afterwards the product was extracted with $CHCl_3$ and water. The product was purified by column chromatography to yield 1.3 g (40%) of the desired product **4**.

^{1}H NMR (300 MHz, $CDCl_3$): 8.87-8.55 (m, 8H, Ar-H), 8.02 (bs, 1H, NH), 4.33 (qu, 1H, CH), 4.18 (t, CH_2), 1.28(m, 24H, CH_2)1.23 (s, 9H, CH_3), 0.87 (t, 6H, CH_3)

MS: ESI m/z: 742.8

UV vis(THF): λ_{max} : 520 nm, 485 nm, 454 nm.

photoluminescence (THF) (exc. 520 nm): 535 nm, 569 nm, 617 nm.

For deprotection of the Boc group product **4** was dissolved in THF and stirred with trifluoro acetic acid (1.5 eq). After 30 min all acid was reacted with NEt_3 until the solution was basic to yield 5 in situ (mass spectroscopy analysis correct).

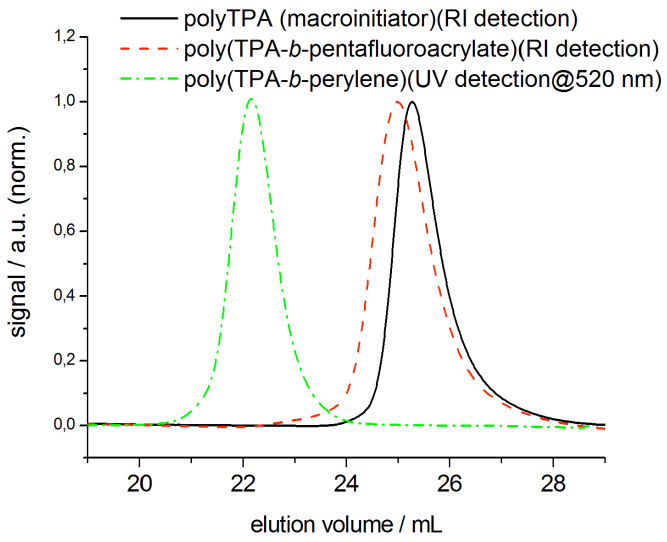

Figure S1.
GPC elugrams of the synthesized polymers.

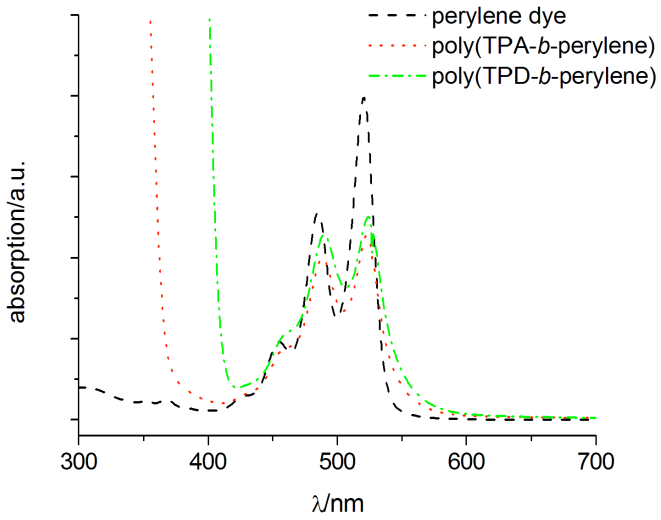

Figure S2.
UV—Vis spectra of the polymer 1 and 2.

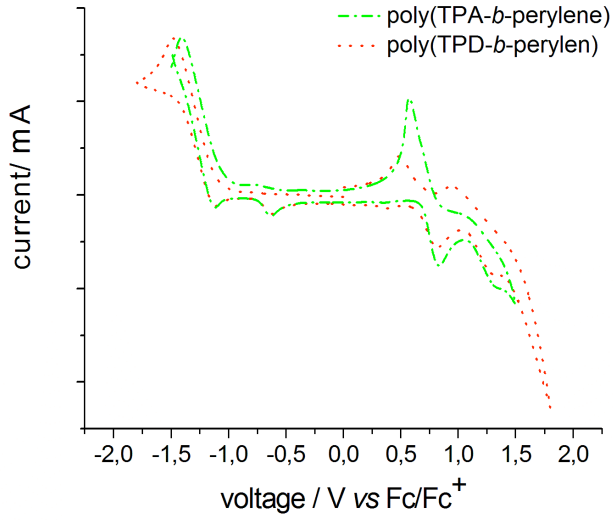

Figure S3.
Cyclovoltammograms of polymers 1 and 2.

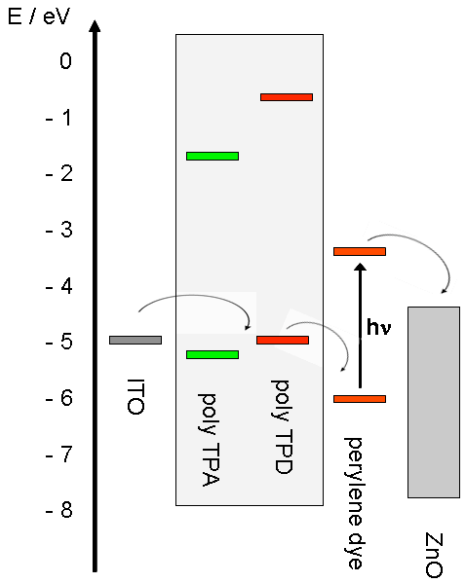

Figure S4.
Energy diagram.

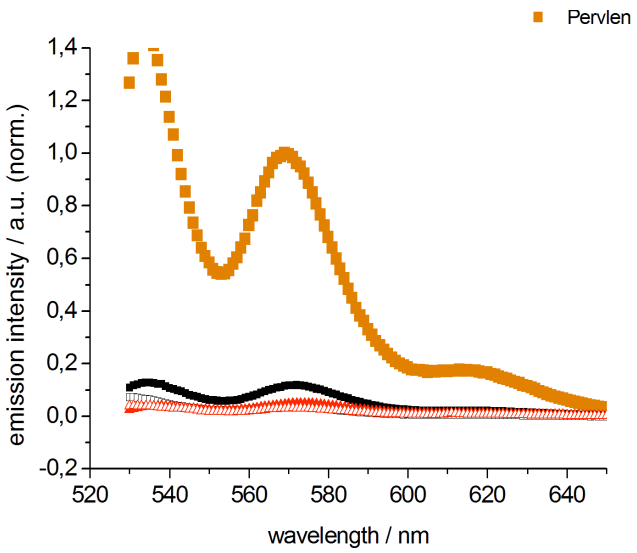

Figure S5.
Full sized PL spectra.

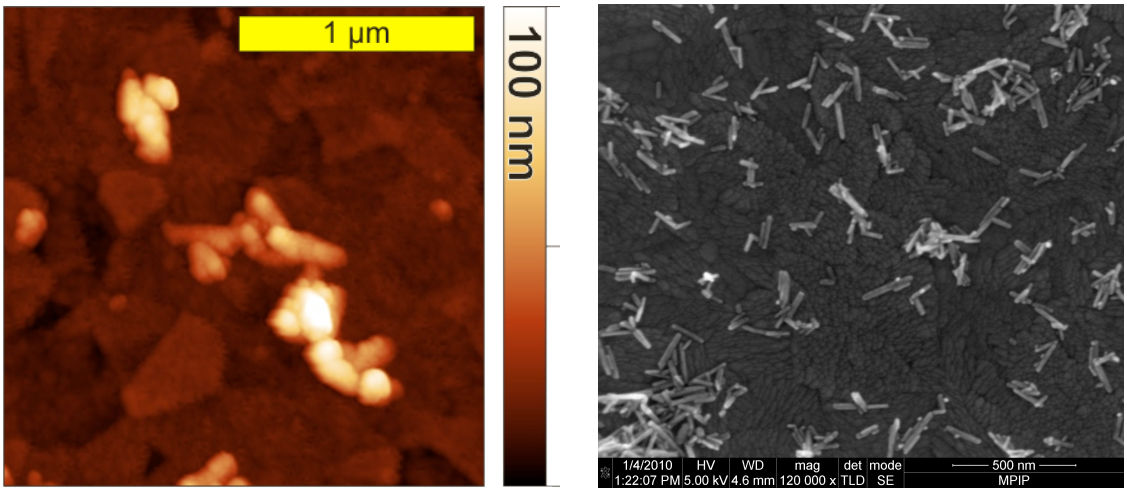

Figure S6.
Topography to the potential images in Fiures 2 (b) and (c) and SEM image of the same sample

Supporting Information to 3.5

Quantum Dot-Block Copolymer Hybrids with Improved Properties and Their Application to Quantum Dot Light-Emitting Devices (p.107-124)

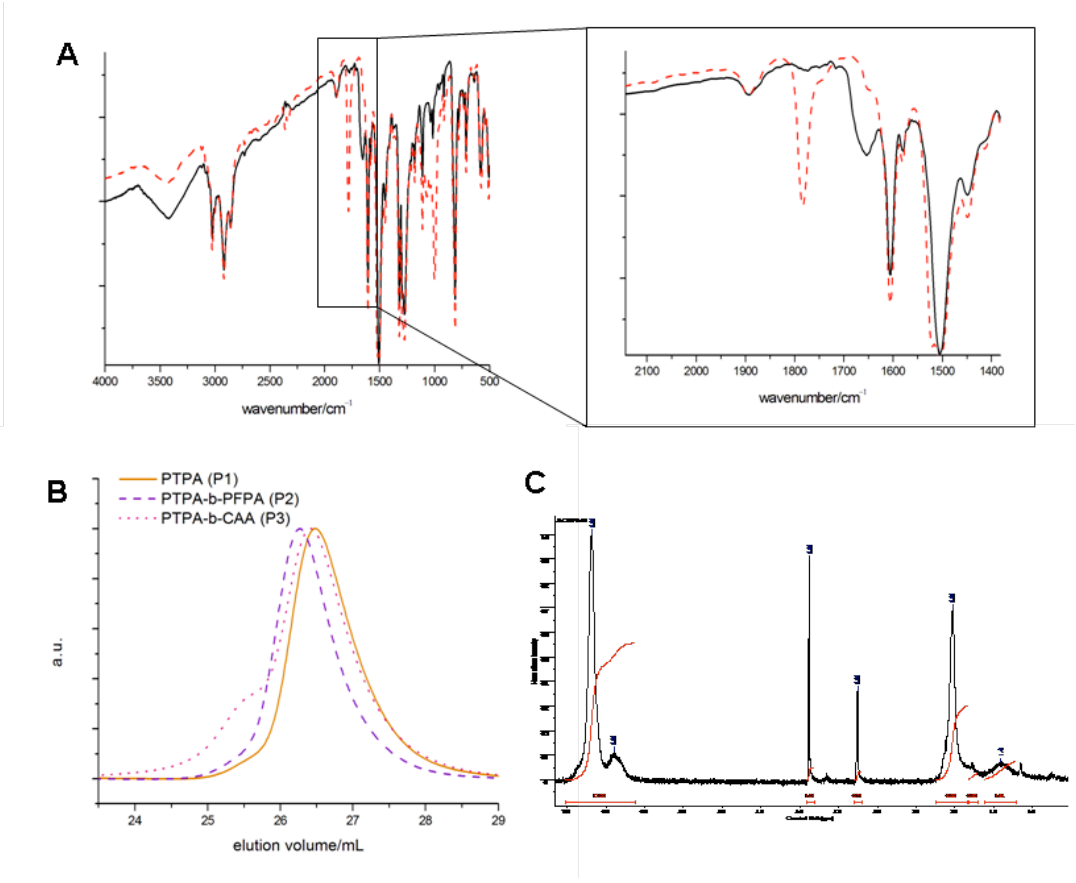

Figure S1.
Analytical details for BCP 2: A: FT-IR spectrum of P2 (red dotted line) and BCP (black line): The disappearance of the ester band shows the transformation of the reactive ester polymer. (see enlargement) B: GPC traces C: NMR spectrum in $CDCl_3$ and MeOH.

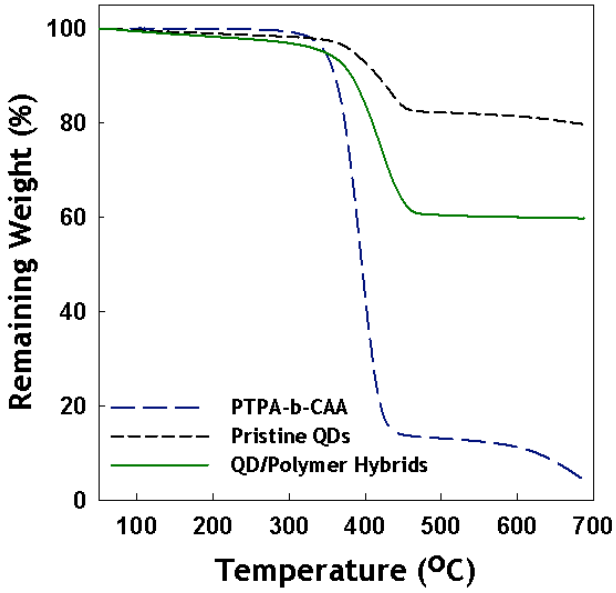

Figure S2.
Thermal gravimetric analysis of pristine QDs, QD/PTPA-*b*-CAA hybrids and PTPA-*b*-CAA.

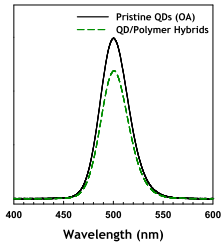

Figure S4.
Photoluminescence intensities of pristine QDs and QD/ PTPA-*b*-CAA hybrids.

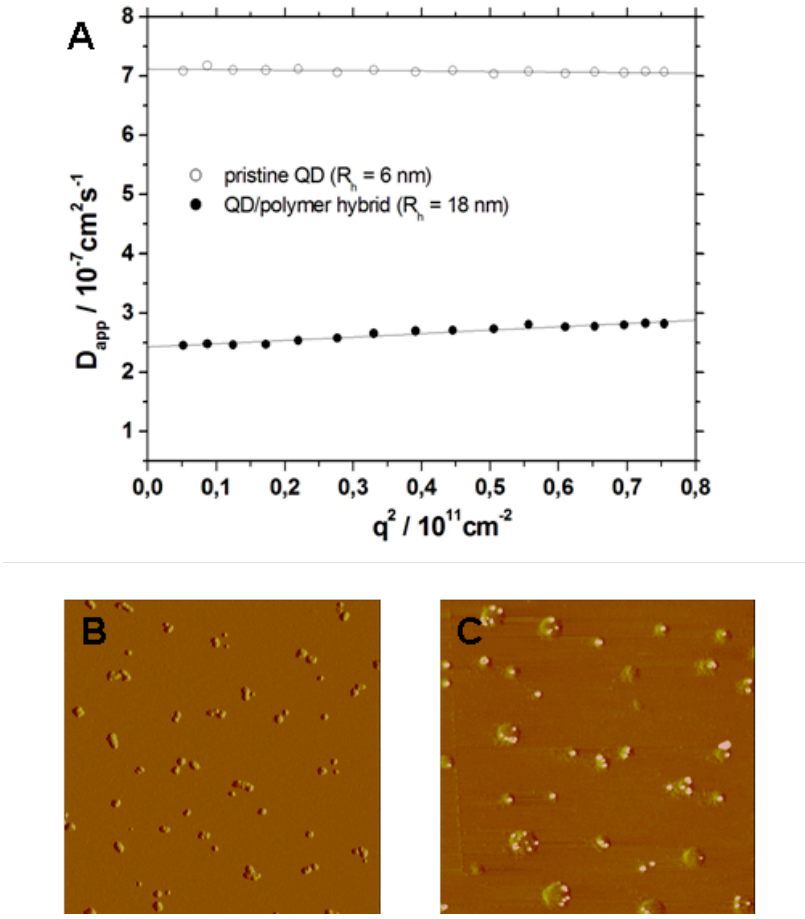

Figure S3.
A: dynamic light scattering data, B: AFM image: pristine QDs, C: AFM image: QD/polymer hybrid, the soft polymers shell can clearly be visualized around the hard inorganic core. (thanks to Karl Fischer, Sandra Muth and Prof. Manfred Schmidt, Mainz).

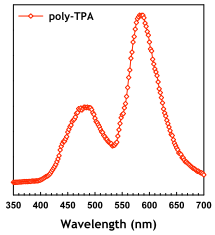

Figure S5.
Electroluminescence spectrum of PTPA-*b*-CAA. (Strong emission at 590 nm is due to exciplex formation at the interface between TPBI and P1).

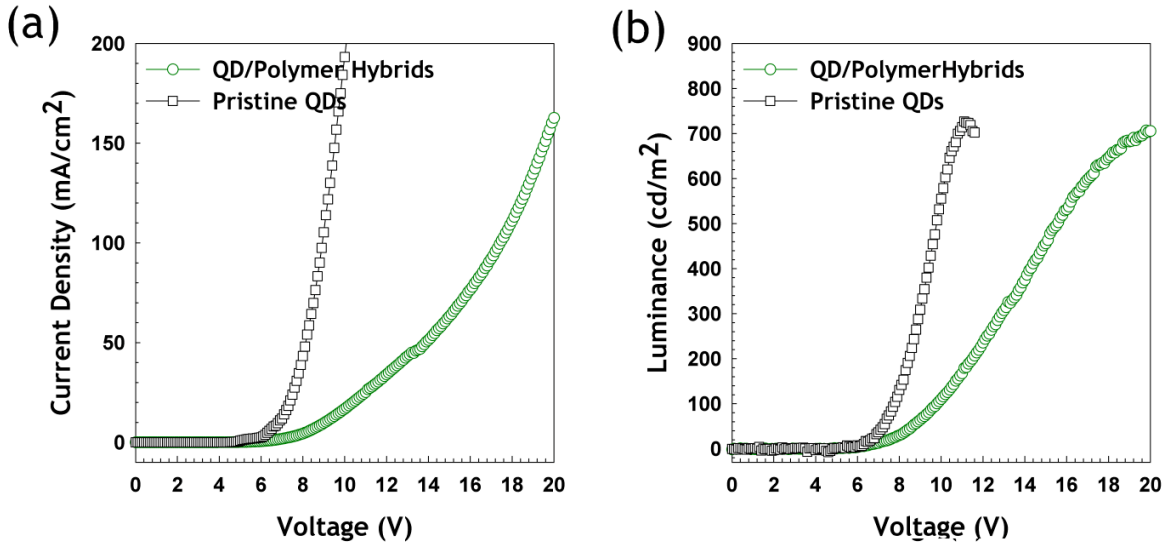

Figure S6.
I-V (left) and L-V (right) characteristics of QLEDs based on pristine QD and QD/PTPA-*b*-CAA hybrid emitting layers.

Supporting Information to 3,6

Reduced Efficiency Roll-Off in Light-Emitting Diodes Based on Quantum Dot-Conducting Polymer Hybrids Reduced Efficiency (p. 125-136)

1. Chemicals

CdO (99.9 %), zinc acetate ($Zn(Ac)_2$, 99.99 %), oleic acid (OA, 90 %), 1-octadecene (1-ODE, 90 %), trioctylphosphine (TOP, 90 %), anhydrous toluene, methanol, hexane and ethanol was purchased from Sigma-Aldrich. AIBN and cysteamine were purchased from Fluka. TPD monomer was synthesized according to literature by a Buchwald-Hartwig coupling of 4-Iodoanisol with N,N´diphenyl(1,1´biphenyl)4,4´diamin with subsequent Vilsmeyer formylation and Wittig reaction. PFPA was synthesized by esterification of acryloylchloride with pentafluorophenol. THF used for polymerisation was freshly distilled over sodium in a nitrogen atmosphere. All chemicals were used as purchased.

2. Synthesis of CdSe@ZnS QDs

CdSe@ZnS QDs with chemical composition gradient were prepared by single-step synthesis. For the typical synthesis, 0.2 mmol of CdO, 4 mmol of $Zn(Ac)_2$ and 4 mmol of OA were loaded in 100 ml flask, evacuated at 150 °C under 100 mTorr pressure for 30 min to form $Zn(OA)_2$. Then the reactor was filled with N_2, added with 15 mL of 1-ODE, and heated up to 305 °C. At the elevated temperature, 2 mL of TOP dissolving 0.1 mmol of Se and 3.5 mmol of Se was swiftly injected into the reactor. The reaction temperature was maintained at 300 °C for further growth of CdSe@ZnS QDs. After 10 min of reaction, the reactor was cooled down to room temperature to complete the reaction. The as-prepared QDs were purified by precipitating with ethanol and redispersing in toluene repeatedly (3 times) to remove residual surfactants and unreacted precursors. Final products were dispersed either in hexane or toluene and kept in the refrigerator.

3. Synthesis of poly(TPD-*b*-PFP) and poly(TPD-*b*-SSMe)

Synthesis of poly(TPD-*b*-PFP)

1.2 g of Vinyl-methoxy TPD (2 mmol, 100 eq), 5 mg of benzylbenzodithionate (0.02 mmol, 1eq) and 1 mg of AIBN (0.01 mmol, 0.1 eq) were dissolved in 3 mL dioxane in a Schlenck tube. The reaction vessel was filled with N_2 through repeated freeze-pump-thaw cycles (3 times). Polymerization was carried out at 90 °C for 48 h. The polymer was precipitated three times in methanol and petrolether to yield in 0.67 g (55 %) of polymer (yellow color).

M_n: 3.157 x 10^4 g mol^{-1}, PDI: 1.10 (PS equivalents)

0.67g (0.02 mmol, 1 eq) homopolymer as a macroinitiator, 0.13 g pentafluorophenylacrylate (0.5 mmol, 50 eq) and 1 mg of AIBN (0.002 mmol, 0.1 eq) were dissolved in 3 mL of dioxane. Polymerization was carried out at 90 °C in N_2 atmosphere for 3 d. The polymer was purified by precipitation with methanol to yield in 0.7 g (%) of the reactive block copolymer PTPA-*b*-PFP. The polymer was stored in refrigerator under N_2 atmosphere.

M_n: 3.871 x 10^4 g mol^{-1}, PDI: 1.24 (PS equivalents)

^{1}H-NMR(d^8-THF, 300 MHz): 6.84 (m, 25H, ArH), 3.73 (m, 6H, -OMe), 2.54 (m, 1H, CH_2-C*H*), 1.88 (m, 3H, C*H*-CH_2), 1.21 (m, 2H, CH-CH_2).

Synthesis of poly(TPD-b-SSMe)

To synthesize PTPD-*b*-SSMe, 0.2 g of PTPD-b-PFP (1eq) was dissolved in tetrahydrofuran, followed by sequential addition with 60 mg of 2-(2-methyldisulfanyl)ethanamine (2 eq according to PFP units) and 0.08 mL of triethylamine. The

mixed solution was stirred over night under N_2 atmosphere. The polymer solution was filtered and precipitated in methanol for three times to yield in 0.76 g (96 %) of PTPD-*b*-SSMe.

IR: ν_{max}/cm^{-1}: 3027 (CH), 1658 (CONH), no ester band

^{19}F-NMR: no signal

4. Characterization

NMR spectra were obtained with a Bruker AC 300MR. IR spectroscopy was performed with a Bruker Vector 22. Gel permeation chromatography (GPC) was carried out in THF as solvent and the detector system contained refractive index (Jasco), UV-Vis (Jasco) and light scattering (Wyatt) detectors. The values given here were calculated in relation to PS standards. UV-Vis. absorption spectra were measured with an Agilent 8454 UV-Vis diode array spectrometer. Photoluminescence (PL) spectra were collected on an ACTON spectrometer.

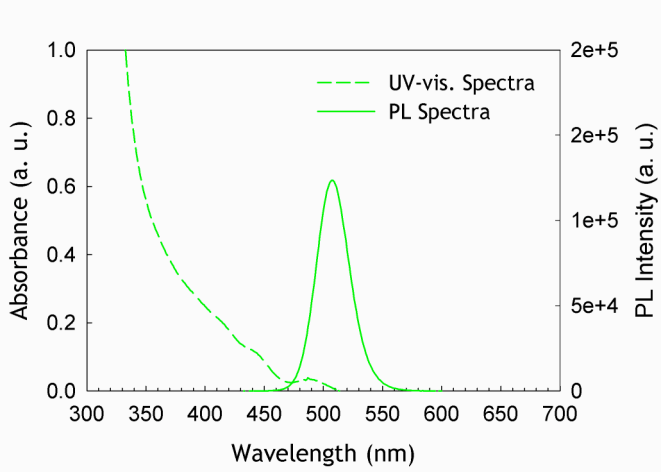

Figure S1.
UV-Vis and PL spectra of CdSe@ZnS QDs with chemical composition gradient.

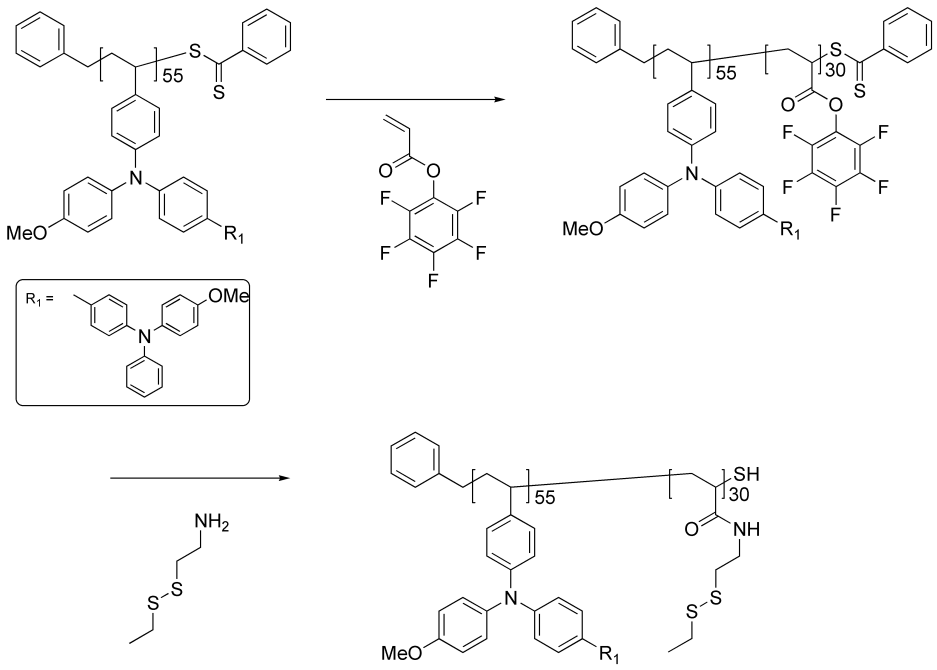

Figure S2.
Schematics for the synthesis of poly(TPD-*b*-SSMe).

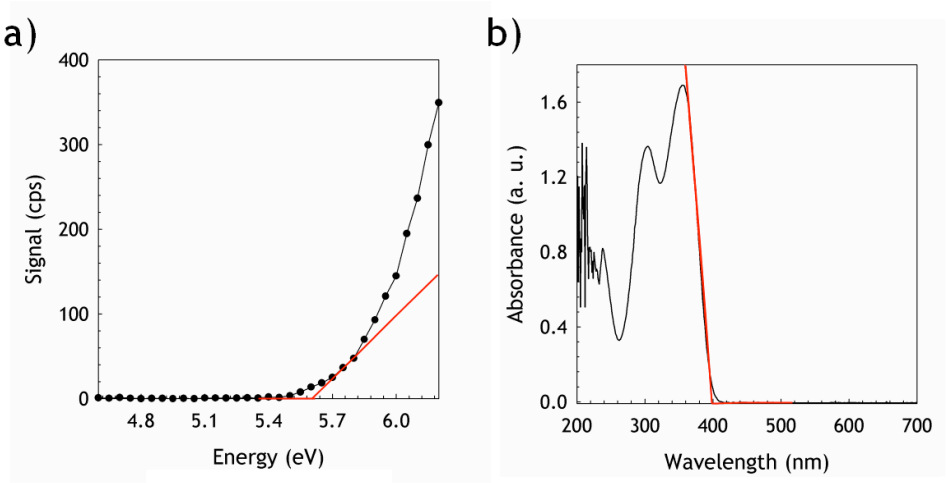

Figure S3.
a) UPS and b) UV-vis. spectra of poly(TPD-*b*-SSMe). The HOMO energy level and LUMO energy level of poly(TPD-*b*-SSMe) are determined as 5.6 eV and 2.6 eV, respectively.

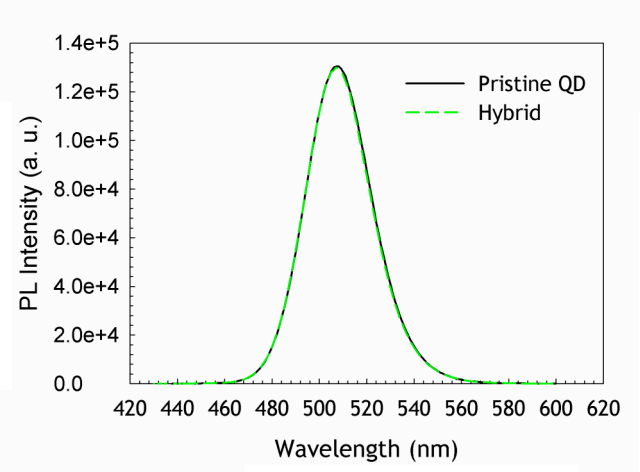

Figure S4.
PL spectra (excited at 420 nm) of pristine QDs stabilized with oleic acid (solid line, optical density at 420 nm = 0.1) and the QD-poly(TPD-*b*-SSMe) hybrids (dotted line, extinction coefficient at 420 nm = 0.1) dispersed in toluene.

List of Publications

H-C. Kim, J. Träger, **M. Zorn**, N. Haberkorn, N. Hampp; Ophthalmic drug delivery utilizing two-photon absorption: A novel approach to treat posterior capsule opacification, *SPIE-OSA*/ Vol. 6632 66321E-1.

M. Zorn, S. Meuer, N. M. Tahir, Y. Khalavka, C. Sönnichsen, W. Tremel, R. Zentel; Liquid crystalline phases from polymer functionalised semiconducting nanorods, *J. Mater. Chem.* **2008**, 18, 3050 – 3058.

M. Zorn, R. Zentel; Liquid Crystalline Orientation of Semiconducting Nanorods in a Semiconducting Matrix, *Macromol. Rapid Commun*. **2008**, 29, 922 - 927.

M. Zorn, W.K. Bae, J. Kwak, H. Lee, C. Lee, R. Zentel, K. Char; Quantum Dot-Block Copolymer Hybrids with Improves Properties and Their Application to Quantum Dot Light Emitting Devices, *ACS Nano* **2009**, 3 (5), 1063-1068

W. Pisula, **M. Zorn**, J.Y. Chang, K. Müllen, R. Zentel; Liquid Crystalline Ordering and Charge Transport in Semiconducting Materials, *Macromol. Rapid Commun*. **2009**, 30, 1179-1202.

M. Zorn, S. Meuer, M.N. Tahir, W. Tremel, K. Char, R. Zentel, Orientation of Polymer Functionalized Nanorods in Thin Films, *J. Nanosci. Nanotech.* **2009**, accepted.

J. Kwak, W. K. Bae, **M. Zorn**, H. Woo, H. Yoon, J. Lim, S. W. Kang, S. Weber, H.-J. Butt, R. Zentel, S. Lee, K. Char, C. Lee; Characterization of Quantum Dot/Conducting Polymer Hybrid Films and Their Application to Light-Emitting Diodes, *Adv. Mater* **2009**, 21, 5022-5026.

M. Zorn, N.M Tahir, W. Tremel, G. Floudas, R. Zentel, Orientation and Dynamics of ZnO Nanorod Liquid Crystals in Electric Fields, *Macromol. Rapid Commun* **2010**, DOI: marc.201000049

W. K. Bae, J. Kwak, **M. Zorn**, H. Woo, D. Lee, J. Lim, S. Lee, R. Zentel, K. Char, C. Lee, Reduced Efficiency Roll-Off in Light-Emitting Diodes Based on Quantum Dot-Conducting Polymer Hybrids, *Angew. Chem. Int. Ed.* **2010**, submitted

M. Zorn, S. Weber, N.M Tahir, W. Tremel, R. Berger, R. Zentel, Light Induced Charging of Polymer Functionalized Nanorods: A “Solar Cell” Concept for a Single Particle, *Nano Lett.* **2010**, submitted

Acknowledgement

Thanks to:

- [redacted] for giving me an interesting project and the chance to make my doctoral studies in an international working group. Thanks for giving me scientific advice and the chance to go to international conferences.
- [redacted], for giving me the chance to visit his group and scientific discussions.
- [redacted], for the chance to use the produced materials in real applications.
- [redacted] for reviewing my thesis.
- the DFG for financial support (International Research Training Group "Self-Organized Materials for Optoelectronics" IRTG 1404) and to the Graduate School of Excellance MAINZ.
- the [redacted] for the good and funny working environment. It was a great time in Mainz.
- the whole Char group for their help in every situation during my time in Korea.
- [redacted], for her synthetical help.
- [redacted] for the translation of the Abstract of this thesis in Korean.
- all the co-authors of the publications for their help, discussions and great work they did. Especially to
    - [redacted] for the interesting and successful cooperation.
    - [redacted] for delivering their wonderful nanorods.
- [redacted] for the work they did during their internship in our group.
- the members of the IRTG for the great time in Seoul, Mainz and in Nierstein.

- [redacted], who accompanied me during the last eight years in Marburg, Mainz and Seoul. Thank you for the good times!
- all the people that participated the time in Seoul (especially [redacted], but all the others too). It was a fantastic experience with you!
- [redacted]., for your encouragement and all the time we shared.
- my parents, my sisters and my whole family for all their help in every situation. I´m glad to know that you are always there. Thank you!